Multivariate assessment of linear and non-linear causal coupling pathways within the central-autonomic-network in patients suffering from schizophrenia

Dissertation
zur Erlangung des akademischen Grades
Doktoringenieur (Dr.-Ing.)

vorgelegt der Fakultät für Informatik und Automatisierung
der Technischen Universität Ilmenau

von Dipl.-Ing. (FH) Steffen Schulz

1. Gutachter: Univ.-Prof. Dr.-Ing. habil. Jens Haueisen
(Technische Universität Ilmenau)
2. Gutachter: Prof. Dr. Mathias Baumert
(The University of Adelaide)
3. Gutachter: Prof. Dr.-Ing. Andreas Voß
(Ernst-Abbe Hochschule Jena)

Tag der Einreichung: 25.11.2022
Tag der wissenschaftlichen Aussprache: 05.06.2023

DOI: 10.22032/dbt.57589
URN: urn:nbn:de:gbv:ilm1-2023000141

Abstract

In the field of time series analysis, increasing interest focuses on insights gained how the coupling pathways of regulatory mechanisms work in healthy and ill states. Recent advances in non-linear dynamics, information theory and network theory lead to a new sophisticated body of knowledge about coupling pathways within (patho)physiological (sub)systems. Coupling analyses aim to provide a better understanding of how the different integrated physiological (sub)systems, with their complex structures and regulatory mechanisms, describe the global behaviour and distinct physiological functions at the organism level. The understanding of driver-response relationships between regulatory (sub)systems is of growing interest. In particular, the detection and quantification of the coupling strength and direction are important aspects for a more detailed understanding of physiological regulatory processes. This thesis aimed to characterize short-term instantaneous central-autonomic-network coupling pathways (top-to-bottom and bottom to top) by analysing the coupling of heart rate, systolic blood pressure, respiration and central activity (EEG) in schizophrenic patients and healthy participants. Therefore, new multivariate causal and non-causal linear and non-linear coupling approaches (HRJSD, mHRJSD, NSTPDC) that are able to determine the coupling strength and direction were developed. Whereby, the HRJSD and mHRJSD approaches allow the quantification and classification of deterministic regulatory coupling patterns within and between the cardiovascular- the cardiorespiratory system and the central-autonomic-network were developed. These coupling approaches have their own unique features, even as compared to well-established coupling approaches. They expand the spectrum of novel coupling approaches for biosignal analysis and thus contribute in their own way to detailed information obtained, and thereby contribute to improved diagnostics/therapy. The main findings of this thesis revealed significantly weaker non-linear central-cardiovascular and central-cardiorespiratory coupling pathways, and significantly stronger linear central information flow in the direction of the cardiac- and vascular system, and a significantly stronger linear respiratory information transfer towards the central nervous system in schizophrenia in comparison to healthy participants. This thesis provides an enhanced understanding of the interrelationship of central and autonomic regulatory mechanisms in schizophrenia. The detailed findings on how variously-pronounced, central-autonomic-network pathways are associated with paranoid schizophrenia may enable a better understanding on how central activation and autonomic responses and/or activation are connected in physiology networks under pathophysiological conditions.

Kurzfassung

Im Bereich der Zeitreihenanalyse richtet sich das Interesse zunehmend darauf, wie Einblicke in die Interaktions- und Regulationsprozesse von pathophysiologischen- und physiologischen Zuständen erlangt werden können. Neuste Fortschritte in der nichtlinearen Dynamik, der Informationstheorie und der Netzwerktheorie liefern dabei fundiertes Wissen über Kopplungswege innerhalb (patho)physiologischer (Sub)Systeme. Kopplungsanalysen zielen darauf ab, ein besseres Verständnis dafür zu erlangen, wie die verschiedenen integrierten regulatorischen (Sub)Systeme mit ihren komplexen Strukturen und Regulationsmechanismen das globale Verhalten und die unterschiedlichen physiologischen Funktionen auf der Ebene des Organismus beschreiben. Dabei spielt das Verständnis von Sender-Empfänger Beziehungen zwischen regulatorischen (Sub)Systemen eine bedeutende Rolle. Insbesondere die Erfassung und Quantifizierung der Kopplungsstärke und -richtung sind wesentliche Aspekte für ein detaillierteres Verständnis physiologischer Regulationsprozesse. Ziel dieser Arbeit war die Charakterisierung kurzfristiger unmittelbarer zentral-autonomer Kopplungspfade (top-to-bottom und bottom to top) durch die Kopplungsanalysen der Herzfrequenz, des systolischen Blutdrucks, der Atmung und zentraler Aktivität (EEG) bei schizophrenen Patienten und Gesunden. Dafür wurden in dieser Arbeit neue multivariate kausale und nicht-kausale, lineare und nicht-lineare Kopplungsanalyseverfahren (HRJSD, mHRJSD, NSTPDC) entwickelt, die in der Lage sind, die Kopplungsstärke und -richtung, sowie deterministische regulatorische Kopplungsmuster innerhalb des zentralen-autonomen Netzwerks zu quantifizieren und zu klassifizieren. Diese Kopplungsanalyseverfahren haben ihre eigenen Besonderheiten, die sie einzigartig machen, auch im Vergleich zu etablierten Kopplungsverfahren. Sie erweitern das Spektrum neuartiger Kopplungsansätze für die Biosignalanalyse und tragen auf ihre Weise zur Gewinnung detaillierter Informationen und damit zu einer verbesserten Diagnostik/Therapie bei. Die Hauptergebnisse dieser Arbeit zeigen signifikant schwächere nichtlineare zentral-kardiovaskuläre und zentral-kardiorespiratorische Kopplungswege und einen signifikant stärkeren linearen zentralen Informationsfluss in Richtung des Herzkreislaufsystems auf, sowie einen signifikant stärkeren linearen respiratorischen Informationsfluss in Richtung des zentralen Nervensystems in der Schizophrenie im Vergleich zu Gesunden. Die detaillierten Erkenntnisse darüber, wie die verschiedenen zentral-autonomen Netzwerke mit paranoider Schizophrenie assoziiert sind, können zu einem besseren Verständnis darüber führen, wie zentrale Aktivierung und autonome Reaktionen und/oder Aktivierung in physiologischen Netzwerken unter pathophysiologischen Bedingungen zusammenhängen.

Danksagung

An erster Stelle möchte ich mich bei meiner Familie bedanken, bei meinen lieben Eltern Dieter und Renate, die mir immer mit Rat und Tat zur Seite gestanden haben. Ohne deren unermüdliche Unterstützung wäre diese Dissertation nicht zustande gekommen. Meinen geliebten Söhnen, Arien und Aurel, danke ich für Ihre Liebe, Geduld und Ihr Vertrauen während der langen und manchmal doch anstrengenden Zeit.

Darüber hinaus möchte ich mich bei meinen Betreuern und Mentoren Prof. Dr.-Ing. Andreas Voß, Prof. Prof. Dr.-Ing. habil. Jens Haueisen, und Prof. Dr. Karl-Jürgen Bär für die tatkräftige und fachliche Unterstützung, sowie für die vielen zielführenden Diskussionen, Anregungen und die großartige Betreuung während der Arbeit erkenntlich zeigen. Sehr dankerfüllt bin ich darüber, dass ich Prof. Dr.-Ing. habil. Jens Haueisen und Prof. Dr.-Ing. Andreas Voß als meine Betreuer hatte. Ich konnte auf ihre hervorragende Unterstützung zählen, wann immer ich vor einer wissenschaftlichen Herausforderung stand. Sie haben mich bei wichtigen Schritten meiner wissenschaftlichen Laufbahn begleitet, und ich konnte von Ihrem breiten Spektrum an Fachwissen in Wissenschaft und Technik profitieren. Ich danke Ihnen beiden für das Begutachten meiner Veröffentlichungen und dieser Arbeit. Herrn Prof. Dr. Karl-Jürgen Bär danke ich für seine Unterstützung und medizinische Expertise, die es mir ermöglichte, meine Dissertation in Kooperation mit dem Universitätsklinikum Jena in der Klinik für Psychosomatische Medizin und Psychotherapie durchzuführen.

Ich danke auch meinem ehemaligen Kollegen und Freund aus der Arbeitsgruppe Biosignalverarbeitung Dipl.-Ing. Rico Schröder, der mir mit seinem Fachwissen bei der Lösung von Programmierproblemen, die während der Arbeit auftraten, geholfen hat. Die erfolgreiche, langjährige Zusammenarbeit mit ihm hat den Inhalt dieser Arbeit stark beeinflusst. Danken möchte ich auch Herrn Prof. Dr. Georg Seifert, der mich mit seinem sehr fundierten Fachwissen und Vertrauen in meine fachliche Kompetenz unterstützt hat.

Vor allem aber möchte ich meiner wunderbaren, geliebten Freundin Caro für ihre Liebe, Geduld und Motivation danken, deren liebevolle Art mir in den schwierigen Phasen dieser Arbeit immer wieder Kraft und Energie gegeben hat.

Mein herzlicher Dank gilt auch all jenen Menschen, die durch Ihre fachliche und persönliche Unterstützung zum Gelingen dieser Dissertation beigetragen haben. Ich spreche Ihnen meine tiefste Dankbarkeit, Wertschätzung und Achtung aus.

Abbreviations

ANS	Autonomic nervous system
AR	Autoregressive
BBI	Beat-to-beat intervals
BPV	Blood pressure variability
BRS	Baroreflex sensitivity
BWD	Bivariate word distribution
CAD	Cardiac autonomic dysfunction
CAN	Central-autonomic-network
CF	Coupling factor
CNS	Central nervous system
CVD	Cardiovascular disease
dACC	Dorsal anterior cingulate cortex
DSM	Dual sequence method
DTF	Directed transfer function
EEG	Electroencephalogram
FB	Feed-back
FD	Frequency domain
FF	Feed-forward
GC	Granger causality
HR	Heart rate
HRJSD	High resolution joint symbolic dynamics
HRV	Heart rate variability
JSD	Joint symbolic dynamics
LP	Level of predictability
MAR	Multivariate autoregressive
MDA	Multivariate dynamical adjustment
mHRJSD	Multivariate high resolution joint symbolic dynamics
MUI	Mutual information
NAARX	Nonlinear additive autoregressive
NAR	Nonlinear autoregressive
NARX	Nonlinear autoregressive exogenous
NF	Normalized factor
NIBP	Non-invasive blood pressure
NLD	Non-linear dynamics
pACC	Perigenual anterior cingulate cortex
PCC	Posterior cingulate cortex

PDC	Partial directed coherence
P_{EEG}	Mean power of EEG activity
PI	Predictability improvement
PSD	Power spectral density
pTE	Partial transfer entropy
RBF	Radial basis function
RESP	Respiratory frequency
RESPV	Respiratory variability
RSA	Respiratory sinus arrhythmia
SCT	Symbolic coupling traces
SP	Systolic blood pressure
STE	Symbolic transfer entropy
SYS	Systolic blood pressure
TD	Time domain
TE	Transfer entropy
VMPFC	Ventromedial prefrontal cortex

Contents

Chapter 1

1. Introduction

The following content was previously published in:

Schulz, S., Haueisen, J., Bär, K. J. & Voss, A. (2019) Altered Causal Coupling Pathways within the Central-Autonomic-Network in Patients Suffering from Schizophrenia. Entropy, 21(8), 733.

Schulz, S., Bolz, M., Bär, K. J. & Voss, A. (2016) Central- and autonomic nervous system coupling in schizophrenia. Philos Trans A Math Phys Eng Sci, 374(2067), 20150178.

1.1 Motivation

Schizophrenia is considered to be one of the most severe mental disorders in the world. Its health consequences are associated with higher cardiac mortality rates, an approximately 15 to 20-year shorter life expectancy, and up to triple the risk of attaining cardiovascular disease (CVD) compared to the general population, independent of age groups (Hennekens et al, 2005; Laursen et al, 2014; McGrath et al, 2008). Schizophrenia is characterized by a point prevalence of 4.5 per 1000 and a median lifetime risk of approximately 1%. Pharmacologic therapeutic strategies have revolutionized treatment options for schizophrenia over the past 50 years and have led to improvements in psychiatric treatment approaches. However, the disorder continues to be associated with a statistical reduction in life expectancy. A particular

cause for concern is that the mortality gap between the general population and schizophrenia patients seems to have increased during recent decades (Saha et al, 2007). Suicide and accidents account only partially for the excess mortality, while a substantial proportion is due to physical illness (Brown, 1997). The largest single cause of death in schizophrenia patients leading to an increased mortality rate is due to CVD, with CVD mortality ranging from 40 to 50% (Ringen et al, 2014). Causal factors for patients with this condition are still being discussed, and have not yet been fully clarified. However, possible complicating factors are related to lifestyle, the lack of physical activity, smoking, obesity, poor diet, substance abuse, diabetes, hypertension, the cardiac side effects of antipsychotics and the imbalanced autonomic nervous system (ANS) during acute psychosis (Hennekens et al, 2005; Ringen et al, 2014; Straus et al, 2004). Two important differences from other patient populations suffering from primary cardiac conditions (e.g. myocardial infarction, cardiomyopathy) and which present signs of cardiac autonomic dysfunction (CAD) need to be considered. The first difference is the fact that severe CAD is not initially caused by major structural or functional alterations of the heart in schizophrenia patients. Moreover, it seems to be associated with an altered brain–heart interaction influenced by a lack of cortical inhibitory control over sympatho-excitatory subcortical regions (Bär et al, 2007a; Schulz et al, 2019; Williams et al, 2004). The second difference to patient populations suffering from primary to cardiac conditions is caused by the relative "longevity" of patients with schizophrenia when compared to more frequent shorter survival rates of cardiac patients.

My own preliminary work and other studies clearly demonstrated that the regulation of the ANS is altered and impaired in schizophrenia, shown by analysing heart rate variability (HRV) (Bär et al, 2007b; Bär et al, 2005; Chang et al, 2009; Schulz et al, 2013c; Valkonen-Korhonen et al, 2003), respiratory variability (RESPV) (Bär et al, 2012; Peupelmann et al, 2009; Schulz et al, 2012a; Schulz et al, 2012b; Schulz et al, 2013b; 2014b), and cardiovascular- and cardiorespiratory couplings (Aguirre et al, 2018; Schulz et al, 2012a; Schulz et al, 2015a; Schulz et al, 2016; Schulz et al, 2017a; Schulz et al, 2019; Schulz et al, 2013b). The coupling between the variability of heart rate and respiration have been an illustrated inherent disease feature and hallmark of these studies. In addition, other studies have shown that structural and functional defects within the brain network are central features of schizophrenia (Castro et al, 2015; Kohler et al, 2019; Suttkus et al, 2021; Wagner et al, 2015). The cardiovascular and cardiorespiratory system and their subsystems (ANS) are linked to the central nervous system (CNS) (sophisticated interplay between ANS and CNS). Therefore, it can be assumed that this causes an interplay based on a feedback-feedforward system, supporting flexible and adaptive responses to environmental demands.

Different studies have indicated that people with reduced HRV, as seen in the case of schizophrenia, exhibit behavioural- and adaptive emotional responses on executive

cognitive tasks (Hansen et al, 2003; Ruiz-Padial et al, 2003). Thayer and Lane (2000) proposed the *neurovisceral integration model*, which suggests that neural networks implicated in emotional and cognitive self-regulation are also involved in the control of cardiac autonomic activity. Frontal, cingulate and subcortical brain regions have been hypothesized to play a critical role in such self-regulatory functions through top-down control from the frontal cortex over subcortical regions involved in reward and emotion, such as the amygdala (Heatherton & Wagner, 2011). A recent meta-analysis (Thayer et al, 2012) revealed that resting HRV is tied to the functioning of frontal-subcortical circuits. Higher resting HRV is associated with the effective functioning of frontal-top-down control over subcortical brain regions that support flexible and adaptive responses to environmental demands (Thayer & Lane, 2000). It is noteworthy that a disruption of frontal-subcortical circuits has been associated with a wide range of psychopathologies including schizophrenia (Callicott et al, 2003). Cognitive impairment is thus known to be a universal and core symptom of schizophrenia. This impairment critically influences treatment response, a patient's insight into their illness, their employment status, ability to communicate, social relationships and living status (Harvey et al, 1998). Cardiovascular adjustments due to a shift in central autonomic control and modulation of the heart are most prominent features of exercising (Brum et al, 2000; Negrao et al, 1993).

The complex interplay of the CNS and ANS with their large number of subsystems (parasympathetic and sympathetic activity) is also known as the central-autonomic-network (CAN) (Bartsch et al, 2015; Bashan et al, 2012; Ivanov et al, 2016). It has been shown, that the output of CAN is directly linked to ANS (heart rate) as well as that sensory information from peripheral end organs provide feedback to the CAN (i.e. baroreceptor reflex). The information transfer between the CNS and ANS is characterized as a feedback-feedforward system that responds to substantial demands of the body. The cerebral cortex in autonomic control of the cardiovascular system is gaining increased attention in medicine. Different cardiovascular control centres in the brainstem deal with different reflex mechanisms of cardiovascular adjustment (i.e. the cardiopulmonary reflex, the chemoreflex and the baroreflex) (Dampney, 1994). Here, neurons in the caudal and rostral ventrolateral medulla affecting efferent sympathetic reflexes, and contribute to the maintenance of heart rate and blood pressure via the intermediolateral cell column of the spinal cord. The two medullary areas, the nucleus ambiguous and the dorsal motor nucleus of the vagus nerve are preganglionic parasympathetic neurons mediating the efferent parasympathetic reflex mechanism (McAllen, 1976; Taylor et al, 2001).

The parasympathetic nervous system is responsible for “rest and digest” function, while sitting, resting and relaxing. It constricts the pupils, slows the heart rate and contractility, contracts the bronchial musculature and stimulates bronchial secretions, and enhances gut motility for digestion. The preganglionic neurons synapse onto

postganglionic neurons in the parasympathetic ganglion that are located next to, or in, the effector end organs. The sympathetic nervous system predominates during "fight-or-flight" reactions and during exercise and thus prepares the body for stressful physical activity. Sympathetic nervous activity increases the flow of blood that is well-oxygenated and rich in nutrients to the tissues that need it, in particular, the working skeletal muscles. The preganglionic sympathetic neurons arise from the thoracic and lumbar regions of the spinal cord (segments T1 through L2) and are located about halfway between the CNS and the effector tissue (McCorry, 2007). The preganglionic neurons of both the sympathetic and parasympathetic divisions release the neurotransmitter acetylcholine. The postganglionic neurons of the parasympathetic system also release acetylcholine, whereas, the postganglionic sympathetic neurons release norepinephrine (Rea, 2016). The cardiac or respiration-related activity (parasympathetic) is connected to preganglionic neurons. It has been shown, that brain regions like the insula, thalamus, hypothalamus, amygdala, and the medial prefrontal cortex are involved in the autonomic regulation at rest and during cognitive or emotional stress conditions proven by functional brain imaging (Shoemaker et al, 2015; Ziegler et al, 2009). Beissner et al. (Beissner et al, 2013) showed that largely divergent brain networks were associated with sympathetic and parasympathetic activity. The ventromedial prefrontal cortex (VMPFC), the perigenual anterior cingulate cortex (pACC), the dorsal anterior cingulate cortex (dACC), the posterior cingulate cortex (PCC), the insular cortices and amygdala seem to be the main cortical and subcortical areas involved in ANS regulation processes, that are created by a network of interactions related to task and autonomic division.

Schizophrenia and other psychopathological conditions i.e. anxiety, depression and post-traumatic stress disorder are linked with prefrontal hypoactivity and a lack of inhibitory neural processes denoted by poor affective information processing and regulation (Thayer & Friedman, 2004). For healthy adults, Beissner et al. (Beissner et al, 2013) suggested that asymmetric frontal EEG responses to emotional arousal in the form of positive and negative emotions may elicit different patterns of cardiovascular reactivity. Different studies using both pharmacological and neuroimaging approaches have provided the evidence that activity of the prefrontal cortex is associated with vagally-mediated HRV (Thayer, 2007). In sum, for schizophrenia it has been assumed that a vagal withdrawal and an over activation of the sympathetic branches of the ANS are present.

Investigating the coupling between these ANS subsystem with their variability and brain activity may lead to a better understanding of pathophysiological regulatory processes within the central-autonomic-network in those patients. For the quantitative analysis of the brain-heart (CNS-ANS) network coupling pathways and its integrated interacting subsystems as the cardiovascular and cardiorespiratory system several linear/non-linear univariate and multivariate approaches are

available. These approaches focus on characterizing the multivariate information transfer. These concepts (Bartsch et al, 2015; Faes et al, 2015; Ivanov et al, 2016; Schulz et al, 2013a) are applicable in the following domains: entropy, Granger causality; non-linear prediction; phase synchronization, symbolization, recurrence quantification analysis (RQA) and functional connectivity analysis techniques (Aguirre et al, 2018; Lombardi et al, 2019; Marwan et al, 2013). It has been demonstrated, that the information transfer between the cardiovascular and cardiorespiratory system acts strongly non-linear (Novak et al, 1993), and therefore linear approaches alone are not fully able to quantify physiological as well as pathophysiological regulatory processes. There is no generally superior approach capable of taking into account all aspects of coupling analysis (linearity, non-linearity, causality, multivariate analysis, directionality, coupling strength) and its quantitative evaluation. Some of these approaches include one or more of these aspects, but usually not to a sufficient extent, so that the time series with their mutual interactions and couplings can only be interpreted and analysed incompletely and only in parts. Furthermore, many of these approaches are not standardized, not user friendly (degrees of freedom, preconditions, model selection and model order estimation, scale dependency, …), and are based on purely mathematical concepts, making it difficult to select the "right" approach to apply them to quantify physiological as well as pathophysiological regulatory processes.

Therefore, a logical conclusion was to develop new coupling approaches for the following reasons: simple basic mathematical principles (e.g. symbolization) are easier to use, limitations of already established coupling approaches can be removed, approaches with new features that allow a more comprehensive understanding of the couplings to be analysed would be improved.

1.2 Objectives

This section outlines the main objectives of this thesis.

- The development of new multivariate coupling approaches to describe causal and non-causal relationships (coupling strength and direction) as well as to quantify and classify deterministic regulatory coupling patterns within and between the cardiovascular system, the cardiorespiratory system and the central-autonomic-network.

- The characterization of short-term instantaneous central-autonomic-network coupling pathways (top-to-bottom and bottom-to-top) by analysing the interaction between heart rate, systolic blood pressure, respiration and central activity in schizophrenia and healthy subjects.

- To contribute to the understanding of (patho)physiological regulatory processes of the central autonomic network in schizophrenia that could potentially lead to an improvement of treatment strategies in these patients, and finally, possibly contributing to cardiac risk stratification strategies able to identify schizophrenic patients at higher risk for cardiovascular disease at an early stage.

1.3 Structure of the thesis

This section outlines the structure of this thesis.

Chapter 2:

In chapter 2, the state of the art regarding coupling analyses is presented. Approaches such as Granger causality, non-linear prediction, entropy, symbolization, and phase synchronization most commonly applied to detect direct and indirect couplings between time series are described. In particular their usefulness for detecting linear and non-linear interdependencies, their theoretical background as well as their basic requirements/conditions for their application are shown.

Chapter 3:

Chapter 3 presents the new coupling analysis approaches for biomedical time series developed in this thesis.

In the first part of chapter 3, I introduce the high-resolution joint symbolic dynamics approach (HRJSD) based on a redundancy reduction strategy to group single word types into 8 pattern families, allowing a detailed quantification of bivariate short-term cardiovascular- and cardiorespiratory couplings which were due to changes of the different branches of autonomic regulation. In addition, a directionality index D_{HRJSD} is introduced and shown to be able to detect the dominating coupling direction in linear coupled systems.

In the second part of chapter 3, I introduced the multivariate high-resolution joint symbolic dynamics approach (mHRJSD) able to determine the driver-responder relationship in multivariate coupled systems, and overcoming limitations of the HRJSD. The mHRJSD approach contains multivariate directionality indices allowing to determine the primary driver, the secondary driver and the dominant responder in a multivariate system.

In the third part of chapter 3, I proposed the normalized short time partial directed coherence (NSTPDC) approach as an improvement of the standard partial directed coherence to overcome its restrictions, and to allow for a better classification of the coupling strength and direction in multivariate linear and non-linear coupled systems. The NSTPDC approach applies a normalization procedure enabling to analyse non-stationary and scale-invariant time series, a Normalized Factor (NF) enabling the characterization of the coupling direction, and distinguish between direct and indirect causal information transfer.

Chapter 4:

In chapter 4, the previously developed coupling analysis approaches are applied in application studies to analyse and quantify the central-autonomic-network in schizophrenia.

The study aims to characterise short-term instantaneous central-autonomic-network couplings by analysing the interaction of heart rate, systolic blood pressure, respiration and central activity in schizophrenic patients compared to healthy subjects. I applied the newly developed causal and non-causal linear and non-linear multivariate coupling approaches (HRJSD, mHRJSD, NSTPDC) that are able to quantify the coupling strength and direction within the central-autonomic-network.

Chapter 5:

Chapter 5 summarizes the results of this thesis in relation to the newly developed coupling analysis approaches and the analysis and quantification of the central-autonomic-network in schizophrenia.

The strengths and limitations of the newly proposed coupling approaches, and the detailed findings of the application studies in respect to central-autonomic-network pathways (the cardiovascular network, the cardiorespiratory network, the central-cardiovascular-network, and the central- cardiorespiratory-network) which are associated with schizophrenia are summarized.

Chapter 2

2. Coupling analyses of linear and non-linear systems

The following content was previously published in:

Schulz, S., Voss, A. Editors. Cardiovascular and cardiorespiratory coupling analysis—State of the art and future perspectives. Cardiovascular Oscillations (ESGCO), 2014 8th Conference of the European Study Group on; 25-28 May 2014 Trento: IEEE.

Schulz, S., Adochiei, F. C., Edu, I. R., Schroeder, R., Costin, H., Bar, K. J. & Voss, A. (2013a) Cardiovascular and cardiorespiratory coupling analyses: a review. Philos Trans A Math Phys Eng Sci, 371(1997), 20120191.

2.1 Introduction

The analysis of causal and non-causal relationships within and between dynamic systems has become more and more of interest in different fields of science e.g. economics, neuroscience, physics or physiology. Especially in the medical field, the understanding of driver-response relationships between regulatory systems and within subsystems is of growing interest. In particular, the detection and quantification of the strength and direction of couplings are two major aspects of investigations for a more detailed understanding of physiological regulatory

mechanisms (Porta & Faes, 2013). The cardiovascular and cardiorespiratory systems are characterised by a complex interplay of several linear and non-linear subsystems (Voss et al, 2009).

Interactions of these physiological subsystems within the cardiovascular system can be described as closed-loops with feedforward and feedback mechanisms. On the one hand, blood pressure changes detected by baroreceptors lead to changes in heart rate regulation through the arterial baroreflex control loop, and on the other hand, heart rate variations affect blood pressure via the Windkessel function (Cohen & Taylor, 2002). Interactions within the cardiorespiratory system are mainly reflected in the respiratory sinus arrhythmia (RSA), the rhythmic fluctuation of cardiac cycle intervals (RR-interval) in relation to respiration. RSA is commonly described as an alteration between inspiratory heart rate acceleration and expiratory heart rate deceleration under normal physiological conditions (Eckberg, 2003). Under these circumstances, two major mechanisms are discussed: the central influence of respiration on vagal cardiac motoneurons and the impact of respiration on intrathoracic pressure and stroke (Eckberg, 2003; 2009; Gilbey et al, 1984; Triedman & Saul, 1994).

In the field of cerebral activity, the concept of causality can be applied to better understand functional connectivity and neurophysiological brain processes. For example, a causal approach to the visual cortex would be able to separate the bottom-up processing of information in the visual system, which is related to perception and takes place from the areas of the sensory receptors to hierarchically higher areas, from the top-down processing, which is related to perception and flows in the opposite direction, so that lower areas are supplied with information about stored knowledge or expectations (Porta & Faes, 2013).

For the analyses of the cardiovascular, cardiorespiratory, and central regulatory networks as well as the quantification of their interactions, a variety of different methods have been proposed. Commonly applied linear approaches include cross correlation analysis in the time domain and cross-spectral power density or coherence analysis in the frequency domain, both are used to investigate the interrelationships between two time series. However, linear approaches might be insufficient to quantify non-linear structures and the complexity of physiological (sub)systems. Therefore, approaches from non-linear time series analysis seem to be more suited to capture complex interactions between time series. These approaches are partly based on the notion of Granger causality (GC), implying that if one time series has a causal influence on a second time series the knowledge of the past of the first time series is useful to predict future values of the second time series (Granger, 1969). In biomedical applications, evaluation of causality is commonly performed by looking for directional dependencies within a set of multiple time series measured in the

physiological system under investigation (Faes & Nollo, 2010). Here, causality is defined in terms of predictability and uses the directionality of time to determine a causal ordering of dependent time series incorporating both direct and indirect causal influences from one process to another. This definition can be applied to bivariate (two time series) and multivariate (more than two time series) analysis. In the case of multivariate analysis, it is possible to differentiate between direct coupling (from one time series to another) and indirect coupling (effects mediated by one or more other time series).

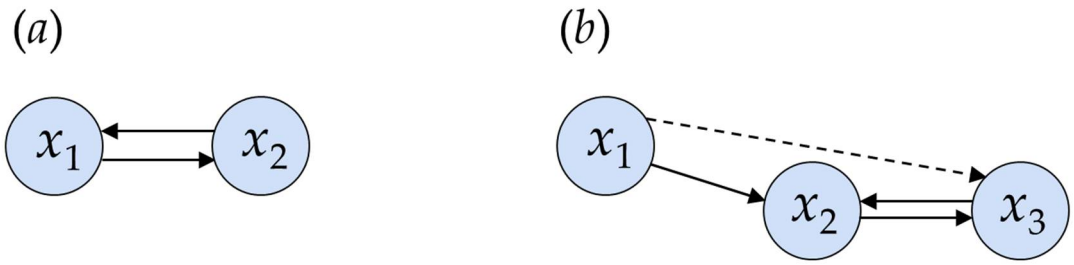

Figure 1. *Examples of directional dependencies for direct and indirect couplings. Interdependence structure for (a) a bivariate and (b) a multivariate case. (a) Direct coupling exists for $x_1 \leftrightarrow x_2$; (b) direct coupling exists for $x_1 \rightarrow x_2$ and $x_2 \leftrightarrow x_3$ and indirect coupling between $x_1 \rightarrow x_3$ mediated by x_2 (direction of coupling: $\rightarrow$,$\leftarrow$ unidirectional, $\leftrightarrow$ bidirectional).*

Direct coupling between two time series x_1 and x_2, exists if $x_1 \rightarrow x_2$ or $x_2 \rightarrow x_1$ (**Figure 1, *a***), whereas indirect coupling occurs when two time series x_1 and x_2 cause a third common time series x_3 mediated by one of the two time series, and also when both time series were caused by a third common time series mediated by one of the two time series x_1 or x_2 (direct coupling: $x_1 \rightarrow x_2$; $x_2 \leftrightarrow x_3$; indirect coupling: $x_1 \rightarrow x_3$ mediated by x_2) (**Figure 1**, ***b***). The coupling definitions generalise the causality definitions by accounting for both forward and backward interactions (Faes et al, 2012a).

In the following sections approaches as Granger causality, non-linear prediction, entropy, symbolization, and phase synchronization most commonly applied to detect direct and indirect couplings between time series are described. In particular their usefulness for detecting causal and non-causal linear and non-linear interdependencies, their theoretical background as well as their basic requirements/conditions for their application are shown.

2.2 Methods and applications

2.2.1 Granger causality

Wiener (Wiener, 1956) defined causality between two time series in a statistical framework by saying that: 'for two simultaneously measured time series, one series can be called causal to the other if we can better predict the second time series by incorporating knowledge of the first' (Kaminski et al, 2001) [p. 145]. Later, Granger adapted this concept to the context of stochastic processes in economics to analyse linear time series based on an autoregressive (AR) model. Today, this concept is known as GC. GC for two processes $X_1(t)$ and $X_2(t)$ is defined as: $X_1(t)$ has causal influence on $X_2(t)$; ($X_1(t) \rightarrow X_2(t)$) if the knowledge of the past of both $X_1(t)$ and $X_2(t)$ reduces the variance of the prediction error of $X_2(t)$ in comparison with the knowledge of the past of $X_2(t)$ alone (the past and the present cause the future but not vice versa) (Gourevitch et al, 2006; Granger, 1969). GC can be assessed by linear and non-linear approaches.

2.2.1.1 Linear Granger causality

Linear GC is based on parametric multivariate autoregressive (MAR) models and favouring the time- and frequency domain.

In the ***time domain*** the linear GC, *F*-test and the Wald-test and approaches based on predictability improvement and partial process decompositions became of importance.

Here, the prediction performance of two stochastic processes X_1 and X_2 can be assessed by comparing the uni- and bivariate AR models. For the univariate case two stationary processes X_1 and X_2 with their time series realisations $x_1(t)$ and $x_2(t)$ with t=1,…,T (T=duration of periods) can be considered which can be expressed as an AR representation (eq. 1, 2):

$$x_1(t) = \sum_{k=1}^{p} a_1(k)\, x_1(t-k) + \varepsilon_1(t) \quad (1)$$

$$x_2(t) = \sum_{k=1}^{p} a_2(k)\, x_2(t-k) + \varepsilon_2(t) \quad (2)$$

where $a_1(k)$ and $a_2(k)$ are the model parameters, p the AR model order and $\varepsilon_1(t)$ and $\varepsilon_2(t)$ are the residual noise and where the prediction error for a signal depends only on its own past values.

In the bivariate case the AR model in Granger's sense can be represented as (eq. 3, 4):

$$x_1(t) = \sum_{k=1}^{p} a_{1,1}(k)\, x_1(t-k) + \sum_{k=1}^{p} a_{1,2}(k)\, x_2(t-k) + \varepsilon_{1,2}(t) \quad (3)$$

$$x_2(t) = \sum_{k=1}^{p} a_{2,2}(k)\, x_2(t-k) + \sum_{k=1}^{p} a_{2,1}(k)\, x_1(t-k) + \varepsilon_{2,1}(t) \quad (4)$$

where the prediction error for a signal depends on the past values of the two signals. For the univariate and the bivariate AR models the prediction performance can be estimated by the variances of the prediction errors.

Geweke (Geweke, 1982) was the first to propose a linear bivariate time series approach assessing ***linear Granger causality (LGC)*** based on the prediction error variance of the time series associated with an statistical test for causality (Gourevitch et al, 2006). If process X_2 has no causal influence on process X_1 then $\mathrm{LGC}_{X_1 \to X_2}$ becomes close to zero which means that the knowledge of past values of X_2 does not improve the prediction of X_1 but if $\mathrm{LGC}_{X_2 \to X_1} > 0$, then a causal influence can be assumed. High values of $\mathrm{LGC}_{X_1 \to X_2}$ and $\mathrm{LGC}_{X_2 \to X_1}$ indicate a bidirectional coupling or a feedback relationship between the two time series (Pereda et al, 2005).

Bassani et al. (Bassani et al, 2012) estimated the direct causal coupling by applying two GC approaches (the ***F-test*** and the ***Wald-test***) along the baroreflex in two anaesthesiologic procedures. The advantages of conducting two GC tests are that:

- They need not assume that the cardiovascular control mechanisms occur along specific temporal scales as is the case with testing GC in the frequency domain;
- The percentage of false GC detections can be rigorously controlled by assigning the type I error probability accepted by the tests;
- The distribution of the statistics which assesses GC under the null hypothesis assuming no causal relationship between the two series follows a classical statistical distribution (in the case of the ***F*-test**: the ***F*** distribution, and for the ***Wald test***: χ^2 distribution), thus allowing the analytical calculation of the critical value above which the null hypothesis is rejected (Bassani et al, 2012).

These approaches are based on predictability improvement and were later extended to account for the effect of latent confounders such as respiration by Porta et al. (Porta et al, 2012a). To do this, an exogenous signal was added to the bivariate autoregressive closed-loop model to evaluate the bias induced on causality when the exogenous signal source was disregarded. In addition, Porta et al. (Porta et al, 2012b) proposed a ***multivariate dynamical adjustment (MDA) modelling approach*** (open loop: OLMDA, closed loop: CLMDA) to assess the strength of the baroreflex as well as of direct and indirect cardiopulmonary couplings in contrast to the two previously mentioned approaches (Bassani et al, 2012; Porta et al, 2012a), causal coupling was assessed using factorisation signals into partial process decompositions, thus allowing the assessment of both direct and indirect couplings. The coupling strength in the MDA class is estimated as the variance as indicated by the contribution of the partial process to the total variance.

GC approaches in the ***frequency domain*** were targeting the oscillatory nature of physiological variables and the peculiarity of specific control mechanisms of working in accordance to well defined time scales (Porta & Faes, 2013).

Here, an *m*-dimensional MAR process with order *p* is given (eq. 5):

$$\begin{bmatrix} x_1(t) \\ x_2(t) \\ . \\ . \\ . \\ x_m(t) \end{bmatrix} = \sum_{k=1}^{p} A_k \begin{bmatrix} x_1(t-k) \\ x_2(t-k) \\ . \\ . \\ . \\ x_m(t-k) \end{bmatrix} + \begin{bmatrix} \varepsilon_1(t) \\ \varepsilon_2(t) \\ . \\ . \\ . \\ \varepsilon_m(t) \end{bmatrix} \quad (5)$$

where ε_i is independent Gaussian white noise with the covariance matrix $\sum$, and $A_{1,\ldots,}A_p$ are the coefficient matrices ($m \times m$). This time domain representation can be transformed into the frequency domain calculating the joint spectral density matrix S(f) that is given by: $S(f) = H(f) \sum H^H(f)$ with $(.)^H$ as the Hermitian transpose and $H(f) = \bar{A}^{-1}(f) = [I - A(f)]^{-1}$ represents the transfer function matrix, I is the identity matrix, f denotes the frequency and $A(f) = \sum_{k=1}^{p} A(k) e^{-j2\pi fk}$ is the Fourier transform of the coefficients with $\bar{A}(f) = \bar{a}_1(f)\bar{a}_2(f) \ldots \bar{a}_m(f)$ where $\bar{A}_{ij}(f)$ is the i, jth element of $\bar{A}(f)$.

In the frequency domain the ***partial directed coherence (PDC)*** (Baccala & Sameshima, 2001a; b) and the ***directed transfer function (DTF)*** (Kaminski & Blinowska, 1991) and their enhanced versions (gPDC, ePDC, iPDC, tvPDC, NSTPDC, dDTF, SDFT) are the most applied approaches. These approaches are based on a fitted AR model and presuppose the stationarity of signals in the time interval under investigation (Hesse et al, 2003).

PDC is a parametric approach based on *m*-dimensional MAR processes with order *p*. It can detect direct and indirect causal information transfer since it measures exclusively direct effects between signals in multivariate dynamic systems. Based on the Fourier transformation of the coefficient matrix the PDC function quantifies the strength of the causal coupling from X_j to X_i as a function of frequency *f*. The PDC is normalised between 0 and 1, in that way the direct influence from process X_j to process X_i is inferred by PDC≠0 (PDC=0 when X_j does not cause X_i at frequency *f*, PDC=1 when all causal influences originating from X_j at frequency *f* are directed toward X_i (Baccala & Sameshima, 2001b; Faes & Nollo, 2010; Pereda et al, 2005). For PDC, a significance level was introduced to ensure reliable detection of the direct information flow (Schelter et al, 2006).

Faes et al. (Faes & Nollo, 2010) proposed the utilisation of an extended MAR model to investigate either instantaneous and lagged effects (ePDC) or lagged effects (iPDC) only. They showed that the presence of instantaneous correlations may produce misleading profiles of PDC, while ePDC and iPDC provided a correct interpretation

of extended and lagged causality, suggesting that ePDC and iPDC are more interpretable than PDC when applied to known cardiovascular and neuronal data. Milde et al. (Milde et al, 2011) introduced a time-variant version of PDC (tvPDC) for short-term multivariate data analysis which is based on a time-variant multivariate autoregressive model in combination with a Kalman filter for model parameter estimation. The Fourier transform of the AR parameters is used to define tvPDC. Milde et al. demonstrated that tvPDC avoids misinterpretations in HRV analyses and quantifies the partial correlative interaction properties between respiratory movements and RSA.

DTF enables the determination of directed causal interactions between two signals in relation to all other signals of the analysed system by applying on a MAR model using the transfer matrix to describe the causal information transfer (Kaminski & Blinowska, 1991; Korzeniewska et al, 2003). Moreover, DTF measures together both direct and indirect effects from one series to another and for this reason a differentiation between direct and indirect causal interactions or both is not possible, thereby leading to a greater number of interactions than are actually present (Winterhalder et al, 2006).

The DTF is normalised such that describes the ratio between the inflow from signal 2 to signal 1, to all the inflows of the activity to the destination signal 1. DFT takes values between 0 and 1 (DTF=1: most of the signal 1 consists of the signal 2; DTF=0: almost no flow from signal 2 to signal 1 at frequency f) (Kaminski & Blinowska, 1991; Korzeniewska et al, 2003).

The main differences and similarities between PDC and DTF are (Baccala & Sameshima, 2001a; b; Gourevitch et al, 2006; Pereda et al, 2005; Winterhalder et al, 2006):

- DTF uses the transfer matrix, PDC uses coefficient matrix;
- DTF cannot distinguish between direct or indirect causal information transfer, or both, whereas PDC can distinguish between both direct and indirect causal information transfer;
- PDC is more robust and efficient than DTF;
- PDC is normalised to the outflow of information (the structure that receives the signal) whereas DTF is normalised to the total inflow of the information (structure that sends the signal);
- DTF and PDC both depend on the reliability of the fitted MAR model (i.e., optimal model order, epoch length);
- A significance level has to be used for both to avoid spurious interactions;

- PDC and DTF can be sensitive in detecting interactions in non-linear multivariate systems under particular circumstances;
- DTF and time-varying PDC detect various types of time-varying influences (sensitive for time-resolved investigations of non-stationary data);
- In bivariate cases, both PDC and DTF are reduced to the causal coherence introduced by Porta et al. (Porta et al, 2002)

2.2.1.2 Non-linear Granger causality

Clive Granger mentioned that in practice it is usually not possible to use completely optimum predictors, unless all sets of series are assumed to be normally distributed, since such optimum predictors may be non-linear in complicated ways. It would seem obvious to simply use linear predictors and to accept the above definitions under this assumption of linearity (Granger, 1969). The most limiting factor for the assessment of non-linear GC is the choice of the model because it must be appropriately matched to the dynamics of the investigated biosignals. However, there are some promising approaches that can quantify causality in non-linear signals, such as methods based on non-linear global model identification and methods based on local linear models.

Methods based on non-linear global model identification were proposed by Faes et al. (Faes et al, 2008a) who introduced an approach for the detection of coupling as well as the causality between two time series, based on non-linear autoregressive (NAR) and non-linear autoregressive exogenous (NARX) models. This approach is more accurate and sensitive in detecting imposed GC conditions and was more accurate than the least squares methods based on the Akaike Information model order criterion. The main advantages are that it can be applied to short data records, only few parameters have to be defined and a more realistic physiological interpretation of the investigated system is possible. To assess GC by means of NARX models they examined the mean squared prediction error which ranges between 0 and 1, where 0 represents a fully predictable time series and 1 a fully unpredictable time series. Causality from y to x can be investigated by reversing the input-output roles of the two series and by calculating the absolute and normalised relative predictability improvement (PI) obtained by the NARX model compared to the NAR model prediction, what resulted from the inclusion of y samples in the prediction of x.

Another approach is introduced by Riedl et al. based on non-linear additive autoregressive (NAARX) models with external inputs fitted to bivariate time series for a model-based causal coupling analysis (Riedl et al, 2010). They showed, if the additional external input led to a significant reduction in the variance of the predicting error, then the external input could be said to have a causal influence on

the response variable. Here, the models are fitted separately to the time series and the different AR predictors as well as external ones are compared with each other with regard to the best prediction. Thus, the improvement of the prediction was measured by a cross-validation criterion, which is weighted by the cost of adding a new predictor or increasing the roughness of the estimated curve. This approach also allows the quantification of the strength and the morphology of the selected couplings. Therefore, the variance of the separate single step prediction of each external input is calculated and normalised by dividing by the variance of the response variable. The resulting values indicate the strength of coupling between various external inputs and the response (increased values=increased coupling).

Methods based on local linear models were proposed by Chen et al. (Chen et al, 2004), who introduced a conditional extended GC model using a spatial reconstruction of the joint dynamics of non-linear multivariate time series. This is associated with various delays and is able to determine whether the causal relation between two non-linear signals (x, y) is coupled directly or mediated by another process (Gourevitch et al, 2006). Here, the extended Granger causality index (EGCI) $\Delta_{y\to x}$ was introduced as a function of δ (neighbourhood size). If EGCI is less than 1, it implies that y (or x) has causal influence on x (or y). For linear systems, $\Delta_{y\to x}$ will stay roughly the same as δ becomes smaller, whereas for non-linear systems $\Delta_{y\to x}$ in the small δ limit, reveals the true non-linear causal relation which may or may not be captured at the full attractor level (Chen et al, 2004). In the multivariate case, a conditional extended GC index was additionally proposed to distinguish between direct and indirect causal relations.

Ancona et al. (Ancona et al, 2004) and Marinazzo et al. (Marinazzo et al, 2006) used a radial basis function (RBF) approach to assess non-linear GC in the context of predictability improvement between non-linear bivariate time series. This means that in the frame of a linear regression model, if the prediction error of the first time series is reduced by including values from the second time series, then the second time series is said to have a causal influence on the first time series. Ancona et al. (Ancona & Stramaglia, 2006) demonstrated that not all non-linear prediction approaches are suitable to evaluate GC between two time series, since they should be invariant if statistically independent variables are added to the set of input variables (unable to quantify how much knowledge of the other time series counts to improve prediction error). They stated that any prediction scheme providing a non-linear extension of GC should satisfy the following property: if Y is statistically independent of X and x, then $\varepsilon_x=\varepsilon_{xy}$; if X is statistically independent of Y and y, then $\varepsilon_y=\varepsilon_{yx}$ (x, y, X, Y=stochastic variables; ε_x=the prediction error when x is predicted solely on the basis of knowledge of its past values; similarly, for ε_y). Later, they introduced an approach to quantify non-linear *GC* based on kernel Hilbert spaces providing a statistically robust tool to assess driver-response relationships (Marinazzo et al, 2011; Marinazzo et al, 2008). This approach performs linear GC in the feature space of suitable kernel functions,

assuming an arbitrary degree of non-linearity and also fulfils the good properties of linear models in the non-linear case. The problem of overfitting the models was handled by exploiting the geometry of reproducing kernel Hilbert spaces. The kernel algorithms work by embedding data in a Hilbert space and searching for linear relations in that space (Hilbert spaces were spaces of kernel functions) (Marinazzo et al, 2011). The proposed approach has the following features:

- The non-linearity of the regression model can be controlled by choosing the kernel function;
- The problem of false causalities, which arises as the complexity of the model increases, is addressed by a selection strategy of the eigenvectors of a reduced Gram matrix;
- Reduction of unknown model parameters by considering a relatively small number of (possibly non-linear) mixtures of parameters, thus bounds model complexity and ensures that the accuracy of different models is a rough approximation to their evidence (Marinazzo et al, 2011).

2.2.2 Non-linear prediction

Non-linear prediction approaches are based on cross-prediction and are similar to those based on predictability improvement in their underlying methodological framework, but differ from predictability improvement in that they do not measure GC, but rather a causality concept which exploits asymmetry of cross-predictability when performed over the two possible directions of interaction between two series. Farmer and Sidorowich (Farmer & Sidorowich, 1987) were the first to introduce a concept of prediction, called the ***k-nearest neighbour prediction***, which was later integrated into different approaches.

Based on local linear prediction (the nearest neighbour local linear approximation (Farmer & Sidorowich, 1987) an extension of a non-linear bivariate prediction approach for the investigation of causal interdependencies between two time series (x, y) with a specific out-of-sample cross validation approach (to avoid overfitting) was introduced for short-term time series (Faes & Nollo, 2006). This method was based on the principle of the mutual prediction method, which provides a measure for the coupling strength and coupling directionality between two time series (Schiff et al, 1996). The bivariate prediction model is defined using knowledge of similar patterns in the first time series to predict the current values of a second time series. By exploiting the input and output series x and y, the relationship between a pattern of samples of x and a synchronous sample of y was approximated using a linear polynomial whose coefficients were estimated applying an equation system

including the nearest neighbour patterns in x and the corresponding samples in y. Finally, an index describing the level of predictability (LP) was defined (LP=1 when y is completely predictable given patterns of length L in x; LP=0 (also negative) when y is completely unpredictable in relation to x indicating the complete uncoupling. The advantage of this predictor is that it allows the possibility to obtain dependable estimates of predictability without constraining the embedding of the series when dealing with short-term time series as well as the predictor is less biased (overfitting) (Faes & Nollo, 2006).

In 2008 (Faes et al, 2008b) three different ***mutual non-linear prediction*** approaches (k-nearest neighbours) were compared: the cross prediction, the mixed prediction and the predictability improvement to test their ability to assess the coupling strength and directionality of the interactions in bivariate time series. Based on simulations and real physiological data (cardiovascular) it was found that cross prediction is valuable for quantifying the coupling strength and predictability improvement to determine the directionality of interactions in short and noisy bivariate time series. These approaches have the following properties:

- ***Cross-prediction*** quantifies interdependence in terms of the predictability of one of the two series estimated using state space vectors of the other series;
- ***Mixed-prediction*** quantifies interdependence in terms of the predictability of a series using state vectors that contain samples of both series;
- ***Predictability-improvement*** quantifies interdependence in terms of the increase in predictability yielded by mixed prediction compared to self-prediction (Faes et al, 2008b; Schiff et al, 1996).

2.2.3 Entropy

Methods based on entropies have in common that they analyse a putative information transfer between signals/time series. The concept of entropy addresses the uncertainty or predictability of signals. Greater entropy values reflect higher uncertainty and lower predictability. The concept of ***Shannon entropy (H)*** was introduced by Shannon in 1948 (Shannon, 1948) quantifying the information content within a time series. $H(x)$ (eq. 6) describes the statistical properties of a time series x (stationary) and represents a measure of uncertainty of a time series based on probabilities:

$$H(x) = -\sum_{i=1}^{M} p(x_i) log_2 p(x_i), \quad (6)$$

where $p(x_i)$ is the probability distribution of the ith bin of the time series x and M as the total number of all bins.

The concept of ***mutual information (MUI)*** (eq. 8) is based on the determination of the Shannon entropies H_x and H_y as well as the joint entropy H_{xy} (eq. 7)

$$H_{xy} = -\sum_{i,j=1}^{M} p(x_i, y_j)\, log_2\, p\,(x_i, y_j), \tag{7}$$

where $p(x_i)$ and $p(y_i)$ are probability distributions of x and y and $p(x_i,y_j)$ is the joint probability distribution of both time series:

$$\mathrm{MUI}_{xy}[\mathrm{bit}] = H_x + H_y - H_{xy} = \sum_{i,j=1}^{M} p(x_i, y_j)\log_2\left(\frac{p(x_i,y_j)}{p(x_i)p(y_j)}\right) \tag{8}$$

MUI analysis is applied to detect and quantify non-directional linear and non-linear interdependencies within one time series (univariate) or between different (bi- and multivariate) time series. MUI measures the information that x and y share in units called "bits" because of the application of $\log_2$ (Hoyer et al, 2005). Large values of MUI represent strongly dependent time series and low values indicate nearly independent ones (MUI=0, if x and y are completely independent). Moreover, MUI is symmetric ($\mathrm{MUI}_{xy}=\mathrm{MUI}_{yx}$), non-negative ($\mathrm{MUI}_{xy}\geq 0$) and bounded from above by $\min\{H_x,H_y\}$ (Cover & Thomas, 1991; Fraser & Swinney, 1986).

Porta et al. introduced the ***cross conditional entropy***, ***($CE_{x/y}$)*** based on the conditional entropy (CE) as a modification of the Shannon entropy. $CE_{x/y}$ quantifies the degree of coupling between two normalised time series (x, y) and represents a measure of the complexity of x with respect to y (Porta et al, 1999) with the pattern length L, the joint probability $p(y_{L-1})$ of the pattern $y_{L-1}(t)$ and the conditional probability $p(x(t)/y_{L-1})$ of the sample $x(t)$, given the pattern y_{L-1}. $CE_{x/y}$ is obtained in a process of sorting and counting mixed patterns. It describes the amount of information included in the sample $x(t)$ when the pattern of L-1 samples of $y_{L-1}(t)$ is given and measures causality (direct coupling) in analogy to the cross-prediction approaches whereby $y_{L-1}(t)$ is intended as the pattern formed by the past L-1 samples of y, i.e. $y_{L-1}(t)=y(t\text{-}1,\ldots,y(t\text{-}L+1))$. $CE_{x/y}$ has the following inherent properties:

- It is equal to zero when a sufficient number of samples of y allow complete prediction of x;
- It is high and constant if x and y are independent processes;
- It decreases toward a value between these extremes when the knowledge of y is useful to partially estimate x (Porta et al, 2000).

In addition, the synchronisation index: $\chi_{x,y} = 1 - \min\left(\overline{UF}_{x,y}\right)$ (with the uncoupling function $\overline{\mathrm{UF}}$) quantifying the maximum amount of information exchanged between the two time series (Porta et al, 1999). The larger the synchronisation index, the more coupled the two time series are.

Schreiber (Schreiber, 2000) proposed an information-theoretical approach named ***Transfer Entropy (TE)*** to distinguish between driving and responding elements and to detect asymmetries in the interaction and to quantify the extent to which the dynamics of one process influences the conditioned transition probabilities of another. TE measures GC with the prediction improvement approach and extends the concept of Shannon entropy by considering the probabilities of transitions rather than static probabilities. Generally, if no information flow from process Y to process X exists, then the state of Y has no influence on the transition probabilities on X. To analyse the dynamics of the shared information between the two processes, the deviation from the generalized Markov property is measured with its transition probabilities $p\left(x_{n+1}\middle|x_n^{(k)}\right) = p\left(x_{n+1}|x_n^{(k)}, y_n^{(l)}\right)$, where l is the conditioning state from process Y. The Kullback–Leibler divergence is used to measure the deviation from the generalized Markov property leading to TE (eq. 9):

$$\mathrm{TE}_{Y\to X} = \sum p(x_{n+1}, x_n^{(k)}, y_n^{(l)}) \log \frac{p\left(x_{n+1}|x_n^{(k)}, y_n^{(l)}\right)}{p\left(x_{n+1}\middle|x_n^{(k)}\right)}. \tag{9}$$

The most important feature of TE is that it is asymmetric under exchange of X and Y ($\mathrm{TE}_{X\to Y} \neq \mathrm{TE}_{Y\to X}$). The direction of coupling and information flow between coupled processes can be determined more adequately in comparison to MUI and CE (Kaiser & Schreiber, 2002; Verdes, 2005). The main advantage of TE is its "model-free" approach (Vakorin et al, 2009). A model-free causality statistic can be defined as the conditional mutual information between the past of one process and the future of another process, given the knowledge about the past of the latter. Moreover, it can be shown that, under proper conditions, TE is equivalent to the conditional mutual information (Vakorin et al, 2009). In addition, it must be noticed that conditional entropies are estimated directly from sampled probability distributions; results will vary with the estimation technique applied. Thus, a naive estimation of TE, e.g. by partitioning the state space is problematic and might fail to converge to the correct result. In practice, more sophisticated techniques such as kernel or *k*–nearest neighbour estimators will be needed (Barnett et al, 2009; Verdes, 2005). Furthermore, there are close similarities between TE and GC as entirely formal equivalence. This has been demonstrated in the case of Gaussian stochastic processes by Barnett et al. (Barnett et al, 2009), thus bridging autoregressive and information-theoretic approaches to data-driven causal inference. GC approaches are typically implemented within a framework of multivariate autoregressive models but imply many assumptions about how to model the data. Thus, the main problem of a parametric approach is the model misspecification. On the other hand, TE may present severe difficulties of empirical application, despite being theoretically ''model agnostic''.

Vakorin et al. (Vakorin et al, 2009) introduced the partial transfer entropy (pTE), a GC measure based on a multivariate version of TE which quantifies causality between two nodes of an interacting network. They found that pTE is a more sensitive technique for identifying robust causal relations than its bivariate equivalent and demonstrated the confounding effects of the variation in indirect coupling on the detectability of robust causal links. The TE approach was extended by Staniek et al. (Staniek & Lehnertz, 2008) by using a technique of symbolisation to estimate TE, called symbolic transfer entropy (STE). STE is a robust and computationally fast method to quantify the dominating direction of information flow between time series from structurally identical and non-identical coupled systems. Faes et al. (Faes et al, 2011a; 2012b) introduced an enhanced version based on the corrected CE and a sequential procedure for non-uniform embedding to assess non-linear GC in multivariate time series. This approach quantifies causality from one time series to another as the amount of information flowing directly from the first to the second time series, while accounting for the effects of all other time series in the multivariate representation, and separates direct and indirect causal effects.

Investigators have the choice to choose the most suitable approach for their data analysis. Numerical issues aside, analytical equivalence underlines the essential point that under Gaussian assumptions GC has a natural interpretation as TE and vice-versa (Barnett et al, 2009).

2.2.4 Symbolization

Methods based on symbolisation enable a coarse grain quantitative assessment of short-term dynamics of time series. The direct analysis of successive signal amplitudes is based on discrete states (symbols).

Joint Symbolic Dynamics (JSD) was introduced by Baumert et al. (Baumert et al, 2002) and is based on the analysis of bivariate dynamic processes by means of symbols (Voss et al, 1996). JSD considers short-term beat-to-beat changes, allowing the assessment of overall short-term cardiovascular and cardiorespiratory couplings. Therefore, a bivariate sample vector X (eq. 10) of two time series (x, y) is transformed into a bivariate symbol vector S (eq. 11) where n are beat-to-beat values.

$$X = \{[x_n, y_n]^T\}_{n=0,1,\dots} x \in R \quad \xrightarrow{transformation} \tag{10}$$

$$S = \{[s(x_n), s(y_n)]^T\}_{n=0,1,\dots} s \in 0,1 \tag{11}$$

For symbol transformation, a given alphabet A={0,1} was used, where symbol “1” represented increasing amplitude values and symbol "0” decreasing and unchanged amplitude values (JSD2). Afterwards, short patterns (words w) of symbol sequences

with a word length of three symbols were formed. For the quantification of JSD2 from each word type, the normalised joint probability $p(w_{i,j})$ of occurrence was estimated using an 8x8 word distribution density matrix W ranging from $(000,000)^T$ to $(111,111)^T$. In addition, from the matrix W, the probabilities of all single types' occurrences $p(w_{x,y})$, the sum of each column c_y, the sum of each row r_x and the Shannon entropy (eq. 12) as measure of the overall complexity and probability of occurrence of each column and each row can be computed

$$\mathrm{JSD}_{\mathrm{shannon}} = -\sum_{i,j=1}^{8}\left[p\left(w_{i.j}\right)\log_2 p\left(w_{i.j}\right)\right]. \tag{12}$$

The ***High Resolution Joint Symbolic Dynamics (HRJSD)*** represents an enhanced version of the classical JSD which is characterised by three symbols which are formed on the basis of a threshold ($l \neq 0$) and which clusters the coupling behaviour into 8-word type families (HRJSD) for the quantification of short-term couplings which arise from autonomic regulation. For the transformation of X into S new definitions were used (eq. 13, 14):

$$S_n^x = \begin{cases} 0\text{: } (X_{n+1}^x - X_n^x) < -l^x \\ \quad 1\text{: } -l^x \leq (X_{n+1}^x - X_n^x) \leq l^x \\ 2\text{: } (X_{n+1}^x - X_n^x) > l^x \end{cases} \tag{13}$$

$$S_n^y = \begin{cases} 0\text{: } (X_{n+1}^y - X_n^y) < -l^y \\ \quad 1\text{: } -l^y \leq (X_{n+1}^y - X_n^y) \leq l^y \\ 2\text{: } (X_{n+1}^y - X_n^y) > l^y \end{cases} \tag{14}$$

The thresholds l^x and l^y for the symbol transformation are:

- l^x and l^y equal 0 similar to JSD2,
- l^x=5ms and l^y=1mmHg (as for calculating baroreflex sensitivity with sequence techniques) (Bertinieri et al, 1988),
- l^x and l^y equal to 25% and 100% of the standard deviation of the time series as an adapted dynamical threshold to the individual variability.

Thus, HRJSD circumvented the problems encountered by JSD2 to distinguish between decreases and steady state as well as between small and large changes of autonomic regulation due to l=0 and A={0,1}. It is also impossible to differentiate between noise, artefacts (e.g. generated by undersampling or ectopic events) and fluctuations which arise from autonomic regulation. Both approaches have the main advantages that they are not sensitive to non-stationary time series and are capable to capture non-linear bivariate couplings by a simple procedure.

A further JSD extension, the ***symbolic coupling traces (SCT)*** was introduced by Wessel et al. (Wessel et al, 2011). SCT is based on the analysis of structural patterns and enables the detection of the direction (bidirectional) of time-delayed couplings in

short-term bivariate time series. Using the JSD2 algorithm two time series $x(t)$ and $y(t)$ were transformed into symbol sequences $s_x(t)$ and $s_y(t)$ also using the alphabet A={0,1} and afterwards series of word $w_x(t)$ and $w_y(t)$ of length l=3 were formed. In contrast to JSD2, a delay-time probability matrix $\Pi(\tau)=(p_{ij}(\tau))$ was estimated describing how word W_i would occur in w_x at time t and W_j would occur in w_y at time $(t+\tau)$ with p_{ij} as the joint probabilities of the words.

For the quantification of SCT only the symmetric and diametric traces of the bivariate word distribution (BWD) matrix were used, thereby excluding random effects and including only significant coupling information. Here, three indices can be calculated: The trace T of the matrix $\Pi(\tau)$ representing the fraction of both time series, which are structurally equivalent (symmetrical influences) to each other at lag τ. The trace $\bar{T}(\tau)$ describes the fraction of each signal, which is structurally diametric at lag τ (Suhrbier et al, 2010). Both parameters vary from 0 to 1 and comprise the diagonals of the BWD only. Finally, the difference $\Delta T = T - \bar{T}$ can be calculated to determine the exact detection of lags (delayed couplings) between two time series. The lags τ should be limited to $20 \leq \tau \leq 20$ (sampling units) in order to focus on short time-delayed dependencies only. The main advantages of SCT are its ability to detect delayed coupling (time lags), its applicability to moderately noisy time series (<10dB) and its insensitivity to non-stationarity.

2.2.5 Phase synchronization

Rosenblum et al. (Rosenblum et al, 2002; Rosenblum & Pikovsky, 2001) proposed an approach based on phase synchronisation, or the directionality index d, for the detection and quantification of coupling directions of weakly coupled self-sustained bivariate time series, even when the interaction between the two time series is too weak to induce synchronisation. The term "***phase synchronisation***" is used to denote the state when a relation only between the phases (Φ_1, Φ_2) of interacting signals sets in, but the amplitudes remain chaotic and nearly uncorrelated (Pikovsky et al, 2001). In contrast to the other proposed methods for examining signal amplitudes, this approach examines directly the oscillation phases. The idea behind this approach is that if a signal 1 is driven by signal 2, then the evolution of Φ_1 also depends on Φ_2; in other words, the prediction of Φ_1 from its previous values can be improved by taking into account the prehistory of Φ_2 only if signal 2 drives signal 1 (Rosenblum et al, 2002). This means that weak coupling affects the phases of interacting time series (oscillators) whereas the amplitudes of those oscillators remain practically unchanged and the dynamics of the interacting signals can be reduced to those of two phases, $\Phi_{1,2} = \omega_{1,2} + \varepsilon_{1,2} f_{1,2}(\Phi_{2,1}, \Phi_{1,2}) + \xi_{1,2}(t)$, where random terms $\xi_{1,2}$ describe the noisy perturbations, small parameters $\varepsilon_{1,2} \ll \omega_{1,2}$ characterise the strength of the coupling, functions $f_{1,2}$ are 2π periodic and $\omega_{1,2}$ are the natural frequencies of the two oscillators.

If the coupling is bidirectional, f_1 and f_2 depend on both f_1 and f_2. In case of unidirectional driving, say from signal 1 to signal 2, $f_1=f_1(\Phi_1)$ whereas $f_2=f_2(\Phi_1, \Phi_2)$ is the function of two arguments. Thereby, the condition of synchronisation for periodic oscillators can be generally written as a phase locking condition applied for any time t as (Pereda et al, 2005; Pikovsky et al, 2001; Rosenblum et al, 2001), $\varphi_{n,m}(t) = |n\Phi_1(t) - m\Phi_2(t)| \leq$ constant, where $\Phi_1(t)$ and $\Phi_2(t)$ are the phases of the signals associated with each system defined on the real line (unwrapped). Phase locking includes the constant phase shift and (small) fluctuations of the phase difference that means that the phases Φ_1 and Φ_2 are n:m locked if the inequality $|n\Phi_1(t)-m\Phi_2(t)|\leq$constant holds (Pikovsky et al, 2001). Rosenblum et al. (Rosenblum & Pikovsky, 2001) assumed that the two analysed signals are weakly coupled oscillators. The coupled signals are claimed to be in phase synchronisation when the difference of the instantaneous phases are bounded with respect to time (Sun et al, 2012). To detect phase synchronisation between two signals various methods to define the instantaneous phases have been proposed such as the Hilbert transform, the wavelet transform or specific filters applied to the signals (Sun et al, 2012). The main advantages of this approach are:

- Applicable to both noisy and chaotic time series;
- Determination of coupling direction (uni- or bidirectional);
- Quantification of the degree of asymmetry of bidirectional couplings;
- Posterior estimation of the coupling direction (Rosenblum & Pikovsky, 2001).

In the context of analysing instantaneous phases Paluš et al. (Palus & Stefanovska, 2003) introduced an approach based on the ***conditional mutual information*** method for the detection of the direction of coupling from phases of weakly coupled oscillators. This approach is able to distinguish between uni- or bidirectional couplings and to quantify the degree of asymmetry in bidirectional coupling. Here, bivariate time series $x(t)$ and $y(t)$ considered as two stationary ergodic stochastic processes $\{X(t)\}$ and $\{Y(t)\}$ which represent coupled systems were assumed. For the estimation of the directionality of coupling between $\{X(t)\}$ and $\{Y(t)\}$, the ''net'' information about the τ-future of the process (Broadley et al) contained in the process $\{Y\}$ applying the conditional mutual information $I(y;x_\tau|x)$ was used (Palus et al, 2001). Thereby, $\{X(t)\}$ and $\{Y(t)\}$ can be modelled by weakly coupled oscillators and their interactions can be inferred by analysing the dynamics of their instantaneous phases Φ_1 and Φ_2 which can be derived from $\{x(t)\}$ and $\{y(t)\}$. The mutual information $I(\Phi_1,\Phi_2)$ between the instantaneous phases Φ_1 and Φ_2 ($[0,2\pi]$ or $[-\pi,\pi]$) is used for the assessment of phase synchronisation between the two systems. Afterwards, phase increments $\Delta_\tau\Phi_{1,2}=\Phi_{1,2}(t+\tau)-\Phi_{1,2}(t)$ and the conditional mutual information $I(\Phi_1(t);\Delta_\tau\Phi_2|\Phi_2(t))$ and $I(\Phi_2(t);\Delta_\tau\Phi_1|\Phi_1(t))$ or $I(\Phi_1;\Delta_\tau\Phi_2|\Phi_2)$ and $I(\Phi_2;\Delta_\tau\Phi_1|\Phi_1)$ are

considered for causality relations. Finally, the directionality index D (eq. 15) is defined:

$$D(1,2) = \frac{i(1\rightarrow 2) - i(2\rightarrow 1)}{i(1\rightarrow 2) + i(2\rightarrow 1)}, \tag{15}$$

where the measure $i(1\rightarrow 2)$ of how system 1 drives system 2 is either equal to the conditional mutual information $I(\Phi_1;\Delta_\tau\Phi_2|\Phi_2)$ for a chosen time lag τ for equal to an average $I(\Phi_1;\Delta_\tau\Phi_2|\Phi_2)$ over a selected range of lags τ. The measure $i(2\rightarrow 1)$ is analogy defined using $I(\Phi_2;\Delta_\tau\Phi_1|\Phi_1)$. In the case of system 1 driving system 2 $D(1,2)>0$ holds and $D(1,2)<0$ for the opposite case (Palus & Stefanovska, 2003).

Schäfer et al. (Schäfer et al, 1998) used the concept of phase synchronisation of chaotic oscillators to analyse irregular non-stationary and noisy bivariate time series using the cardiorespiratory ***synchrogram***, to detect different synchronous states (n:m) and transitions between the two time series and to distinguish between different periods of synchronisation using their instantaneous phases.

Eckmann et al. introduced (Eckmann et al, 1987) the method of ***recurrence plots (RPs)*** to visualise the recurrences of a dynamical system in its phase space. Bivariate cross recurrence plots (CRPs) are the extensions of the RPs and can be used to analyse the non-linear dependencies between two different systems by comparing their states. CRP is essentially assumed as a generalisation of the linear cross-correlation function. To quantify CRPs, indices of complexity were introduced mainly based on diagonal structures in CRPs. CRP can find non-linear interrelations from bivariate time series, whereas linear correlation tests can't (Marwan & Kurths, 2002).

2.3 Summary

Linear and non-linear approaches quantifying direct or indirect couplings as well as the direction of these couplings (driver-response relationship) provide new insights into alterations of cardiovascular, cardiorespiratory, and central regulatory networks and lead to an improved knowledge of the interacting regulatory mechanisms under different physiological and pathophysiological conditions. One should consider that the application of these approaches cannot be restricted to a single favourable one. There exists no generally superior approach that can solve all problems. However, there are some important points to consider when applying these methods to time series analysis:

- The cardiovascular, cardiorespiratory, and central regulatory networks are complex physiological systems interacting in direct or indirect ways. For the investigation of these systems, bivariate approaches are commonly applied. However, it can be assumed that multivariate approaches will be increasingly used instead of bivariate ones since they improve the characterisation of causal or non-causal interrelationships.

- Cardiovascular, cardiorespiratory and central time series (e.g. from electrocardiogram (ECG), systolic- and diastolic blood pressure, blood flow, plethysmogram, respiratory frequency, respiration flow, electroencephalogram (EEG)) are often noisy and non-stationary or only quasi-stationary over short periods.

- The assessment of coupling and causality can be performed by applying either linear or non-linear time series analysis approaches. While non-linear methods study complex signal interactions, linear methods favour the frequency domain representation of biological signals (characterisation of connectivity between specific oscillatory components).

- The measurement data (time series) represent (patho)physiological processes only very incompletely and can only represent partial aspects.

- The method-specific characteristics used to differentiate between direct and indirect information flows and uni- and bidirectional couplings and to assess the coupling strength are not uniformly combined in one approach.

- PDC analyses are most frequently carried out between signals which are scaled on identical sizing systems (e.g. EEG on a microvolt scale). In contrast, respiration, heart rate and blood pressure amplitudes are scaled in different metric sizing systems. For such cases, it has been recommended to use the generalised PDC as a scale invariant interaction measure (Milde et al, 2011).

In particular, the PDC can take values arbitrarily close to either one or zero if the scale of the target variable is changed accordingly (Schelter et al, 2009).

- The application of time-variant multivariate analysis approaches (i.e. tvPDC) will contribute to an improved understanding of time-variant relationships of the cardiovascular and cardiorespiratory system (Adochiei et al, 2013; Milde et al, 2011).
- For the investigation of pathophysiological conditions, it has to be considered that these approaches are partly not validated since they were often applied either on experimental data, in healthy subjects or in patients with a specific pathophysiological condition. Representative studies are still missing.

Linear and non-linear coupling approaches might provide new insights into alterations of the cardiovascular, the cardiorespiratory and the central system and possibly will lead to an improved knowledge of the interacting regulatory mechanisms under different physiological and pathophysiological conditions. However, due to the large amount of these approaches it seems necessary to standardize these approaches, thus allowing us to select the "optimum" technique for each specific application. To make the application of coupling analyses more user friendly and more efficient the following issues should be solved or at least considered:

- Reduction of the degrees of freedom
- Reduction and standardization of preconditions
- Development of time-variant and multivariate analysis approaches
- Considering specific time delayed couplings (time lags)
- Considering scale independent couplings
- Method validation on larger sample sizes

Further on, such new coupling approaches represent promising tools for detecting information flows in a multivariate sense. They also might be able to provide additional prognostic information in the medical field and might overcome or at least complement other traditional univariate analysis techniques. The interest in coupling analyses of (patho)physiological networks has been growing considerably, and therefore, this will lead to an increasing amount of additional applications in the near future, improving the knowledge about interacting regulatory subsystems.

Chapter 3

3. Novel coupling analyses methods for biomedical time series

The following content was previously published in:

High Resolution Joint Symbolic Dynamics – HRJSD:

Schulz, S., Haueisen, J., Bär, K. J. & Andreas, V. (2015) High-resolution joint symbolic analysis to enhance classification of the cardiorespiratory system in patients with schizophrenia and their relatives. Philos Trans A Math Phys Eng Sci, 373(2034).

Schulz, S., Tupaika, N., Berger, S., Haueisen, J., Bär, K. J. & Voss, A. (2013) Cardiovascular coupling analysis with high-resolution joint symbolic dynamics in patients suffering from acute schizophrenia. Physiol Meas, 34(8), 883-901.

Multivariate High Resolution Joint Symbolic Dynamics – mHRJSD:

Schulz, S., Haueisen, J., Bär, K. J. & Voss, A. (2018) Multivariate assessment of the central-cardiorespiratory network structure in neuropathological disease. Physiol Meas, 39(7), 074004.

Schulz, S., Castro, M. R., Giraldo, B., Haueisen, J. & Voss, A. (2017) Multivariate high resolution joint symbolic dynamics (mHRJSD): a new tool to analyze couplings in physiological networks. Biomedical Engineering / Biomedizinische Technik.

Normalized Short Time Partial Directed Coherence – NSTPDC:

Schulz, S., Haueisen, J., Bär, K. J. & Voss, A. (2019) Altered Causal Coupling Pathways within the Central-Autonomic-Network in Patients Suffering from Schizophrenia. Entropy, 21(8), 733.

Schulz, S., Bär, K. J. & Voss, A. (2015) Analyses of Heart Rate, Respiration and Cardiorespiratory Coupling in Patients with Schizophrenia. Entropy, 17(2), 483-501.

Adochiei, F., Schulz, S., Edu, I., Costin, H. & Voss, A. (2013) A New Normalised Short Time PDC for Dynamic Coupling Analyses. Biomed Tech (Berl), 58 Suppl 1.

3.1 High Resolution Joint Symbolic Dynamics

3.1.1 Introduction

Over the last decades, knowledge of autonomic regulation has increased significantly through the investigation of HRV indices. Apart from linear HRV indices (time- and frequency domain), only a few published studies have applied non-linear dynamics (NLD) for short-term HRV analysis in patients with schizophrenia (Bär et al, 2007b; Chang et al, 2009; Kim et al, 2004; Mujica-Parodi et al, 2005). However, non-linear methods might help to reveal far more information about the dynamics and complexity of cardiovascular regulation and the involved subsystems of patients at higher cardiac risk, such as those with schizophrenia, as demonstrated in studies of heart failure patients (Voss et al, 2009). Interactions of these physiological subsystems within the cardiovascular system can be understood as closed-loops with feedforward and feedback mechanisms.

In addition to classical univariate indices from HRV in the time- and frequency domain, bivariate analysis of autonomic regulation, based on cardiovascular couplings of heart rate and systolic blood pressure time series can provide extra information (heart rate and blood pressure regulation pattern) about the complex cardiovascular system. Traditional bivariate techniques such as cross-correlation, cross-spectral power density analysis or baroreflex sensitivity (BRS) describe only linear dependencies of heart rate and systolic blood pressure. For coupling analysis, these approaches are partly inadequate for physiological data due to the linear as well as the non-linear interactions of the underlying control systems and the non-stationary behaviour and high complexity of these signals (Hoyer et al, 1998). Therefore, it seems to be desirable to apply suitable coupling analysis approaches that can identify and quantify non-linear interactions between heart rate and systolic blood pressure (Schulz et al, 2013a). The well-established joint symbolic dynamics method (JSD) (Baumert et al, 2002) allows a simplified coarse-grained quantification of the dynamics of heart rate and systolic blood pressure using two symbols. JSD has been successfully applied in HRV analysis in different approaches to interpret

physiological data and characterise the system's underlying dynamics (Baumert et al, 2002; Caminal et al, 2005; Voss et al, 2009).

Here, I introduce a new high resolution joint symbolic dynamics (HRJSD) that is based on 3 symbols and a symbol-transformation threshold which can be used to quantify short-term cardiovascular coupling. I further introduce and define pattern families that characterise different interaction aspects of the branches of autonomic regulation based on a redundancy reduction strategy. I hypothesise that HRJSD indices reveal alterations of complexity and cardiovascular coupling patterns in autonomic regulation more precisely and in more detail than the original JSD method. This might improve the understanding of physiological processes of cardiovascular coupling (e.g. feedforward and feedback mechanisms of changes in heart rate regulation through the arterial baroreflex control loop or heart rate variations affecting blood pressure via the Windkessel function) and could provide additional information about altered heart rate/systolic blood pressure coupling resulting from antipsychotic treatment (anti-cholinergic effects of antipsychotic drugs) of patients with acute schizophrenia. In particular, it can be hypothesised that the application of HRJSD will help to quantify and characterise how different antipsychotics influence autonomic modulation in different ways. This will allow prospective studies investigating medicated schizophrenic patients to predict how a specific antipsychotic will influence autonomic regulation (cardiovascular). In addition, HRJSD may help with the selection of an optimal treatment strategy (selection and doses of optimal antipsychotics to prevent affecting ANS modulation) and may contribute to the success of therapy.

3.1.2 Basics of Joint Symbolic Dynamics

The method of joint symbolic dynamics (JSD) was developed by Baumert (Baumert et al, 2002) to analyse non-linear couplings between systolic blood pressure (SP) and heart rate (BBI) time series and is based on the analysis of dynamic processes by means of symbols (Kurths et al, 1995). Therefore, both time series (BBI and SP, or respiration rate (RESP)) were transformed into symbol sequences. In X (eq. 16) as a bivariate sample vector, x^{BBI} and x^{SP} were n beat-to-beat values of BBI and SP, respectively.

$$X = \left\{[X_n^{\mathrm{BBI}}, X_n^{\mathrm{SP}}]^T\right\}_{n=0,1,\ldots} \tag{16}$$

$X \in R$ (R is the subset of real positive numbers)

Then X was transformed into a bivariate symbol vector S (eq. 17) defined as

$$S = \left\{[S_n^{\mathrm{BBI}}, S_n^{\mathrm{SP}}]^T\right\}_{n=0,1,\ldots} \tag{17}$$

$S \in R$ with the following definitions:

$$S_n^{\mathrm{BBI}} = \begin{cases} 0: \left(X_{n+1}^{\mathrm{BBI}} - X_n^{\mathrm{BBI}}\right) \leq l^{\mathrm{BBI}} \\ 1: \left(X_{n+1}^{\mathrm{BBI}} - X_n^{\mathrm{BBI}}\right) > l^{\mathrm{BBI}} \end{cases}$$

$$S_n^{\mathrm{SP}} = \begin{cases} 0: \left(X_{n+1}^{\mathrm{SP}} - X_n^{\mathrm{SP}}\right) \leq l^{\mathrm{SP}} \\ 1: \left(X_{n+1}^{\mathrm{SP}} - X_n^{\mathrm{SP}}\right) > l^{\mathrm{SP}} \end{cases}$$

In the JSD method, the threshold l was set to zero. Hence, increases between two successive BBI and SP, were respectively coded as "1" and consequently decreases and equilibriums were coded as "0". Afterwards, *S* was subdivided into short words (sequences of symbols) w_k of length *k*, where *k* was set to 3. The word types were integrated into an 8×8 vector matrix *W* ranging from $(000,000)^{\mathrm{T}}$ to $(111,111)^{\mathrm{T}}$. To compare the word distributions between time series of different lengths, the probability of occurrence of all word types was normalised to 1.

JSD allows a simplified quantification of the dynamics of BBI and SP using a limited number of symbols and has been successfully applied to HRV analysis (Voss et al, 1996; Voss et al, 2009). However, using a threshold l=0, some problems occur, including:

- The number of word types including decreases and equilibriums increase, because increases between two successive values which are not exceeding l were codes with "0". That is why the word types including the symbol "0" are the most pronounced ones within W especially the word type combination 000,000 is the most pronounced one.
- It is impossible to differentiate between decreases and steady states of autonomic regulation because both states are coded with the symbol "0". This limitation might further lead to misinterpretations of the findings regarding autonomic regulation. For example, the word type combination (000,000) might suggest a sympathetic activation in response to a decrease of blood pressure.
- It is impossible to distinguish between small and large changes in heart rate or blood pressure.

To differentiate between noise, artefacts (e.g. generated by undersampling or ectopic events) and fluctuations that arise from autonomic regulation, I inserted the threshold level $l \neq 0$. This led to a JSD with three symbols (HRJSD). For the transformation of *X* into *S*, new definitions were used (eq. 18, 19):

$$S_n^{\mathrm{BBI}} = \begin{cases} 0: \left(X_{n+1}^{\mathrm{BBI}} - X_n^{\mathrm{BBI}}\right) < -l^{\mathrm{BBI}} \\ 1: -l^{\mathrm{BBI}} \leq \left(X_{n+1}^{\mathrm{BBI}} - X_n^{\mathrm{BBI}}\right) \leq l^{\mathrm{BBI}} \\ 2: \left(X_{n+1}^{\mathrm{BBI}} - X_n^{\mathrm{BBI}}\right) > l^{\mathrm{BBI}} \end{cases} \quad (18)$$

$$S_n^{\mathrm{SP}} = \begin{cases} 0\text{: } (X_{n+1}^{\mathrm{SP}} - X_n^{\mathrm{SP}}) < -l^{\mathrm{SP}} \\ 1\text{: } -l^{\mathrm{SP}} \leq (X_{n+1}^{\mathrm{SP}} - X_n^{\mathrm{SP}}) \leq l^{\mathrm{SP}} \\ 2\text{: } (X_{n+1}^{\mathrm{SP}} - X_n^{\mathrm{SP}}) > l^{\mathrm{SP}} \end{cases} \quad (19)$$

Here, symbol sequences with increasing values were coded as "2", decreasing values were coded as "0" and unchanging (no variability) values were coded as "1". *S* was also subdivided into short words (bins) w_k of length k=3. The application of 3 symbols allowed me to differentiate between fluctuations of bradycardic and tachycardic origin. Furthermore, the influence of blood pressure regulation on heart rate was considered to be associated with the actual SP value X_n^{SP} and with the following BBI value X_{n+1}^{BBI} (one-beat delay (Fritsch et al, 1986)).

Using three symbols led to 27 different word types for BBI and SP time series (word types ranging from: 000, 001, …, 221, 222 (**Figure 2, *a***). The distribution of all single word types ($w_{i,j}$) was normalised by the total number of all word type combinations n=729 (27×27). The word types were sorted into a normalised 27×27 vector matrix W_n ranging from word type $(000{,}000)^{\mathrm{T}}$ to $(222{,}222)^{\mathrm{T}}$ (**Figure 2, *a***). To compare the word type distributions between time series of different lengths, the probability of occurrence $p(w_k)$ of all word types was normalised to 1.

3.1.3 Pattern families and threshold levels

However, the maximum length of words was restricted by the probability $p(w_k)$ (eq. 20) of occurrence of each word type and accordingly by the number of samples within the investigated time series. For a statistically sufficient representation of each single word type, the $\sqrt{N}$ approximation for the histogram construction of *N* observations was applied to estimate the maximum number of word types.

For example, for a short-term recording (here: 30 min) with a mean heart rate of 70 bpm, 3 symbols, word length=3, 729 word types ($3^3 * 3^3$) and a time series length *N* of 2100 beat-to-beat intervals, there are about 2.9 words in each bin.

$$p(w_k) = \frac{N-1}{\text{word types}} = \frac{2099}{3^3 * 3^3} = 2.88 \quad (20)$$

Thus, the accuracy of the word distribution is limited by having only a few words per bin. For a statistically sufficient representation, a heuristic basis of a minimum 20 words per bin would be required. (Voss et al, 1996). As a consequence, at least 3-h recordings (mean heart rate of 70 bpm, number of symbols=3, word length=3, word types=$3^3 * 3^3 = 729$) would be necessary to achieve a statistically sufficient representation of words per bin.

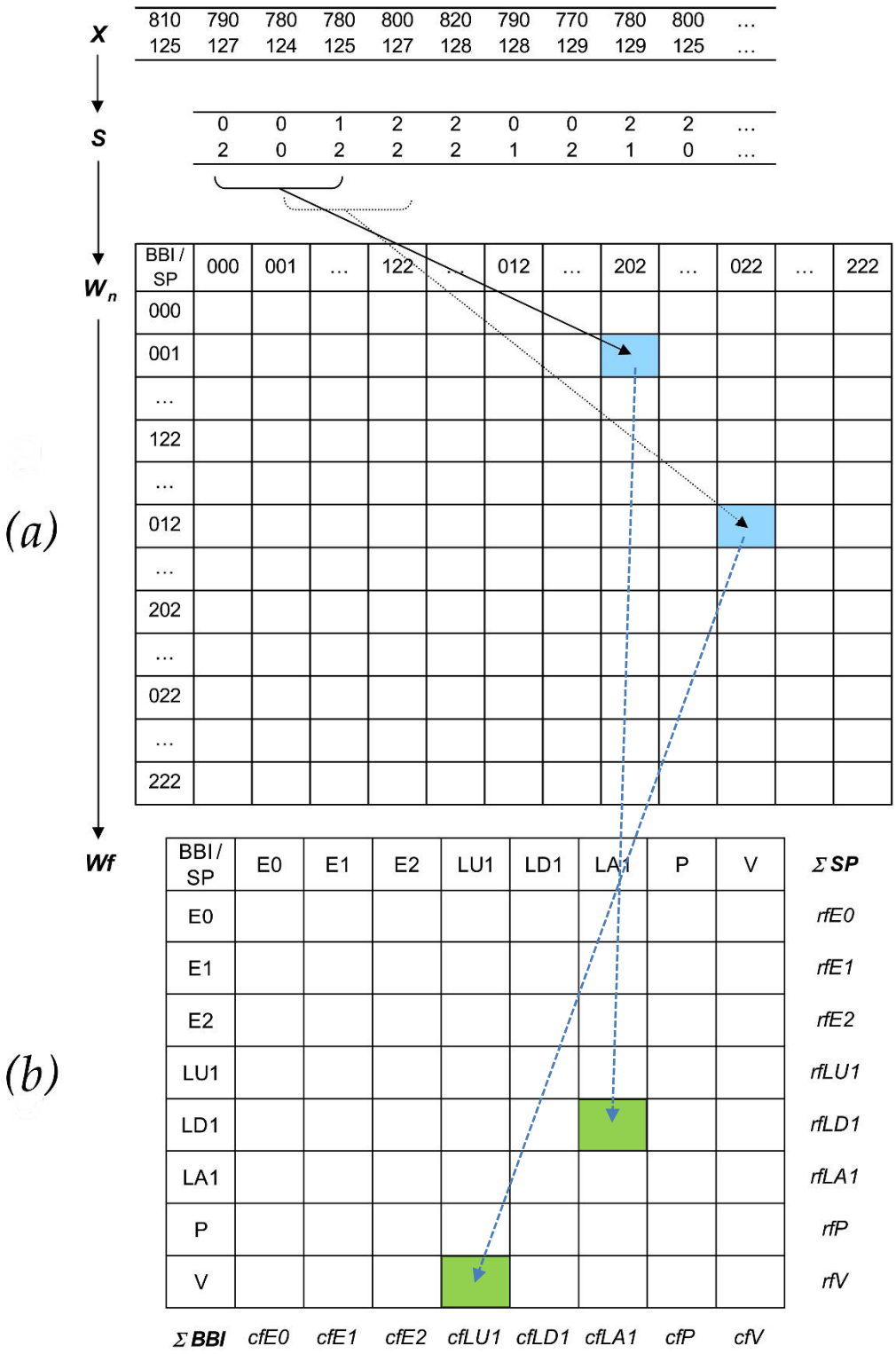

Figure 2. *Basic principle of HRJSD. (a) Transformation of the bivariate sample vector X (BBI=beat-to-beat intervals (msec); SP=systolic blood pressure (mmHg)) into the bivariate symbol vector S (0: decreasing values, 1: equal values 2: increasing values) and word distribution density matrix* W_n *(27×27). (b) Word pattern family distribution density matrix Wf (8×8) with eight pattern families wf created from 27 single word types* $w_{BBI,SP}$*. Rows represent pattern families of BBI intervals changes, column pattern families of SP changes,* rf_{BBI} *(row): sum of specific word family,* cf_{SP} *(column): sum of specific word family.*

To overcome this problem, all single word types $w_{BBI,SP}$ were grouped into 8 pattern families *wf*. The probabilities of all single word family's occurrences *p*(*wf*) (eq. 21) were normalised to 1.

$$p(wf) = \frac{N-1}{\text{word families}} = \frac{2099}{64} = 32.79 \tag{21}$$

These 8 pattern families (*E0*, *E1*, *E2*, *LU1*, *LD1*, *LA1*, *P*, *V*) represent different patterns of interactions between the branches of the autonomic regulation system (strong and weak tachycardic or bradycardic, nearly constant or alternating) (**Figure 3**) and were sorted into an 8x8 pattern family density matrix *Wf* (**Figure 2, *b***) resulting in 64 coupling patterns. The pattern definition (**Figure 3**, **Figure 4**) is as follows:

- ***E0***, ***E1*** and ***E2***: Words consisting of three equal symbols (no variation of symbols) of type '0', '1' and '2', respectively.
- ***LU1*** and ***LD1***: Words consisting of two different symbols with low increasing behaviour (LU1) and low decreasing behaviour (LD1).
- ***LA1***: Words consisting of two different alternating symbols of type '0' and '2' with an increasing-decreasing behaviour.
- ***P*** and ***V***: Words consisting of three different symbols with peak-like behaviour (P) and with valley-like behaviour (V) (Schulz et al, 2013c).

word family	details	effect on HR	RESP	P_{EEG}
E0	no variation within the word consisting of three symbols of type '0' (decreasing BBI, RESP & P_{EEG} behavior; '000')	↑	↓	↓
E1	no variation within the word consisting of three symbols of type '1' (unchanging BBI, RESP & P_{EEG} behavior; '111')	→	→	→
E2	no variation within the word consisting of three symbols of type '2' (increasing BBI, RESP & P_{EEG} behavior; '222')	↓	↑	↑
LU1	one variation within the word consisting of two different symbols with low increasing behavior of BBI, RESP & P_{EEG} ('122', '022', '112', '221', '220', '211', '121', '212')	↘	↗	↗
LD1	one variation within the word consisting of two different symbols with low decreasing behavior of BBI, RESP & P_{EEG} ('011', '001', '002', '110', '100', '200', '010', '101')	↗	↘	↘
LA1	one variation within the word consisting of two different alternating symbols of type '0' and '2' with an increasing-decreasing behavior of BBI, RESP & P_{EEG} ('020', '202')	↗↘	↘↗	↗↘
P	three variations within the word consisting of three different symbols with peak-like behavior of BBI, RESP & P_{EEG} ('120', '201', '210')	↘↗	↗↘	↗↘
V	three variations within the word consisting of three different symbols with valley-like behavior of BBI, RESP & P_{EEG} ('021', '102', '012')	↗↘	↘↗	↘↗

Figure 3. *Definition of 8 pattern families of HRJSD. (HR=heart rate, BBI=beat-to-beat intervals, RESP=respiratory frequency, P_{EEG}=mean power in the BBI-related EEG intervals).*

As an example, the pattern family *"E0"* from BBI time series is coupled with the 8 pattern families from SP as: *BBI-E0/SP-E0*, *BBI-E0/SP-E1*, *BBI-E0/SP-E2*, *BBI-E0/SP-LU1*, *BBI-E0/SP-LD1*, *BBI-E0/SP-LA1*, *BBI-E0/SP-P* and *BBI-E0/SP-V*. Thus, the pattern family "*E0*" (*BBI-E0/SP-E0*) contains word types that consist only of the "0" symbol. On one hand, this means that the BBI decreases over three values and which were therefore coded by "0" three times (represents an increase in mean heart rate over three values) whereas on the other hand, SP values decrease over three values.

In addition, from this matrix *Wf* the sum of each (*n*=8) column cf_{SP} (*cfE0, cfE1, cfE2, cfLU1, cfLD1, cfLA1, cfP, cfV*) (eq. 22) and the sum of each (*n*=8) row rf_{BBI} (*rfE0, rfE1, rfE2, rfLU1, rfLD1, rfLA1, rfP, rfV*) (eq. 23) were computed (**Figure 2, *b***) for each pattern family, resulting in 16 further HRJSD indices.

$$cf_{\mathrm{SP}} = \sum_{\mathrm{BBI}} Wf_{\mathrm{BBI,SP}} \tag{22}$$

$$cf_{\mathrm{BBI}} = \sum_{\mathrm{SP}} Wf_{\mathrm{BBI,SP}} \tag{23}$$

Furthermore, I calculated the Shannon entropy ($\mathrm{HRJSD}_{\mathrm{Shannon}}$) (eq. 24) within *Wf* as a measure of the overall complexity of cardiovascular coupling.

$$\mathrm{HRJSD}_{\mathrm{Shannon}} = -\sum_{i,j=1}^{8}\left[p\left(wf_{i.j}\right)\log_2 p\left(wf_{i.j}\right)\right] \tag{24}$$

To investigate the influence of the threshold *l* level on the density matrices W_n and *Wf* I applied different individual dynamic variability and cardiovascular (l^{BBI}, l^{SP}) and cardiorespiratory (l^{RESP}) physiological settings for the thresholds $l^{BBI,}$ l^{SP}, and l^{RESP} for symbol transformation as:

- l^{BBI}, l^{SP}, and l^{RESP} equal 0 (no threshold=***no_TH***), similar to JSD,
- l^{BBI}=5ms and l^{SP}=1mmHg (as for the non-invasive estimation of the spontaneous baroreflex sensitivity (***BRS_TH***) with the validated sequence technique) (Bertinieri et al, 1988; Laude et al, 2004),
- l^{BBI}, l^{SP}, and l^{RESP} equal to 25% and 100% of the standard deviation (***1/4sd_TH***, ***sd_TH***) of the BBI, SP and RESP time series as an adapted threshold to the individual physiological dynamic variability (**Figure 4**).

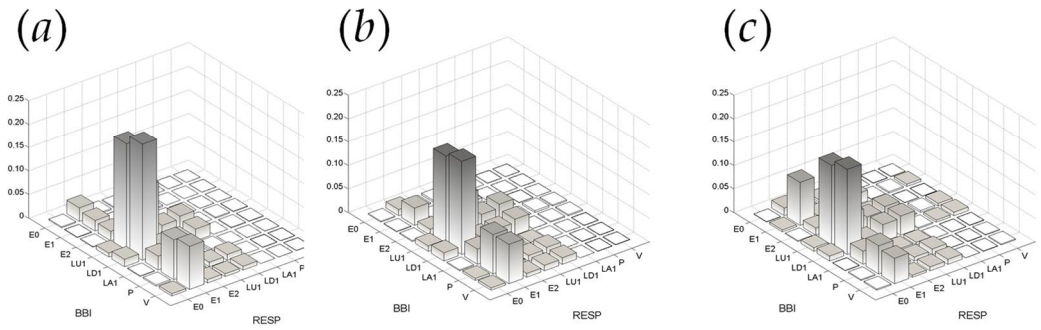

Figure 4. *Visualisation example of the three-dimensional plots of the HRJSD pattern family distribution density matrix Wf (8×8) for the threshold levels l^{BBI} equal to 5ms and l^{RESP} equal to 25% of the standard deviation of the RESP time series for healthy subjects (a), healthy first-degree relatives (b) and schizophrenic patients (c). (BBI=beat-to-beat intervals, RESP=respiratory frequency) (Schulz et al, 2015b)*

3.1.4 Directionality index

In order to evaluate physiological states of biological systems, which are highly complex, it is important and necessary not only to determine synchronization processes within coupled complex systems, but also to determine the predominant direction of their coupling. Therefore, various approaches are available for this purpose. The coupling direction can be determined, e.g. from the amplitudes of the system (properties of the system state) by calculating their mutual predictability (Schiff et al, 1996), from mutual nearest neighbours (Arnhold et al, 1999; Quiroga et al, 2000) in the reconstructed state space or by applying information theoretical approaches (Palus et al, 2001; Palus & Stefanovska, 2003; Schreiber, 2000).

In the field of symbolization there are so far no approaches available that determine the coupling direction neither for bivariate nor for multivariate systems. First attempts for this were integrated in SCT (Wessel et al, 2011). SCT are able to detect delayed couplings (time lags), but not able to assess the coupling direction as well as the driver-response relationships. To close this gap here, I introduced a **Directionality index** ($\boldsymbol{D}_{\mathrm{HRJSD}}$) derived from the 8×8 pattern family density matrix *Wf* from the HRJSD approach. This index is able to determine the dominant coupling direction and assesses the driver-response relationships in bivariate (n=2) and multivariate (n=3) systems (**Figure 1**, **Figure 5**).

For the **bivariate case** (x,y) the columns cf_x (n=8) and the rows rf_y (n=8) from the matrix Wf (**Figure 2**) were used to calculate $D_{HRJSD}(x,y)$ (eq. 25):

$$D_{\mathrm{HRJSD}}(x,y) = -\left(\sum_{i=1}^{n} \frac{cf_{\mathrm{x}}(i) - rf_{\mathrm{y}}(i)}{cf_{\mathrm{x}}(i) + rf_{\mathrm{y}}(i)}\right)/n \tag{25}$$

If $D_{HRJSD}(x,y)$ is positive driving (→) from system 1 (x) to system 2 (y) predominates (eq. 26) and becomes negative for the opposite case (eq. 27).

$$D_{\mathrm{HRJSD}}(x,y) > 0; \quad \boldsymbol{x} \rightarrow y \tag{26}$$

$$D_{\mathrm{HRJSD}}(x,y) < 0; \quad \boldsymbol{y} \rightarrow x \tag{27}$$

3.1.4.1 Simulated coupled linear and non-linear systems to validate D_{HRJSD}

Simulated data were used to validate D_{HRJSD}. Therefore, two different multivariate models were applied (Baccala & Sameshima, 2001b; Montalto et al, 2014), each with 100 simulated time series:

- Linear time series with a normal distribution of the variables, generated by a ***linear Gaussian AR model***, and
- Non-linear time series, generated by a ***non-linear Gaussian AR model***.

For the linear and the non-linear model three different multivariate coupled systems were generated with different mutual influences (unidirectional, bidirectional) between the time series (**Figure 5**).

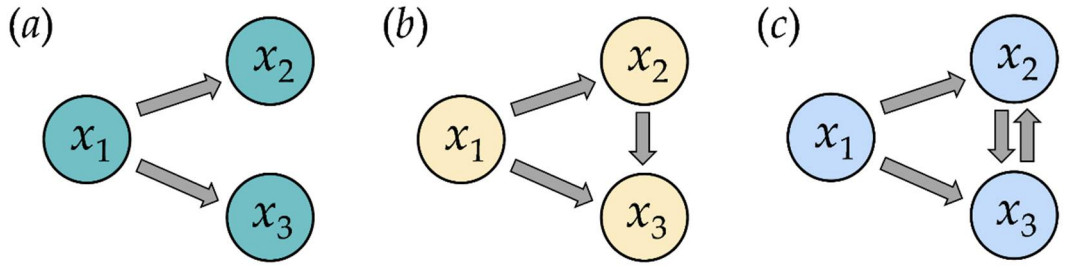

Figure 5. *Simulated multivariate systems with their mutual influence between the time series x_1, x_2, and x_3. Arrows indicating the causal coupling direction from one system to another (e.g. $x_1 \rightarrow x_2$ means a unidirectional driving from system 1 (x_1) to system 2 (x_2), and $x_2 \rightleftarrows x_3$ means a bidirectional driving between system 2 (x_2) to system 3 (x_3)).*

The following equations were used for the three linear Gaussian autoregressive models (Baccala & Sameshima, 2001b; Montalto et al, 2014) (eq. 28-30):

Linear system 1, LS1 (Figure 5, *a*):

$$\begin{aligned} x_1(n) &= 0.95\sqrt{2}x_1(n-1) - 0.9025x_1(n-2) + w_1(n) \\ x_2(n) &= -0.5x_1(n-1) + w_2(n) \\ x_3(n) &= 0.4x_1(n-2) + w_3(n) \end{aligned} \quad (28)$$

Linear system 2, LS2 (Figure 5, *b*):

$$\begin{aligned} x_1(n) &= 0.95\sqrt{2}x_1(n-1) - 0.9025x_1(n-2) + w_1(n) \\ x_2(n) &= 0.5x_1(n-2) + w_2(n) \\ x_3(n) &= -0.4x_1(n-3) - 0.2x_2(n-2) + w_3(n) \end{aligned} \quad (29)$$

Linear system 3, LS3 (Figure 5, *c*):

$$\begin{aligned} x_1(n) &= 0.95\sqrt{2}x_1(n-1) - 0.9025x_1(n-2) + w_1(n) \\ x_2(n) &= 0.5x_1(n-2) + 0.4x_3(n-1) + w_2(n) \\ x_3(n) &= -0.4x_1(n-3) - 0.2x_2(n-2) + w_3(n) \end{aligned} \quad (30)$$

where $w_1(n)$, $w_2(n)$, and $w_3(n)$ were drawn from Gaussian noise with zero mean and unit variance. For the linear system 3, a closed-loop from $x_3(n)$ back to $x_2(n)$ via a direct connection was integrated, with x_3 as the predominant driver.

For the non-linear models (Montalto et al, 2014) (eq. 31-33), $x_2(n)$ was modified by a quadratic term of x_1^2. Thus, the three linear model equations changed to:

Non-linear system 1, NLS1 (Figure 5, *a*):

$$\begin{aligned} x_1(n) &= 0.95\sqrt{2}x_1(n-1) - 0.9025x_1(n-2) + w_1(n) \\ x_2(n) &= -0.5x_1^2(n-1) + w_2(n) \\ x_3(n) &= 0.4x_1(n-2) + w_3(n) \end{aligned} \quad (31)$$

Non-linear system 2, NLS2 (Figure 5, *b*):

$$\begin{aligned} x_1(n) &= 0.95\sqrt{2}x_1(n-1) - 0.9025x_1(n-2) + w_1(n) \\ x_2(n) &= 0.5x_1^2(n-2) + w_2(n) \\ x_3(n) &= -0.4x_1(n-3) - 0.2x_2(n-2) + w_3(n) \end{aligned} \quad (32)$$

Non-linear system 3, NLS3 (Figure 5, *c*):

$$\begin{aligned} x_1(n) &= 0.95\sqrt{2}x_1(n-1) - 0.9025x_1(n-2) + w_1(n) \\ x_2(n) &= 0.5x_1^2(n-2) + 0.5x_3(n-1) + w_2(n) \\ x_3(n) &= -0.4x_1(n-3) - 0.2x_2(n-2) + w_3(n) \end{aligned} \quad (33)$$

where $w_1(n)$, $w_2(n)$, and $w_3(n)$ were drawn from Gaussian noise with zero mean and unit variance. For non-linear system 3, a closed-loop from $x_2(n)$ back to $x_3(n)$ via a direct connection was integrated, with x_2 as the predominant driver.

3.1.4.2 Results of simulated systems to validate D_{HRJSD}

The results of the simulated linear and non-linear AR systems were validated with two further methods, the normalized short-time partial directed coherence (NSTPDC) (Adochiei et al, 2013) and the Multivariate Transfer Entropy (MuTE) (Montalto et al, 2014). Both methods allow to determine the coupling direction. NSTPDC mainly detects linear coupling, whereas MuTE mainly detects non-linear coupling. In short, NSTPDC is based on a m-dimensional AR model with the order p and allows determining linear Granger causality in the frequency domain, and MuTE is an information-theoretical approach detects the information transfer between multivariate joint processes and discovers purely non-linear interactions with a range of interaction delays.

All three methods, the HRJSD, NSTPDC and MuTE calculated a directionality index D (D_{HRJSD}, D_{NSTPDC}, D_{MuTE}). These three indices have in common, that if the index is positive, driving (→) from system 1 (x) to system 2 (y) predominates, and become negative for the opposite case that system 2 (y) is driving system 1 (x).

Linear system 1 (Table 1):

1→2 and **1**→3: D_{HRJSD}, D_{NSTPDC}, D_{MuTE} are positive; correct classification of the predominating coupling directions (1 is driver).

Linear system 2:

1→2, **1**→3, **2**→3: D_{HRJSD}, D_{NSTPDC}, D_{MuTE} are positive; correct classification of the predominating coupling directions (1 and 2 are drivers).

Linear system 3:

1→2, **1**→3: D_{HRJSD}, D_{NSTPDC}, D_{MuTE} are positive; correct classification of the predominating coupling directions (1 is driver).

2⇄**3**: D_{HRJSD}, D_{NSTPDC}, D_{MuTE} are negative; correct classification of the predominating coupling direction (3 is driver).

For the linear AR model with purely linear couplings among the three variables (1, 2, 3) all directionality indices (D_{HRJSD}, D_{NSTPDC}, D_{MuTE}) were able to correctly detect the predominating coupling directions and the related driver variable.

Table 1. *Results of simulated linear and non-linear AR systems to validate the directionality index D_{HRJSD}. (blue: driver variable)*

Simulated driver-response relationship	Coupling	AR model	Directionality index		
			D_{HRJSD}	D_{NSTPDC}	D_{MuTE}
1→2	linear	linear	0.013	2.0	1.0
1→3	linear	linear	0.052	2.0	1.0
1→2	linear	linear	0.012	2.0	1.0
1→3	linear	linear	0.028	2.0	1.0
2→3	linear	linear	0.012	1.8	0.7
1→2	linear	linear	0.011	2.0	1.0
1→3	linear	linear	0.012	2.0	1.0
2⇄3	linear	linear	-0.011	-0.5	-0.6
1→2	non-linear	non-linear	-0.037	1.0	1.0
1→3	linear	non-linear	0.106	2.0	1.0
1→2	non-linear	non-linear	-0.036	1.4	1.0
1→3	non-linear	non-linear	-0.019	2.0	1.0
2→3	non-linear	non-linear	-0.010	2.0	1.0
1→2	non-linear	non-linear	-0.030	1.5	1.0
1→3	non-linear	non-linear	-0.015	2.0	1.0
2⇄3	non-linear	non-linear	-0.002	1.5	0.8

Non-linear system 1 (Table 1):

1→2: D_{NSTPDC} and D_{MuTE} are positive; correct classification of the predominating coupling direction (1 is driver).

D_{HRJSD} is negative; incorrect classification of the predominating coupling direction. D_{HRJSD} detects variable 2 as the driver.

1→3: D_{HRJSD}, D_{NSTPDC}, D_{MuTE} are positive; correct classification of the predominating coupling direction (1 is driver).

Non-linear system 2:

1→2, 1→3, 2→3: D_{NSTPDC} and D_{MuTE} are positive; correct classification of the predominating coupling directions (1 and 2 are drivers).

D_{HRJSD} is negative; incorrect classification of the predominating coupling directions. D_{HRJSD} detects variables 2 and 3 as the drivers.

Non-linear system 3:

1→2, **1**→3, **2**⇄3: D_{NSTPDC} and D_{MuTE} are negative; correct classification of the predominating coupling directions (1 and 2 are drivers).

D_{HRJSD} is negative; incorrect classification of the predominating coupling directions. D_{HRJSD} detects variables 2 and 3 as the drivers.

For the non-linear AR model with purely non-linear couplings among the three variables (1, 2, 3) only NSTPDC and MuTE were able to correctly detect the predominating coupling directions and the related driver variable. D_{HRJSD} was partly able to detect the dominating coupling direction in non-linear systems (non-linear system 1). Due to this limitation, in detailed investigations to determine the coupling direction, other methods should be used in addition to D_{HRJSD} (e.g. MuTe), which can also correctly determine the dominant driver-response relationships in pure non-linear systems.

3.1.5 Evaluation of pattern families and threshold levels

To evaluate and validate the pattern families and the threshold levels real patient data of a clinical study were investigated. Therefore, a high-resolution short-term ECG (1000 Hz sampling frequency) and synchronised non-invasive blood pressure (NIBP, 500 Hz sampling frequency) were recorded over 30 minutes with the Task Force Monitor® (CNSystems, Graz, Austria). From the raw data recordings, time series of heart rate consisting of successive beat-to-beat intervals (BBI) and systolic blood pressure values (SP) were extracted automatically using in-house software (programming environment Delphi 3). Afterwards, all time series were adaptively filtered to exclude artefacts and ventricular premature beats (interpolation) using in-house software. Thus, a normal-to-normal beat time series (NN) was obtained.

In this clinical study BBI and SP time series of 42 unmedicated (UNMED: 34.9±13.0 years, 18 female) and 42 medicated patients (MED: 35.1±12.7 years, 18 female) suffering from acute schizophrenia were analysed. This study complied with the Declaration of Helsinki. All participants gave written informed consent to a protocol approved by the Ethics Committee of the University Hospital, Jena. Patients were advised that the refusal of participating in this study would not affect future treatment. For the statistical evaluation of the results, the nonparametric Wilcoxon signed rank test was applied to determine differences between UNMED and MED. Significance values $p<0.05$ were considered statistically significant (highly significant $p<0.01$). Descriptive statistics were used to describe basic features of data in terms of mean value (*MW*) and standard deviation (*SD*).

3.1.6 Surrogate data

The surrogate data approach (Schreiber & Schmitz, 2000; Theiler et al, 1992) was applied to test the significance and the non-linear nature of the cardiovascular couplings between BBI and SP from HRJSD analysis. Therefore, two types of surrogate data were created:

I) Uncoupled isospectral isodistribution pairs (sI) from the original heart rate and systolic blood pressure time series to preserve linear properties to test for coupling. These surrogate data have the same frequency distribution and power spectra as the original pairs of signals, but were completely uncoupled.

II) Isospectral isodistribution pairs (sII) from the original heart rate and systolic blood pressure time series preserving cross-correlation to test non-linearity of the couplings. These surrogate data preserved the individual BBI and SP spectra as well as the magnitude of their cross-spectrum, obtained by adding the same random number to the Fourier phases of the two series. Thus, the linear coupling was maintained, whereas non-linear interactions were destroyed (Nollo et al, 2002).

Fifteen independent surrogate time series of type I and II were derived from the original time series from each of the unmedicated and medicated schizophrenic patients (UNMED_sI, UNMED_sII, MED_sI, MED_sII). As a consequence, each HRJSD index was calculated from the surrogate time series sets. In addition, it was determined the extent to which different threshold levels l for HRJSD analysis influence cardiovascular couplings of surrogate data. The nonparametric Wilcoxon signed rank test (paired data) was applied to determine differences between UNMED_sI vs. MED_sI and UNMED_sII vs. MED_sII. Differences were considered statistically significant at $p<0.05$.

3.1.7 Results of High Resolution Joint Symbolic Dynamics

3.1.7.1 The influence of different threshold levels on word type probabilities

The application of different settings for the thresholds l^{BBI} and l^{SP} (*no_TH*, *BRS_TH*, *1/4sd_TH*, *sd_TH*) led to a number of significant HRJSD indices (**Table 2**). When only considering HRJSD indices with a significance of less than $p<0.05$, I found that all four threshold settings showed significant differences between UNMED and MED. After a correction of the significance level shifted to $p<0.01$, the threshold level, which is based on baroreflex sensitivity (*BRS_TH*) estimation and the threshold level 25% of the standard deviation (*1/4sd_TH*, *sd_TH*) of the BBI- and SP time series were the most effective ones quantifying the anti-cholinergic effects of drugs and the related specific cardiovascular coupling patterns in MED. As expected, different definitions of

thresholds led to different word type probabilities for MED (the same behaviour was obtained for UNMED) within the density matrix W_n (**Figure 6**).

Table 2. *The influence of different threshold settings on the occurrence of significant word types for quantifying the anti-cholinergic effects of the antipsychotic drugs in medicated schizophrenic patients (MED) in comparison to unmedicated schizophrenic patients (UNMED). (TH=threshold, no=0, BRS=baroreflex sensitivity, 1/4sd=25% standard deviation, sd=100% standard deviation, p=significance level)*

HRJSD thresholds	**number of HRJSD indices**	
	***p*<0.05**	***p*<0.01**
no_TH	5	-
BRS_TH	49	9
1/4sd_TH	28	6
sd_TH	22	5

In (**Figure 6, *a***) (no threshold), various word types from BBI and SP show both lower and higher probability of occurrence. However, the most dominant word type was the combination of both (000,000). Furthermore, some clusters (increased number of similar word types with higher probabilities of occurrence) were found within the word distribution density matrix W_n. A cluster can be understood as those word types within W_n which describe nearly the same type of coupling (e.g. increasing, decreasing, alternating or unchanging (invariable) cardiovascular regulation behaviour), reveal a higher probability of occurrence within W_n and were concentrated side by side (forming a cluster). In this case, the clusters were mainly characterised by combinations of the symbols '0' and '2' for both BBI and SP, representing increasing, decreasing or alternating behaviour of these time series. The symbol '1' (unchanged) revealed a lower probability of occurrence. Regarding the threshold based on baroreflex sensitivity (**Figure 6, *b***) the word type (111) from SP was the most represented, independent of all other BBI word types whereas all other word type combinations were mainly uniformly distributed within W_n.

The application of the individually adapted threshold level *l=1/4sd* (**Figure 6**, ***c***) showed that the word type combination (111,111) became the most frequent one within W_n and was mainly the SP word type (111). This word type revealed a higher probability of occurrence and was independent of all other BBI word types. All other combinations of SP and BBI word types were mainly uniformly distributed within W_n. This higher probability of occurrence (~70%) of word type combination (111,111) was intensified by applying the threshold level *l=sd* (**Figure 6, *d***). Here, the word type (111) with respect to both SP and BBI was the most frequent whereas other word types

revealed a lower probability of occurrence or were even entirely absent. Furthermore, the word type (111) of SP was nearly independent of all other BBI word types.

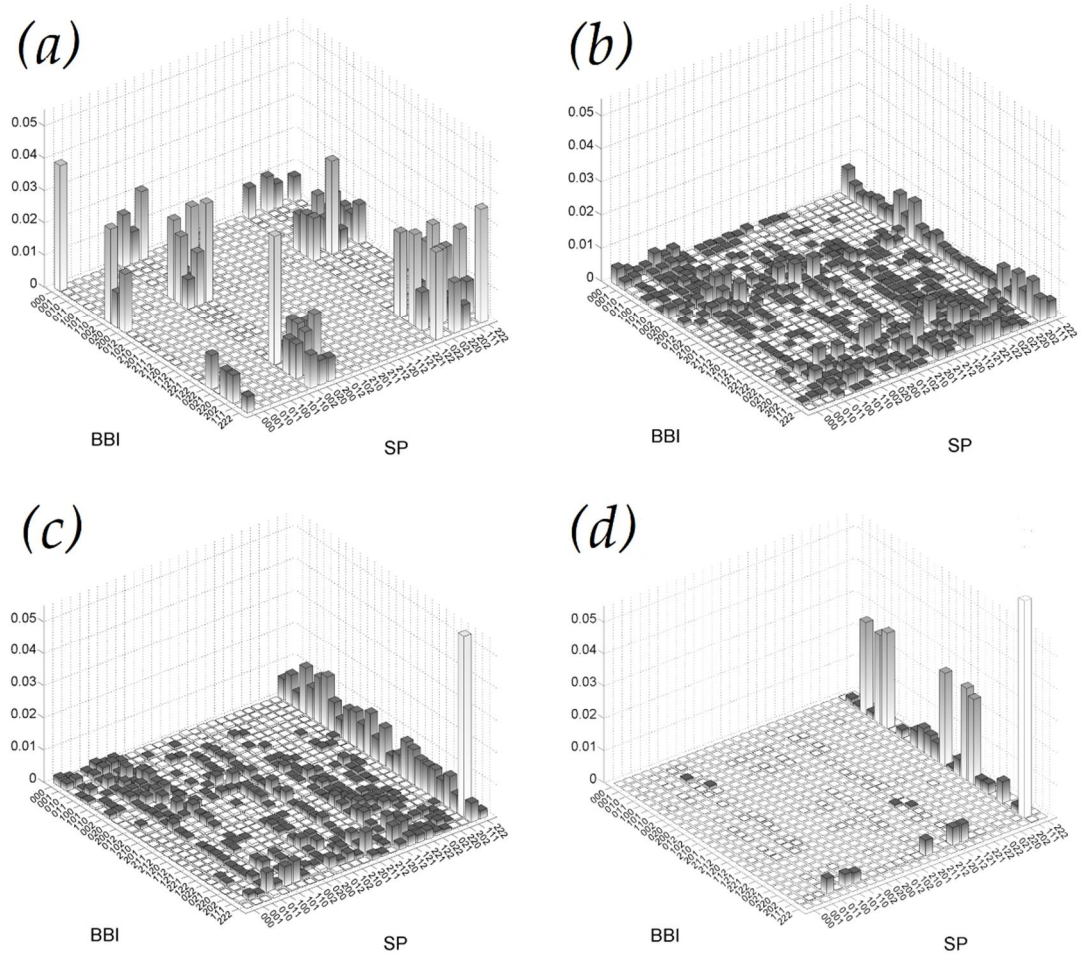

Figure 6. *Three-dimensional plots of the word distribution density matrix W_n (27×27) for the threshold levels no_TH, BRS_TH, 1/4sd_TH and sd_TH (a, b, c, d) from medicated schizophrenic patients. Due to the application of the threshold level sd_TH (d) the word type combination (111,111) was the most frequent, with the highest probability of occurrence (~70%) whereas all other word types revealed a lower probability of occurrence. Note that in plot d the bar chart of the word type (111,111) was cut to archive a uniform scaling of plot a-d. If the axis of plots a, b and c were scaled to the maximum possible value (111,111) shown in plot d, the representation of the predominant word types in plot a, b and c would not be noticeable. (SP=systolic blood pressure, BBI=beat-to-beat intervals)*

3.1.7.2 The influences of different threshold levels on pattern family probabilities

The application of different thresholds for l^{BBI} and l^{SP} (*no_TH*, *BRS_TH*, *1/4sd_TH*, *sd_TH*) resulted in different distributions in the 8x8 pattern family density matrix *Wf* (**Table 3**) and 12 significant (p<0.05) HRJSD pattern family indices. 9 HRJSD pattern family indices were found to be significantly different when applying *BRS_TH*. This threshold was most suitable for revealing specific cardiovascular coupling patterns resulting from treatment with antipsychotics (anti-cholinergic effects of drugs) in MED (p<0.05) in comparison to UNMED (**Figure 7**).

The combination of *SP-E2/BBI-E1* was particularly highly significant different (p<0.01) in this approach. This combination is characterised by increased systolic blood pressure values (*SP-E2*) and nearly invariable BBI (heart rate) (*BBI-E1*) variations. The combination *SP-E2/BBI-E1* was considerably reduced in UNMED and increased in MED (**Table 3**). Increased single pattern family probabilities *BBI-E1* of MED (6.15±11.94), indicating a high increase of invariable heart rate patterns, were found in MED in comparison to UNMED (2.52±4.79). Out of all the significant cardiovascular HRJSD combinations, 50% (n=4) showed increased mean values and 50% (n=4) revealed reduced mean values in MED in comparison to UNMED. Here, the single pattern family probabilities *BBI-E1* were involved in all 4 combinations which showed increased mean values (*SP-E2/BBI-E1*, *SP-LU1/BBI-E1*, *SP-P/BBI-E1*, *SP-V/BBI-E1*) in MED in comparison to UNMED.

Table 3. ***Left*****:** *The influence of different threshold settings on the occurrence of HRJSD pattern family indices used to quantify the anti-cholinergic effects of the antipsychotic drugs in medicated schizophrenic patients (MED) in comparison to unmedicated schizophrenic patients (UNMED).* ***Right:*** *Group mean value (MV) and standard deviation (SD) in arbitrary units [%] for HRJSD indices for UNMED and MED applying the baroreflex sensitivity threshold (BRS_TH). (SP=systolic blood pressure, BBI=beat-to-beat time series (heart rate), E0, E1, E2, LA1, LU1, LD1, P, V=pattern families, TH=threshold, no=0, BRS=baroreflex sensitivity, 1/4sd=25% standard deviation, sd=100% standard deviation, *p<0.05, **p<0.01, n.s.=not significant, #=significant cardiovascular coupling index with respect to surrogate type I analysis, §=non-linear cardiovascular coupling index with respect to surrogate type II analysis)*

					BRS_TH	
Index	***no_TH***	***BRS_TH***	***1/4sd_TH***	***sd_TH***	**UNMED**	**MED**
					MV ± SD	**MV ± SD**
SP-E0/BBI-E2	n.s.	*, #, §	n.s.	n.s.	0.04 ± 0.07	0.01 ± 0.03
SP-E2/BBI-E1	n.s.	**, #	n.s.	n.s.	0.03 ± 0.10	0.14 ± 0.34
SP-E2/BBI-V	n.s.	n.s.	*, #, §	n.s.	0.08 ± 0.09	0.12 ± 0.13
SP-LU1/BBI-E1	n.s.	*, #, §	n.s.	n.s.	0.77 ± 1.63	1.83 ± 3.60
SP-LU1/BBI-LA1	n.s.	*, #, §	n.s.	n.s.	3.08 ± 2.69	2.40 ± 2.38
SP-LD1/BBI-E0	n.s.	*	n.s.	n.s.	3.15 ± 2.71	2.37 ± 2.21
SP-P/BBI-E1	n.s.	*	n.s.	n.s.	0.22 ± 0.43	0.48 ± 1.07
SP-P/BBI-LA1	n.s.	*, #, §	n.s.	n.s.	1.58 ± 1.63	1.23 ± 1.63
SP-V/BBI-E1	n.s.	*	n.s.	n.s.	0.24 ± 0.44	0.56 ± 1.13
SP-E2	*	n.s.	n.s.	n.s.	3.82 ± 2.61	3.90 ± 2.50
BBI-E0	n.s.	*	n.s.	n.s.	6.71 ± 5.42	5.26 ± 4.30
BBI-E1	n.s.	n.s.	n.s.	n.s.	2.52 ± 4.79	6.15 ± 11.94

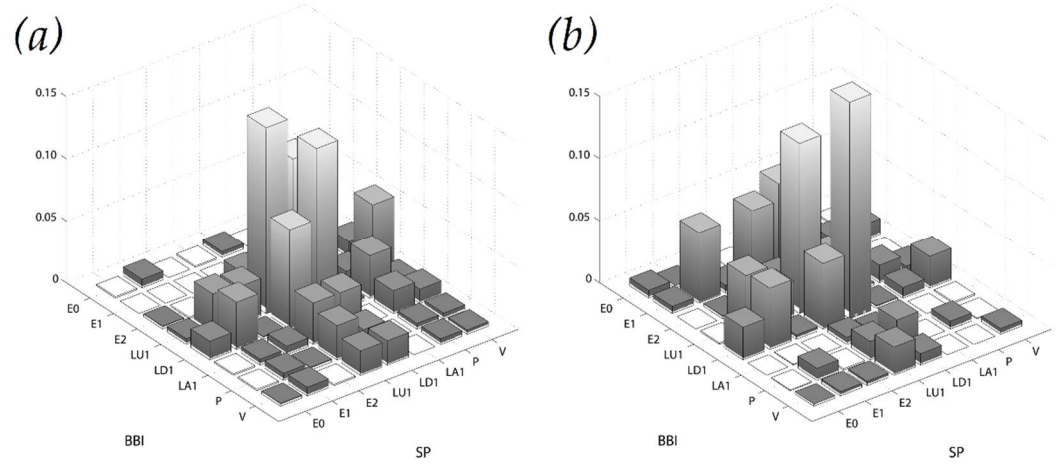

Figure 7. *Three-dimensional plots of the HRJSD pattern family distribution density matrix Wf (8×8) for the baroreflex sensitivity related threshold level (BRS_TH) for a unmedicated schizophrenic patient (a) and the medicated state (b). (SP=systolic blood pressure, BBI=beat-to-beat intervals)*

3.1.7.3 Surrogate data analysis - Probabilities of occurrence of HRJSD indices in surrogate time series and the influence of different threshold levels on pattern families' probabilities

The application of different thresholds for l^{BBI} and l^{SP} (*no_TH*, *BRS_TH*, *1/4sd_TH*, *sd_TH*) on surrogate data time series (UNMED_sI, UNMED_sII, MED_sI MED_sII) revealed a similar behaviour of different and nearly identical significant HRJSD indices within *Wf* as it was found for the original time series (**Table 4**). When the thresholds *no_TH* and *1/4sd_TH* were applied, type I and II surrogates did not show significant differences between the time series of unmedicated and medicated schizophrenic patients, whereas the *sd_TH* led to significant word type combinations (type I: n=3, type II: n=1) in contrast to the original time series, where no significant differences were found. The physiological threshold level based on baroreflex sensitivity (*BRS_TH)* revealed most of the significant differences between the surrogates for type I (9%) and II (10%) as found for the original time series (11%).

Table 4. *Surrogate data – The effect of different threshold settings on the occurrence of significant HRJSD indices (pattern families) used to identify significant differences between the unmedicated and medicated state of acute schizophrenic patients due to the antipsychotic drugs treatment derived from surrogate time series (type I and II). (TH=threshold, no=0, BRS=baroreflex sensitivity, 1/4sd=25% standard deviation, sd=100% standard deviation, p<0.05)*

	Number of significant HRJSD word family indices			
	sd_TH	***1/4sd_TH***	***BRS_TH***	***no_TH***
Original	0	1	9	1
Type I surrogates	3	0	7	0
Type II surrogates	1	0	8	0
	Percentage [%] of significant HRJSD word family indices			
	sd_TH	***1/4sd_TH***	***BRS_TH***	***no_TH***
Original	0	1	11	1
Type I surrogates	4	0	9	0
Type II surrogates	1	0	10	0

In summary, the surrogates (type I and II) revealed similar probabilities of occurrence of significant HRJSD indices as in the original time series which means that the patterns found are not based on chance but are physiological in nature. Especially noteworthy was that the baroreflex-related threshold (*BRS_TH*) illustrated its potential and significance in the uncovering of short-term cardiovascular coupling pattern.

3.1.7.4 The significance and non-linearity nature of coupling of derived HRJSD indices

With the type I surrogates (uncoupled) it was investigated the extent to which the significant HRJSD indices between UNMED and MED refer to different threshold levels. As a result, I focused only on the thresholds *BRS_TH* and *1/4sd_TH* and found that the bivariate coupling pattern *SP-E2/BBI-V* for *1/4sd_TH* (1 of 1) and the patterns *SP-E0/BBI-E2*. *SP-E2/BBI-E1*, *SP-LU1/BBI-E1*, *SP-LU1/BBI-LA1* and *SP-P/BBI-LA1* for *BRS_TH* (5 of 8) are real significant short-term coupling patterns due to the anti-cholinergic effects of the antipsychotic in medicated schizophrenic patients.

In the second step, the presence of non-linear features underlying the couplings between BBI and SP was investigated by the means of type II surrogate data analysis. Hence, I tested the non-linear nature of the significant cardiovascular coupling indices and found that *SP-E2/BBI-V* for the threshold *1/4sd_TH* and 4 of the 5 HRJSD indices (*SP-E0/BBI-E2*. *SP-LU1/BBI-E1*, *SP-LU1/BBI-LA1*, *SP-P/BBI-LA1*) for the threshold *BRS_TH* were significant non-linear cardiovascular coupling indices.

As a result, the application of the thresholds *1/4sd_TH* and *BRS_TH* seem to be the most suitable thresholds to use applying HRJSD to characterise short-term non-linear cardiovascular coupling patterns in UNMED and MED since the baroreflex sensitivity method (e.g. sequence method) only describes linear dependencies of HR and SP.

3.1.8 Summary of High Resolution Joint Symbolic Dynamics

Here, I introduced the HRJSD approach based on a redundancy reduction strategy to group single word types into 8 pattern families, allowing a detailed quantification of bivariate short-term cardiovascular- and cardiorespiratory coupling patterns which were due to changes of the different branches of autonomic regulation. This redundancy reduction strategy and the bivariate pattern family density matrix allows for a more robust statistical analysis of autonomic modulation. These are very promising and novel features of coupling analyses, emphasising the novelty of the HRJSD approach. My bivariate redundancy reduction strategy was based on the idea of the classification of frequent deterministic patterns lasting three beats (symbols), as proposed by Porta et al. (Porta et al, 2001). However, their approach was applied to univariate time series only (heart rate time series). The proposed HRJSD approach was enlarged to create a bridge between univariate and bivariate symbolic analyses.

In a first study (Schulz et al, 2013c), I applied the HRJSD approach to unmedicated and medicated patients with acute schizophrenia to quantify and characterise how different antipsychotics influence autonomic regulation (cardiovascular coupling). Applying the HRJSD approach, I was able to demonstrate that the baroreflex threshold (*BRS_TH*) based on the sequence technique in combination with three symbols reveals specific cardiovascular coupling patterns resulting from the anti-cholinergic effects of the antipsychotic drugs in medicated patients with acute schizophrenia. In addition, the HRJSD approach seems to be superior to non-invasive BRS analysis and the JSD approach in uncovering detailed changes of short-term cardiovascular regulation patterns.

I showed that the application of the HRJSD approach seems to be more suitable than univariate HRV indices and the JSD approach for providing detailed insights into the complex physiological regulation of heart rate and blood pressure couplings in patients with schizophrenia. The JSD approach codes a decreased and equilibrium change between two BBIs by means of the same symbol and might therefore miss important aspects of autonomic regulation. In addition, it can be assumed that small changes which do not arise from autonomic regulation, such as noise (e.g. generated by undersampling) or artefacts (e.g. ectopic events) can be excluded by the HRJSD approach, applying a physiologically based threshold for symbol transformation. The

grouping of different single word types into 8 pattern families, each of which characterising different interactions of the branches of the autonomic regulation of heart rate and blood pressure coupling patterns led to a further enhancement of the HRJSD approach.

I conclude that the HRJSD approach offers more detailed information about non-linear cardiovascular couplings than the standard JSD approach and standard variability analysis. Thus, may lead to an improved understanding of short-term cardiovascular regulatory mechanisms and processes (heart rate/ blood pressure regulation pattern) of autonomic regulation in patients with schizophrenia under treatment with antipsychotics. This might therefore contribute to an optimal selection of therapy strategies and thus to more successful therapy.

In a second study (Schulz et al, 2015b; Schulz et al, 2020), I applied the HRJSD approach to investigate cardiorespiratory regulation and to quantify short-term non-linear cardiorespiratory couplings in patients suffering from schizophrenia and their healthy first-degree relatives in comparison to healthy subjects. I demonstrated an altered heart rate pattern, respiratory pattern and cardiorespiratory coupling in patients with schizophrenia and only marginal changes for their healthy first-degree relatives in comparison to healthy subjects applying the HRJSD approach. These findings might be based on a decreased vagal activity within the brainstem, an altered or suppressed interaction of the brainstem and higher regulatory centres or of panic and anxiety related changes in the brainstem due to acute psychosis in these patients. Patients with schizophrenia revealed cardiorespiratory coupling patterns which were characterized as less predominant but more widely distributed than those in healthy subjects, indicating a decreased cardiorespiratory coupling in schizophrenia. I was able to demonstrate that the threshold with 25% of the standard deviation of the cardiorespiratory time series as an adapted dynamical threshold to the individual variability reveals specific cardiorespiratory coupling patterns in patients suffering from schizophrenia and their healthy first-degree relatives in comparison to healthy subjects.

The HRJSD approach enables the classification and characterization of short-term cardiovascular- and cardiorespiratory regulatory bivariate coupling patterns which are dominating the interaction generated by the ANS. As a new feature in contrast to the classical JSD approach or other coupling approaches (Schulz et al, 2013a) the HRJSD approach emphasizes a clear characterization of how the couplings are composed by the different regulatory aspects of the ANS.

The proposed directionality index D_{HRJSD} derived from the HRJSD approach is able to correctly detect the dominating coupling direction in linear coupled systems, but is only partly able to detect the dominating coupling direction in non-linear coupled systems.

3.2 Multivariate High Resolution Joint Symbolic Dynamics

3.2.1 Basics of High Resolution Joint Symbolic Dynamics

In recent years methods for analysing complex physiological regulatory networks have been developed. These methods allow analysing couplings in dynamic systems. Recent advances in non-linear dynamics and information theory facilitate a *multivariate* study of information transfer between time series. For the analyses of the cardiovascular-, cardiorespiratory- and central regulatory networks as well as the quantification of their interactions, varieties of methods have been proposed. For the characterization of linear and non-linear couplings in the brain-heart network several concepts are available (Bartsch et al, 2015; Faes et al, 2015; Ivanov et al, 2016; Schulz et al, 2013a) based on Granger causality; non-linear prediction; entropies; symbolization and phase synchronisation. The multivariate coupling analysis, e.g. of heart rate, systolic blood pressure and respiration might provide further information about the complex autonomic-network in physiological and pathophysiological conditions than uni- and bivariate approaches can do.

The idea behind the HRJSD approach was to analyse bivariate non-linear cardiovascular and cardiorespiratory couplings in acute schizophrenia (Schulz et al, 2015b; Schulz et al, 2013c) based on the analysis of dynamic processes by means of symbols (Voss et al, 1996). Thereby, the HRJSD approach classifies frequent deterministic patterns lasting three beats, and based on a symbolisation procedure permitting a coarse-grain quantitative assessment of bivariate short-term dynamics of time series. To overcome the limitation of analysing bivariate couplings only, I adopted HRJSD in a further step for the quantification of multivariate couplings – the ***multivariate High Resolution Joint Symbolic Dynamics (mHRJSD)*** (Schulz et al, 2018; Schulz et al, 2017b).

Therefore, the set of three investigated time series (e.g. BBI, SP, and RESP) were transformed into symbol sequences based on their signal amplitudes using a given alphabet A={0, 1, 2} The trivariate sample vector X (eq. 34) of these time series x^{BBI}, x^{SP} and x^{RESP} were then transformed into a trivariate symbol vector S, where n were the nth beat-to-beat values of BBI, SP and RESP, respectively (**Figure 8**).

$$X = \left\{[X_n^{\mathrm{BBI}}, X_n^{\mathrm{SP}}, X_n^{\mathrm{RESP}}]^T\right\}_{n=0,1,\ldots} \tag{34}$$

$X \in R$ (R is the subset of real positive numbers)

Then X was transformed into a trivariate symbol vector S (eq. 35) defined as

$$S = \left\{[S_n^{\mathrm{BBI}}, S_n^{\mathrm{SP}}, S_n^{\mathrm{RESP}}]^T\right\}_{n=0,1,\ldots} \tag{35}$$

$S \in R$

The trivariate symbol vector S was defined using the following definitions (eq. 36-38)

$$S_n^{\mathrm{BBI}} = \begin{cases} 0: \left(X_{n+1}^{\mathrm{BBI}} - X_n^{\mathrm{BBI}}\right) < -l^{\mathrm{BBI}} \\ 1: -l^{\mathrm{BBI}} \leq \left(X_{n+1}^{\mathrm{BBI}} - X_n^{\mathrm{BBI}}\right) \leq l^{\mathrm{BBI}} \\ 2: \left(X_{n+1}^{\mathrm{BBI}} - X_n^{\mathrm{BBI}}\right) > l^{\mathrm{BBI}} \end{cases} \quad (36)$$

$$S_n^{\mathrm{SP}} = \begin{cases} 0: \left(X_{n+1}^{\mathrm{SP}} - X_n^{\mathrm{SP}}\right) < -l^{\mathrm{SP}} \\ 1: -l^{\mathrm{SP}} \leq \left(X_{n+1}^{\mathrm{SP}} - X_n^{\mathrm{SP}}\right) \leq l^{\mathrm{SP}} \\ 2: \left(X_{n+1}^{\mathrm{SP}} - X_n^{\mathrm{SP}}\right) > l^{\mathrm{SP}} \end{cases} \quad (37)$$

$$S_n^{\mathrm{RESP}} = \begin{cases} 0: \left(X_{n+1}^{\mathrm{RESP}} - X_n^{\mathrm{RESP}}\right) < -l^{\mathrm{RESP}} \\ 1: -l^{\mathrm{RESP}} \leq \left(X_{n+1}^{\mathrm{RESP}} - X_n^{\mathrm{RESP}}\right) \leq l^{\mathrm{RESP}} \\ 2: \left(X_{n+1}^{\mathrm{RESP}} - X_n^{\mathrm{RESP}}\right) > l^{\mathrm{RESP}} \end{cases} \quad (38)$$

and the threshold levels l^{BBI}, l^{SP} and l^{RESP} (with: l^{BBI}=5ms and l^{SP}=1mmHg (non-invasive estimation of the spontaneous baroreflex sensitivity), and l^{RESP}=25% of the standard deviation of the RESP time series as an adapted threshold to the individual physiological dynamic variability).

Symbol sequences with increasing values were coded as "2", decreasing values were coded as "0" and unchanging (no variability) values were coded as "1". The symbol vector S was subdivided into short words (bins) w_k of length k=3. Thus, using three symbols led to 27 different word types for BBI (w_{BBI}), SP (w_{SP}) and RESP (w_{RESP}). The derived different word types (word types ranging from: 000, 001,…, 221, 222) were sorted into a normalized 27×27×27 vector matrix W_n (with x-, y- and z-plane) (eq. 39) ranging from word type $(000,000,000)^{\mathrm{T}}$ to $(222,222,222)^{\mathrm{T}}$.

$$W_n = \begin{bmatrix} x_{000}, y_{000}, z_{000} & \cdots & x_{000}, y_{222}, z_{222} \\ \vdots & \ddots & \vdots \\ x_{222}, y_{000}, z_{000} & \cdots & x_{222}, y_{222}, z_{222} \end{bmatrix} \quad (39)$$

Afterwards, all single word types $w_{\mathrm{BBI,SP,RESP}}$ were grouped into 8 pattern families' w_f whereby the probabilities of all single word family's occurrences $p(w_f)$ were normalized to 1. These 8 pattern families (*E0*, *E1*, *E2*, *LU1*, *LD1*, *LA1*, *P*, *V*) were sorted into an 8×8×8 pattern family density matrix W_f resulting in 512 coupling patterns (**Figure 8**) (e.g. *BBI-E0/SP-E0/RESP-E0* = HR↑, SP↓, RESP↓).

Furthermore, from the matrix W_f, the sum of each (n=8) x-, y-, and z-plane (pf_{BBI}, pf_{SP}, pf_{RESP}) as pfE0, pfE1, pfE2, pfLU1, pfLD1, pfLA1, pfP, and pfV were calculated describing how one family pattern in one time series is coupled with all other 8 pattern families of the other two time series (**Figure 9**). In addition, to quantify the complexity of the coupling network, the Shannon entropy ($\mathrm{mHRJSD}_{\mathrm{Shannon}}$) (eq. 40) and/or the Renyi entropy ($\mathrm{mHRJSD}_{\mathrm{renyi2}}$, α=2) can be computed from W_f

$$\mathrm{mHRJSD}_{\mathrm{Shannon}} = -\sum_{i,j=1}^{8}\left[p\left(wf_{i.j}\right)\log_2 p\left(wf_{i.j}\right)\right]. \quad (40)$$

For a statistical representation, the probabilities of occurrences of the coupling pattern has to be $p(w_j)>0.05$ and has to fulfil the Bonferroni-Holm adjustment ($p<0.000098$, for $n=512$ coupling patterns) (**Figure 9**).

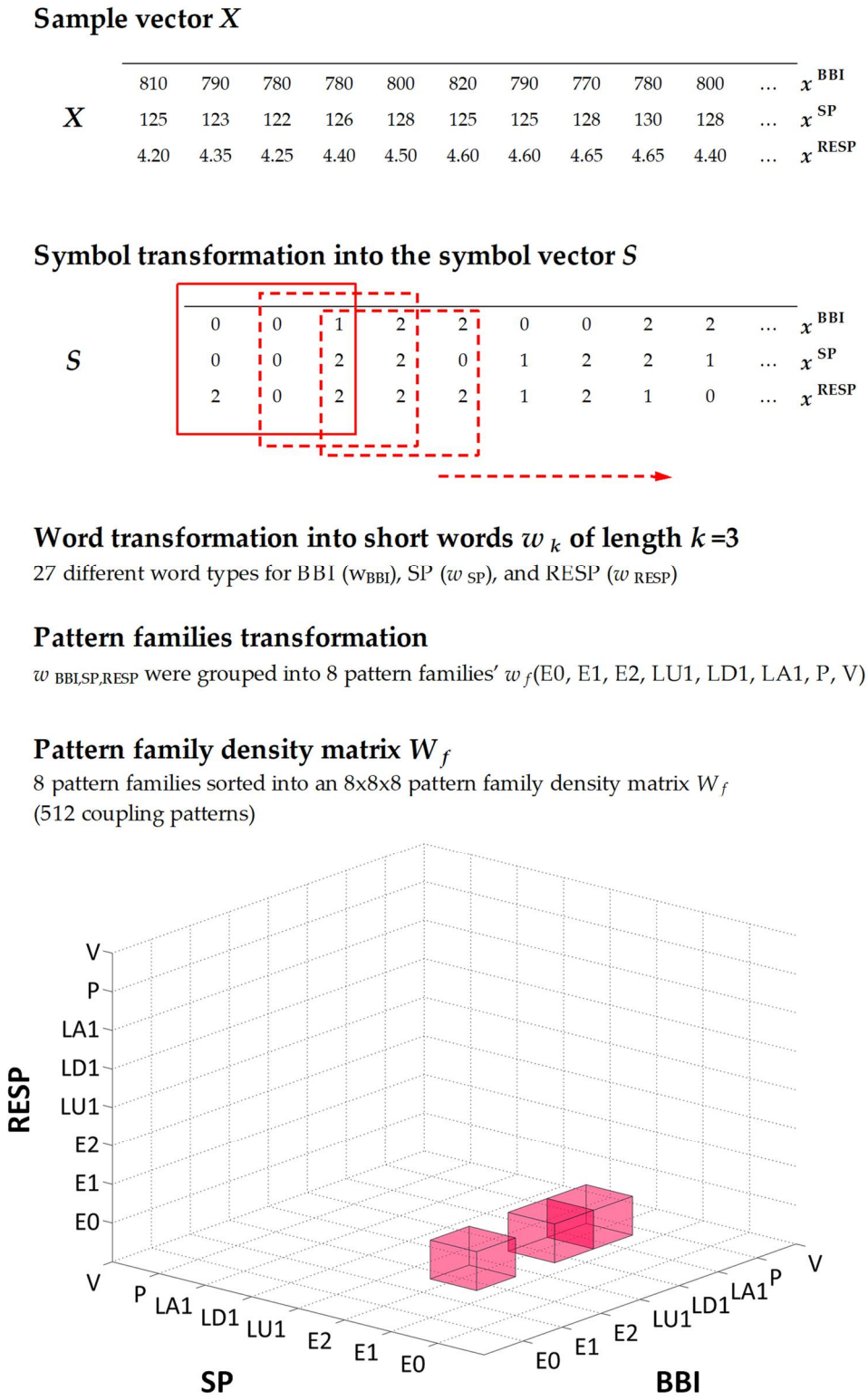

Figure 8. *Basic principle of mHRJSD. Transformation of the trivariate sample vector X into the trivariate symbol vector S (0: decreasing values; 1: equal values; 2: increasing values); Word transformation and word pattern family distribution density matrix W_f (8×8×8) with 8 pattern families E0, E1, E2, LU1, LD1, LA1, P, and V with word pattern probabilities $p(w_f)>0.05$ (red cubes). (BBI=beat-to-beat intervals, SP=systolic blood pressure, RESP=respiratory frequency)*

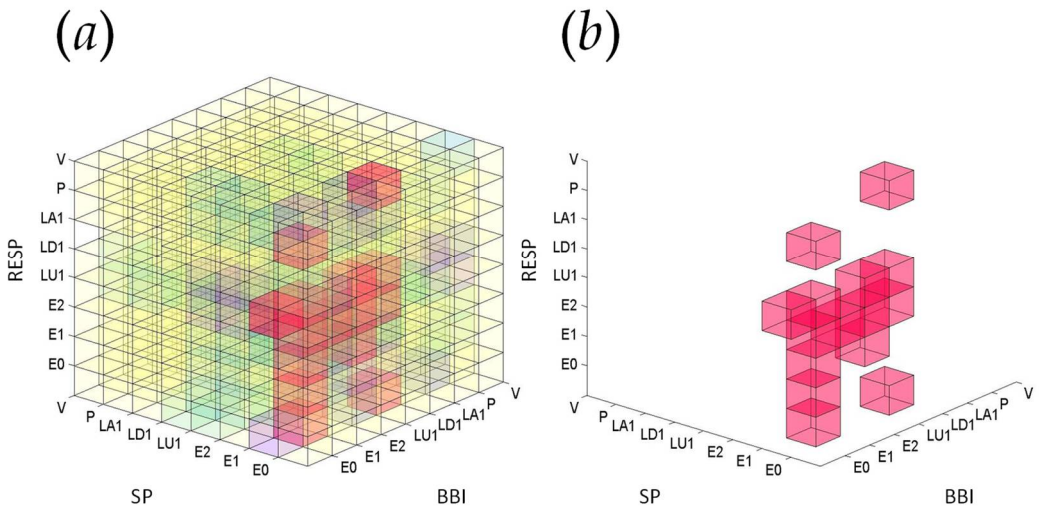

Figure 9. *Visualisation example of mHRJSD for a healthy subject. Word pattern family distribution density matrix W_f (8×8×8) with 8 pattern families E0, E1, E2, LU1, LD1, LA1, P, and V with (a) all word pattern probabilities $p(w_f)$=[yellow: <0.001; green: <0.0025; turquoise: <0.005; blue: <0.01; violet: <0.015, red: >0.05], and (b) only for $p(w_f)$>0.05. (BBI=beat-to-beat intervals, SP=systolic blood pressure, RESP=respiratory frequency)*

3.2.2 Simulations

The mHRJSD approach was validated by artificial time series with different patterns of autonomic regulation. Therefore, specific time series with different pattern families w_f (ranging from simple ones to highly complex ones, e.g. *E0/E0/E0* or *E1-P-LU1/E1-V-LA1/E0-LD1-LU1*) were simulated including all possible types of word of the pattern families w_f (*E0*, *E1*, *E2*, *LU1*, *LD1*, *LA1*, *P*, *V*). The obtained mHRJSD results were verified, whether the family patterns were correctly detected and classified. A selection of 5 simulation examples carried out is shown below.

Simulation 1 – E0/E0/E0 (Figure 10):

This is a simple simulation. All time series consist only of the pattern E0 (no variation within the time series, consisting of three symbols of type "0") leading to different probabilities of the single word family's occurrences $p(w_f)$ from the *x*-, *y*- and *z*-plane (pf_xE0, pf_yE0, pf_zE0) and the coupling pattern (*x-E0/y-E0/z-E0*).

- pf_xE0 **= 1,** pf_yE0 **= 1**, pf_zE0 **= 1**
- *x-E0/y-E0/z-E0* **= 1**

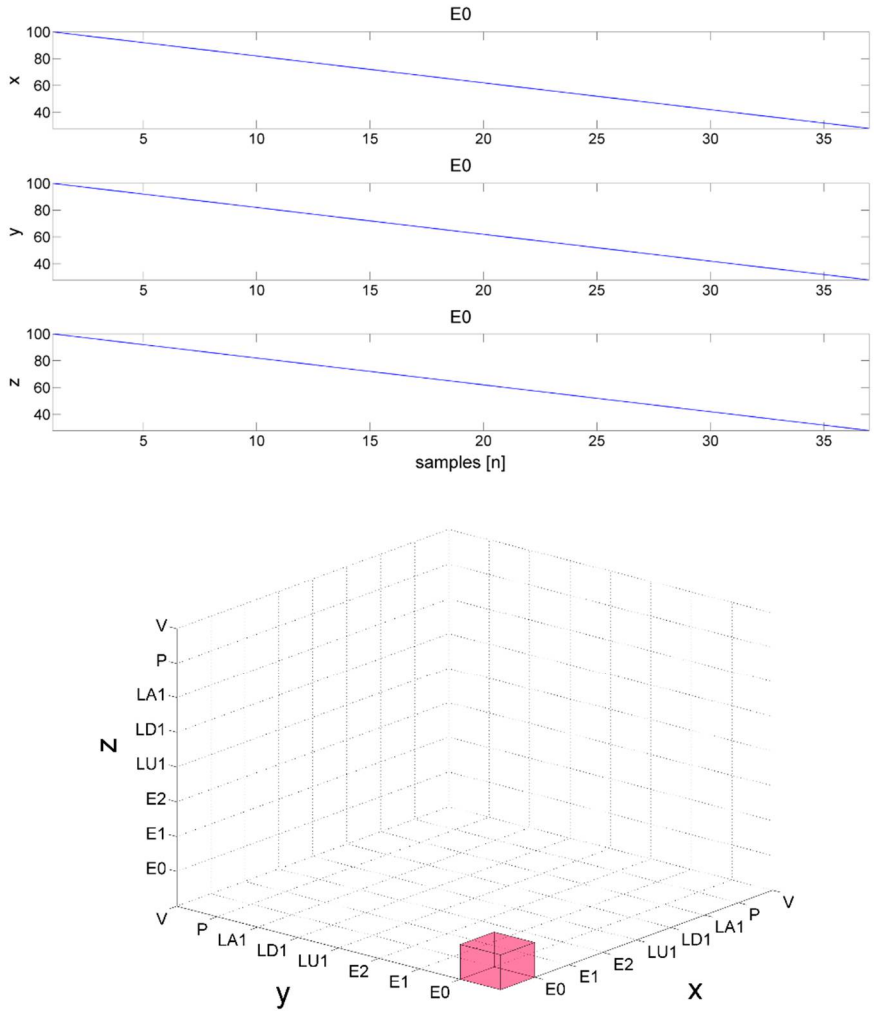

Figure 10. *mHRJSD simulation example 1 – Visualisation of the time series x, y, z and the word pattern family distribution density matrix W_f (8×8×8) with 8 pattern family E0 with the word pattern probabilities $p(w_f)$>0.05.*

Simulation 2 – E2/E1/E0 (Figure 11):

This is also a simple simulation. The time series consist of the pattern E2, E1 and E0 (no variation within each time series, consisting each of three symbols of type "2", "1", and "0").

- pf_xE2 **= 1**, pf_yE1 **= 1**, pf_zE0 **= 1**
- *x-E2/y-E1/z-E0* **=1**

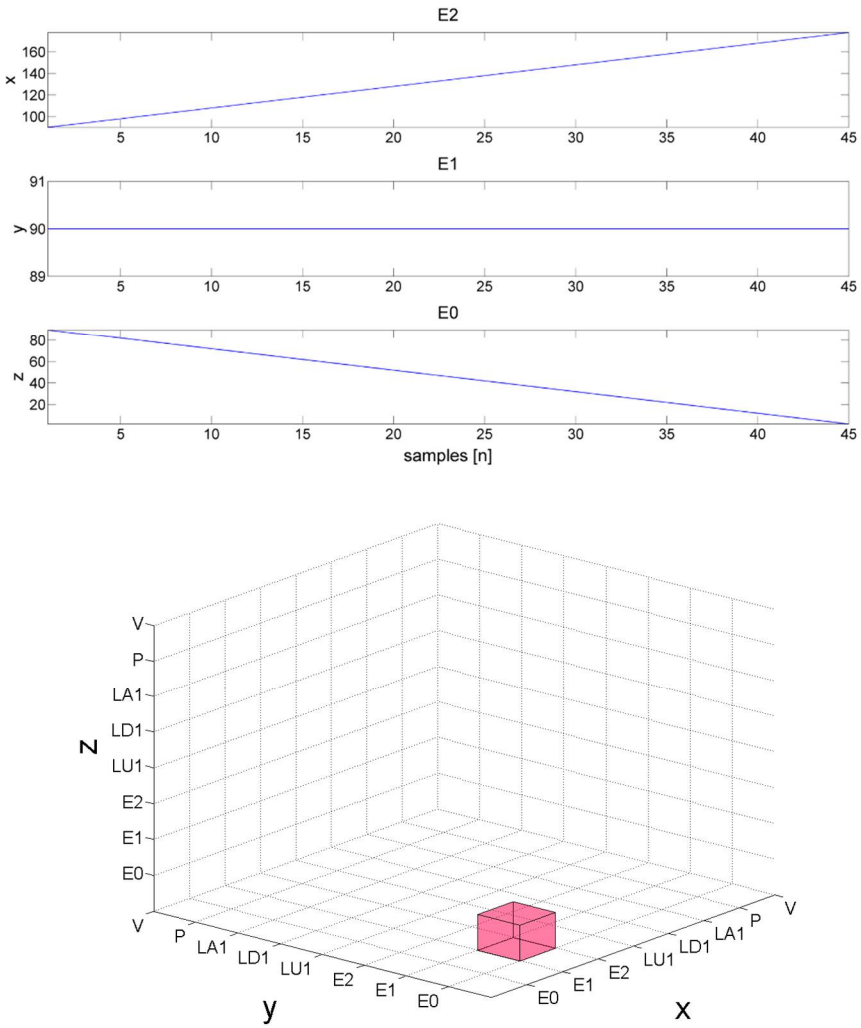

Figure 11. *mHRJSD simulation example 2 – Visualisation of the time series x, y, z and the word pattern family distribution density matrix W_f (8×8×8) with 8 pattern families E0, E1, and E2 with the word pattern probabilities $p(w_f)$>0.05.*

Simulation 3 – LU1-LA1/LD1-LA1/LA1-LD1 (Figure 12):

This simulation includes the pattern families LU1, LD1, and LA1 (one variation within the word consisting of two different symbols with low increasing, decreasing and alternating behaviour) different distributed in each of the time series.

- pf_xLU1=0.66667 + pf_xLA1=0.33333 = **1**
- pf_yLD1=0.66667 + pf_yLA1=0.33333 = **1**
- pf_zLA1=0.33333 + pf_zLD1=0.66667 = **1**
- *x-LU1/y-LD1/z-LD1*=0.33333 + *x-LU1/y-LA1/z-LD1*=0.33333 + *x-LA1/y-LD1/z-LA1*=0.33333 = **1**

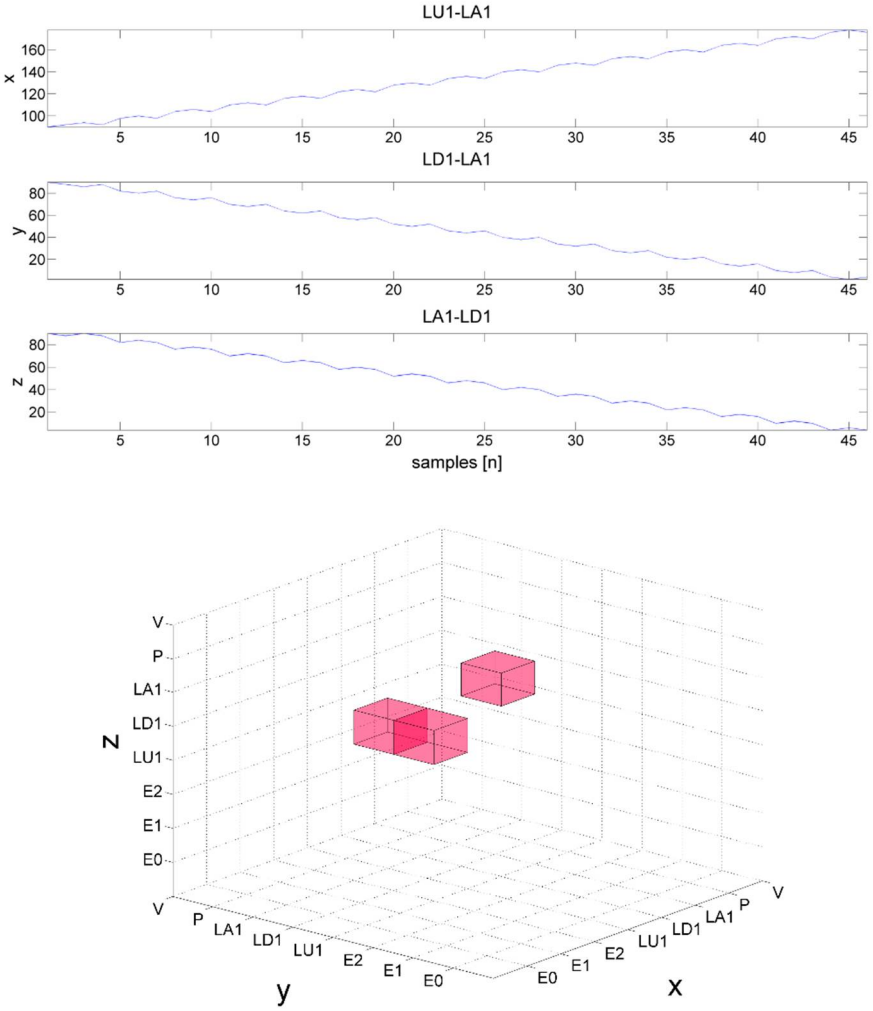

Figure 12. *mHRJSD simulation example 3 – Visualisation of the time series x, y, z and the word pattern family distribution density matrix W_f (8×8×8) with 8 pattern families LU1, LD1, and LA1 with the word pattern probabilities $p(w_f)$>0.05.*

Simulation 4 – V-P/P-V/V-P (Figure 13):

This simulation contains the pattern families P and V (three variations within the word consisting of three different symbols with peak-like and valley-like behaviours) different distributed in each of the time series.

- pf_xV=0.66667 + pf_xP=0.33333 = **1**
- pf_yP=0.66667 + pf_yV=0.33333 = **1**
- pf_zV=0.33333 + pf_zP=0.66667 = **1**
- *x-V/y-P/z-P*=0.33333 + *x-V/y-V/z-P*=0.33333 + *x-P/y-P/z-V*=0.33333 = **1**

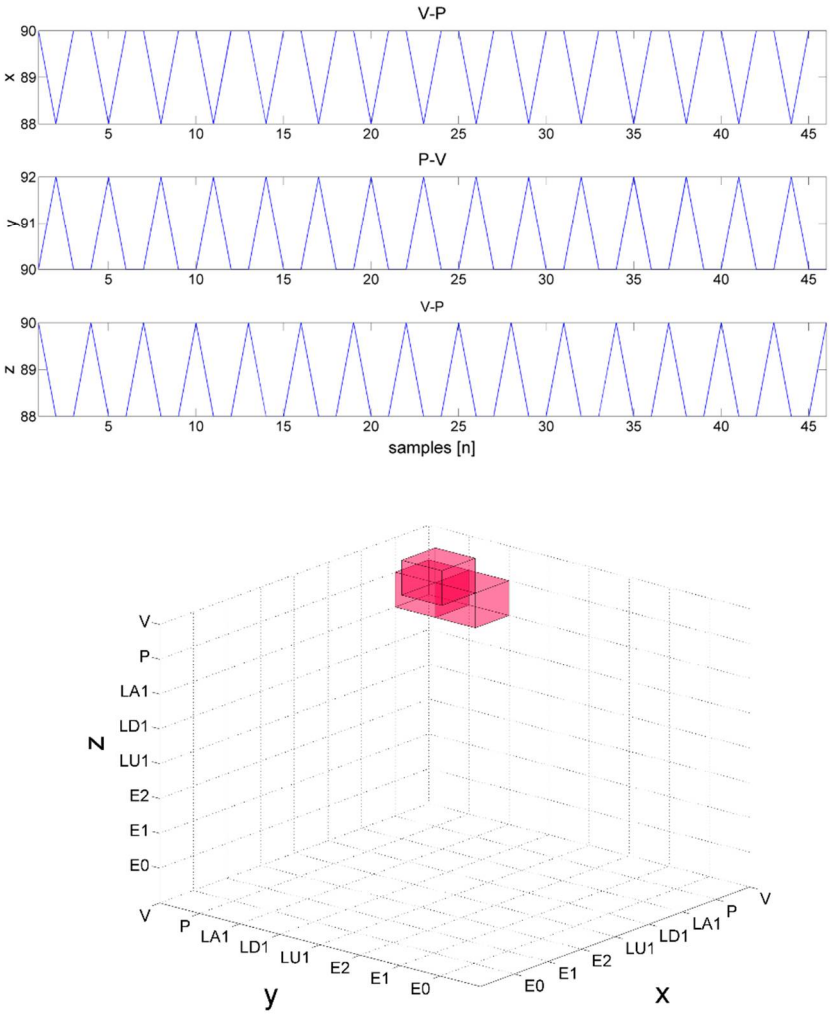

Figure 13. *mHRJSD simulation example 4 – Visualisation of the time series x, y, z and the word pattern family distribution density matrix W_f (8×8×8) with 8 pattern families P and V with the word pattern probabilities $p(w_f)$>0.05.*

Simulation 5 – E2-LA1/P-V-LU1/E0-LD1 (Figure 14):

The last simulation represents a highly complex combination of several pattern families consisting of the pattern families E2, LA1 and LU1 for time series *x*, P, V, LU1 and LA1 time series *y*, and E0, LD1, LA1, and V time series *z*.

- pf_xE2=0.47727 + pf_xLA1=0.51136 + pf_xLU1=0.01136 **= 1**
- pf_yLU1=0.51136 + pf_yLA1=0.02273 + pf_yP=0.30682 + pf_yV=0.15909 **= 1**
- pf_zE0=0.46591 + pf_zLD1=0.51136 + pf_zLA1=0.01136 + pf_zV=0.01136 **= 1**
- *x-E2/y-P/z-E0*=0.30682 + *x-E2/y-V/z-E0*=0.15909 + *x-E2/y-LA1/z-LD1*=0.01136 + *x-LU1/y-LA1/z-LA1*=0.01136 + *x-LA1/y-LU1/z-V*=0.01136 + *x-LA1/y-LU1/z-LD1*=0.5 **= 1**

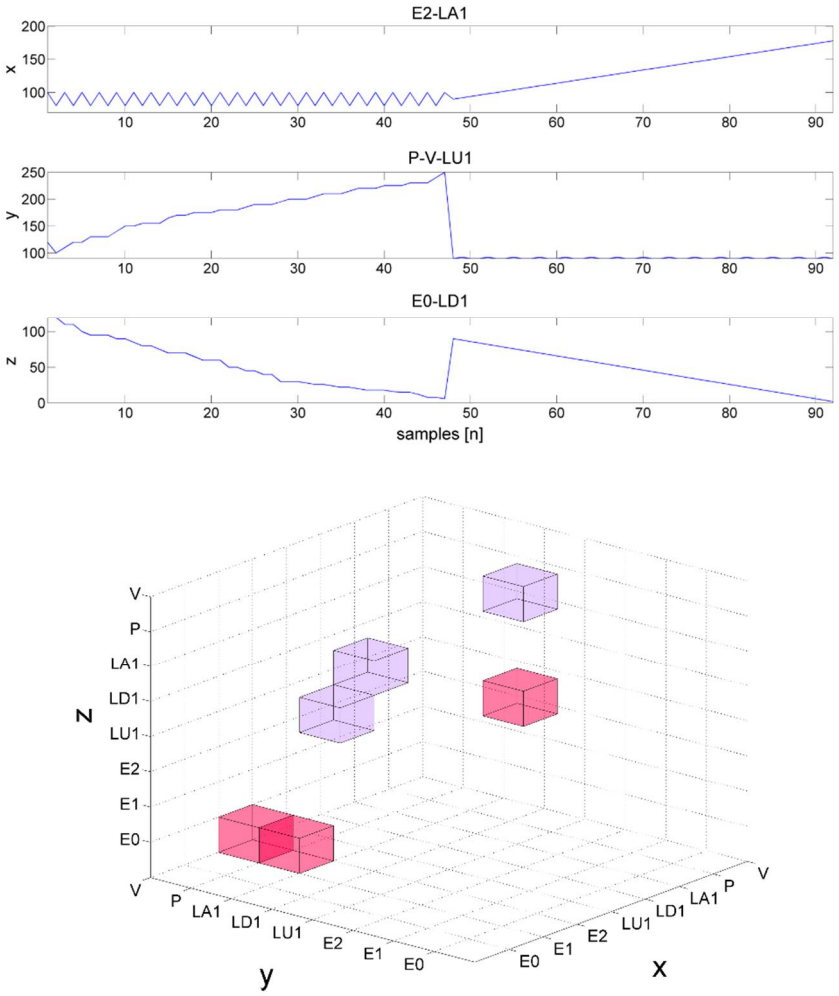

Figure 14. *mHRJSD simulation example 5 – Visualisation of the time series x, y, z and the word pattern family distribution density matrix W_f (8×8×8) with 8 pattern families E0, E2, LU1, LD1, LA1, P, and V with the word pattern probabilities $p(w_f)$<0.015 (violet cubes) and $p(w_f)$>0.05 (red cubes).*

The results of the simulations (here only 5 presented) clearly showed that the mHRJSD approach correctly detected all possible probabilities of the single word family's occurrences $p(w_f)$ from the *x*-, *y*- and *z*-plane (pf_xE0, pf_yE0, pf_zE0) and the coupling pattern within artificial time series.

The mHRJSD approach extends univariate and bivariate symbolic approaches by including a third time series enabling multivariate time series coupling analysis based on a coarse graining of the dynamics of the time series under investigation.

3.2.3 Directionality index

3.2.3.1 Introduction

In section 3.1.4, I introduced the directionality index (D_{HRJSD}) for bivariate systems derived from the 8×8 pattern family density matrix W_f from the HRJSD approach. The introduced directionality index D_{HRJSD} is able to correctly detect the dominating coupling direction in linear bivariate coupled systems, and only partly able to detect the dominating coupling direction in non-linear bivariate coupled systems. However, there is no methodical approach, based on symbolization that allows to detect the coupling direction in multivariate coupled systems. Rather there is no coupling approach available, which is able to determine the primary driver, the secondary driver and dominant responder in multivariate weakly coupled systems. Therefore, for the mHRJSD approach I further extended this directionality index to determine the dominant coupling direction and assesses the driver-response relationships in multivariate (n=3) systems (**Figure 1**).

For the **multivariate case** (x,y,z) the single word family's occurrences $p(w_f)$ from the x-, y- and z-plane (pfx, pfy, pfz) from the 8×8×8 pattern family density matrix W_f were used to calculate $D_{\mathrm{mHRJSD}}(x,y|z)$ (eq. 41-43). Thereby, for each coupling pathway one directionality index was calculated (e.g., 2 interacting time series: x and y with z as the covariate |).

Thus, for the coupling between the time series x and y with covariate z, the directionality index (eq. 41) is defined as:

$$D_{\mathrm{mHRJSD}}(x,y|z) = -\left(\sum_{i=1}^{n} \frac{pf_{\mathrm{x|z}}(i) - pf_{\mathrm{y|z}}(i)}{pf_{\mathrm{x|z}}(i) + pf_{\mathrm{y|z}}(i)}\right)/n \qquad (41)$$

For the coupling between the time series x and z with covariate y, the directionality index (eq. 42) is defined as:

$$D_{\mathrm{mHRJSD}}(x,z|y) = -\left(\sum_{i=1}^{n} \frac{pf_{\mathrm{x|y}}(i) - pf_{\mathrm{z|y}}(i)}{pf_{\mathrm{x|y}}(i) + pf_{\mathrm{z|y}}(i)}\right)/n \qquad (42)$$

For the coupling between the time series y and z with covariate x, the directionality index (eq. 43) is defined as:

$$D_{\mathrm{mHRJSD}}(y,z|x) = -\left(\sum_{i=1}^{n} \frac{pf_{\mathrm{y|x}}(i) - pf_{\mathrm{z|x}}(i)}{pf_{\mathrm{y|x}}(i) + pf_{\mathrm{z|x}}(i)}\right)/n \tag{43}$$

If $D_{\mathrm{mHRJSD}}(x,y|z)$ is positive driving (→) from system 1 (x) to system 2 (y) predominates (eq. 44) and becomes negative for the opposite case (eq. 45).

$$D_{\mathrm{mHRJSD}}(x,y|z) > 0; \quad \boldsymbol{x}|z \rightarrow y|z \tag{44}$$

$$D_{\mathrm{mHRJSD}}(x,y|z) < 0; \quad \boldsymbol{y}|z \rightarrow x|z \tag{45}$$

If $D_{\mathrm{mHRJSD}}(x,z|y)$ is positive driving (→) from system 1 (x) to system 2 (z) predominates (eq. 46) and becomes negative for the opposite case (eq. 47).

$$D_{\mathrm{mHRJSD}}(x,z|y) > 0; \quad \boldsymbol{x}|y \rightarrow z|y \tag{46}$$

$$D_{\mathrm{mHRJSD}}(x,z|y) < 0; \quad \boldsymbol{z}|y \rightarrow x|y \tag{47}$$

If $D_{\mathrm{mHRJSD}}(y,z|x)$ is positive driving (→) from system 1 (y) to system 2 (z) predominates (eq. 48) and becomes negative for the opposite case (eq. 49).

$$D_{\mathrm{mHRJSD}}(y,z|x) > 0; \quad \boldsymbol{y}|x \rightarrow z|x \tag{48}$$

$$D_{\mathrm{mHRJSD}}(y,z|x) < 0; \quad \boldsymbol{z}|x \rightarrow y|x \tag{49}$$

Thus, three indices were derived, which are subsequently used to determine the strongest driver and the most dominant responder in the overall system. Therefore, all three indices were compared to whether they were greater or less than 0 (**Table 5**).

Table 5. *Determination of the primary driver (**D_{mHRJSD}), secondary driver (*D_{mHRJSD}) and the dominant responder ($\bar{}D_{mHRJSD}$) in a multivariate system derived from the directionality indices $D_{mHRJSD}(x,y|z)$, $D_{mHRJSD}(x,z|y)$, and $D_{mHRJSD}(y,z|x)$.*

$\boldsymbol{D_{\mathrm{mHRJSD}}(x,y\|z)}$	$\boldsymbol{D_{\mathrm{mHRJSD}}(x,z\|y)}$	$\boldsymbol{D_{\mathrm{mHRJSD}}(y,z\|x)}$	$^{**}\boldsymbol{D_{\mathrm{mHRJSD}}}$	$^{*}\boldsymbol{D_{\mathrm{mHRJSD}}}$	$\bar{}\boldsymbol{D_{\mathrm{mHRJSD}}}$
+ = x	+ = x	+ = y	x	y	z
- = y	- = z	- = z	z	y	x
+ = x	+ = x	- = z	x	z	y
- = y	- = z	+ = y	y	z	x
+ = x	- = z	- = z	z	x	y
- = y	+ = x	+ = y	y	x	z
+ = x	- = z	+ = y	x-y-z	x-y-z	x-y-z
- = y	+ = x	- = z	x-y-z	x-y-z	x-y-z

In the following, the sum of the three comparisons was determined. If a time series is present twice as a driver, it dominates the overall system as the **primary driver** $^{**}D_{\mathrm{mHRJSD}}$, and if a time series is present only once, it is the **secondary driver** $^{*}D_{\mathrm{mHRJSD}}$ of the overall system, and the non-occurring time series is the **dominant responder** $\bar{D}_{\mathrm{mHRJSD}}$.

For the cases, that $D_{\mathrm{mHRJSD}}(x,y|z) > 0$, $D_{\mathrm{mHRJSD}}(x,z|y) < 0$, and $D_{\mathrm{mHRJSD}}(y,z|x) > 0$ (+ - +) or that $D_{\mathrm{mHRJSD}}(x,y|z) < 0$, $D_{\mathrm{mHRJSD}}(x,z|y) > 0$, and $D_{\mathrm{mHRJSD}}(y,z|x) < 0$ (- + -) the indices $^{**}D_{\mathrm{mHRJSD}}$, $^{*}D_{\mathrm{mHRJSD}}$ and $\bar{D}_{\mathrm{mHRJSD}}$ are determined by their absolute values, in descending order of importance of their values. In these both cases, closed-loops are present without any feedback-loops.

3.2.3.2 Simulated multivariate coupled linear systems to validate D_{mHRJSD}

Similar to the validation of D_{HRJSD} for the bivariate case (3.1.4), simulated data were used to validate D_{mHRJSD}. Therefore, a ***multivariate linear Gaussian AR model*** was applied to generate a set of multivariate linear time series (n=100) with a normal distribution of the variables (Baccala & Sameshima, 2001b; Montalto et al, 2014). For the linear model two different multivariate coupled systems were generated (eq. 50, 51) with different mutual influences (unidirectional, bidirectional) between the time series (**Figure 5, *b*, *c***). Non-linear AR models were not applied since D_{HRJSD} seems to be only partly able to detect the correct driver-responder relationship between non-linear coupled time series.

I. Coupled multivariate linear AR model (Figure 5, *b*):

$$\begin{aligned} x_1(n) &= 0.95\sqrt{2}x_1(n-1) - 0.9025x_1(n-2) + w_1(n) \\ x_2(n) &= 0.5x_1(n-2) + w_2(n) \\ x_3(n) &= -0.4x_1(n-3) - 0.2x_2(n-2) + w_3(n) \end{aligned} \quad (50)$$

II. Coupled multivariate linear AR model (Figure 5, *c*):

$$\begin{aligned} x_1(n) &= 0.95\sqrt{2}x_1(n-1) - 0.9025x_1(n-2) + w_1(n) \\ x_2(n) &= 0.5x_1(n-2) + 0.4x_3(n-1) + w_2(n) \\ x_3(n) &= -0.4x_1(n-3) - 0.2x_2(n-2) + w_3(n) \end{aligned} \quad (51)$$

where $w_1(n)$, $w_2(n)$, and $w_3(n)$ were drawn from Gaussian noise with zero mean and unit variance. For the II. coupled multivariate linear AR model a closed-loop from $x_3(n)$ back to $x_2(n)$ via a direct connection was integrated, with x_3 as a driver.

3.2.3.3 Results of simulated multivariate coupled linear systems to validate D_{mHRJSD}

The results of the two multivariate coupled linear AR systems showed that the determination of the multivariate directionality index D_{mHRJSD} works properly as well as the determination of the **primary driver** $^{**}D_{\mathrm{mHRJSD}}$, the **secondary driver** $^{*}D_{\mathrm{mHRJSD}}$ and **dominant responder** $\bar{D}_{\mathrm{mHRJSD}}$ in the multivariate systems (**Table 6**).

I. Coupled multivariate linear AR model (Figure 5, *b*):

$\boldsymbol{x_1 \rightarrow x_2}$: $D_{\text{mHRJSD}}(x_1,x_2 \mid x_3)$ is positive; correct classification of the dominating coupling direction (x_1 is driver).

$\boldsymbol{x_1 \rightarrow x_3}$: $D_{\text{mHRJSD}}(x_1,x_3 \mid x_2)$ is positive; correct classification of the dominating coupling direction (x_1 is driver).

$\boldsymbol{x_2 \rightarrow x_3}$: $D_{\text{mHRJSD}}(x_2,x_3 \mid x_1)$ is positive; correct classification of the dominating coupling direction (x_2 is driver).

From this results that:

$D_{\text{mHRJSD}}(x_1,x_2 \mid x_3) = x_1$ and $D_{\text{mHRJSD}}(x_1,x_3 \mid x_2) = x_1 \Rightarrow \mathbf{^{**}D_{mHRJSD} = x_1}$

$D_{\text{mHRJSD}}(x_2,x_3 \mid x_1) = x_2 \Rightarrow \mathbf{^{*}D_{mHRJSD} = x_2}$

$\Rightarrow \mathbf{\bar{D}_{mHRJSD} = x_3}$

For the coupled multivariate linear AR model (I.) the correct driver-responder relationships were classified with x_1 as the primary driver, x_2 as the secondary driver, and x_3 as the responder of the system, as it was simulated.

II. Coupled multivariate linear AR model (Figure 5, *c*):

$\boldsymbol{x_1 \rightarrow x_2}$: $D_{\text{mHRJSD}}(x_1,x_2 \mid x_3)$ is positive; correct classification of the dominating coupling direction (x_1 is driver).

$\boldsymbol{x_1 \rightarrow x_3}$: $D_{\text{mHRJSD}}(x_1,x_3 \mid x_2)$ is positive; correct classification of the dominating coupling direction (x_1 is driver).

$x_2 \rightleftarrows \boldsymbol{x_3}$**:** $D_{\text{mHRJSD}}(x_2,x_3 \mid x_1)$ is negative; correct classification of the dominating coupling direction (x_3 is driver).

From this results that:

$D_{\text{mHRJSD}}(x_1,x_2 \mid x_3) = x_1$ and $D_{\text{mHRJSD}}(x_1,x_3 \mid x_2) = x_1 \Rightarrow \mathbf{^{**}D_{mHRJSD} = x_1}$

$D_{\text{mHRJSD}}(x_2,x_3 \mid x_1) = x_3 \Rightarrow \mathbf{^{*}D_{mHRJSD} = x_3}$

$\Rightarrow \mathbf{\bar{D}_{mHRJSD} = x_2}$

For the coupled multivariate linear AR model (II.) the correct driver-responder relationships were classified with x_1 as the primary driver, x_3 as the secondary driver, and x_2 as the responder of the system, as it was simulated.

Table 6. *Determination of the primary driver (**D_{mHRJSD}), secondary driver (*D_{mHRJSD}) and the dominant responder ($\bar{}D_{mHRJSD}$) derived from the directionality indices $D_{mHRJSD}(x,y|z)$, $D_{mHRJSD}(x,z|y)$, and $D_{mHRJSD}(y,z|x)$ for two simulated multivariate coupled systems.*

	$D_{\mathrm{mHRJSD}}(x_1,x_2\|x_3)$	$D_{\mathrm{mHRJSD}}(x_1,x_3\|x_2)$	$D_{\mathrm{mHRJSD}}(x_2,x_3\|x_1)$	$^{**}D_{\mathrm{mHRJSD}}$	$^{*}D_{\mathrm{mHRJSD}}$	$\bar{}D_{\mathrm{mHRJSD}}$
I	x_1	x_1	x_2	x_1	x_2	x_3
II	x_1	x_1	x_3	x_1	x_3	x_2

3.2.4 Summary of multivariate High Resolution Joint Symbolic Dynamics

I developed the multivariate high-resolution joint symbolic dynamics approach (mHRJSD) to overcome the limitation of the HRJSD approach that is only able to analyse bivariate couplings and to determine the driver-responder relationship. Therefore, the HRJSD approach was enhanced in a further step allowing the quantification of multivariate couplings and the determination of the driver-responder relationships.

The mHRJSD approach extending the bivariate HRJSD approach by including a third time series enables multivariate time series coupling analyses based on a coarse graining of the dynamics of the time series under investigation.

To prevent that spurious couplings were detected a statistical significance level was applied whereby the probabilities of occurrences of the coupling pattern have been set to $p(w_f)>0.05$ and have to fulfil the Bonferroni-Holm adjustment ($p<0.000098$, $n=512$ coupling patterns).

The multivariate redundancy reduction strategy with the multivariate pattern family density matrix allows for a robust statistical analysis and provides more detailed information about short-term physiological regulatory processes of complex multivariate physiological networks.

The mHRJSD approach contains multivariate Directionality indices D_{mHRJSD} ($D_{\mathrm{mHRJSD}}(x,y|z)$, $D_{\mathrm{mHRJSD}}(x,z|y)$, and $D_{\mathrm{mHRJSD}}(y,z|x)$) allowing to determine the primary driver $^{**}D_{\mathrm{mHRJSD}}$, the secondary driver $^{*}D_{\mathrm{mHRJSD}}$ and dominant responder $\bar{}D_{\mathrm{mHRJSD}}$ in multivariate systems. Therefore, it has to be assumed that the time series to be analysed are at least weakly coupled with each other.

Limiting factors are that the proposed directionality index D_{mHRJSD} derived from the mHRJSD approach is only able to correctly detect the driver-responder relationships in linear coupled systems, and is not able to detect the driver-responder relationships in non-linear coupled systems. The mHRJSD approach is able to evaluate direct causal information transfer in multivariate systems.

Despite this limitation of D_{mHRJSD}, the feature to assess the driver-response relationships in multivariate systems is not implemented in none of the existing symbolization approaches and thus clearly complements the already existing coupling approaches.

The clinical validation of the mHRJSD approach is presented in chapter 4.

3.3 Normalized Short Time Partial Directed Coherence

3.3.1 Basics of partial directed coherence

For two processes $X(t)$ and $Y(t)$ Granger causality can be defined as: $X(t)$ has causal influence on $Y(t)$; ($X(t)\rightarrow Y(t)$) if the knowledge of the past of both $X(t)$ and $Y(t)$ reduces the variance of the prediction error of $Y(t)$ in comparison with the knowledge of the past of $Y(t)$ alone (the past and the present cause the future but not vice versa). Granger causality approaches in the frequency domain as, the partial directed coherence (PDC) and the enhanced version the normalized short time partial directed coherence (NSTPDC) targeting to the oscillatory nature of physiological variables and the peculiarity of specific control mechanisms of working in accordance to well defined time scales (Porta & Faes, 2013). These approaches are based on a fitted AR model and presuppose the stationarity of signals in the time interval under investigation (Hesse et al, 2003).

The main methodological principles of the PDC approach have already been described in chapter 2.2.1.

PDC is a parametric approach based on m-dimensional MAR processes with order p. It can detect direct and indirect causal information transfer since it measures exclusively direct effects between signals in multivariate dynamic systems. Based on the Fourier transformation of the coefficient matrix $A(f)$ the PDC function quantifies the strength of the causal coupling from X_j to X_i as a function of frequency f. PDC between two processes X_j and X_i is given by (eq. 52):

$$\pi_{i\leftarrow j}(f) = \frac{\bar{A}_{ij}(f)}{\sqrt{\bar{a}_j^H(f)\bar{a}_j(f)}} \tag{52}$$

Following normalisation properties have to hold for PDC estimation: $0 \leq \left|\pi_{ij}(f)\right|^2 \leq 1$ and $\sum_{i=1}^{m}\left|\pi_{ij}(f)\right|^2 = 1$ (for all $1\leq j\leq m$) indicate that the squared magnitude of the PDC function $\pi_{ij}(f)$. The PDC is normalised between 0 and 1, in that way the direct influence from process X_j to process X_i is inferred by PDC≠0 (PDC=0 when X_j does not cause X_i at frequency f, PDC=1 when all causal influences originating from X_j at frequency f are directed toward X_i (Baccala & Sameshima, 2001b; Faes & Nollo, 2010; Pereda et al, 2005). Due to, that the original introduced PDC method cannot be applied to non-stationary signals a time-variant version is needed providing information about the partial correlative short-time interaction properties. To overcome this problem, Milde et al. introduced the time-variant partial directed coherence approach (tvPDC, $\pi_{ij}(f,n)$) (eq. 53) (Milde et al, 2011).

Here, I introduced an extended version of the tvPDC approach the ***Normalized Short Time Partial Directed Coherence (NSTPDC)*** (Adochiei et al, 2013; Schulz et al, 2015a) NSTPDC provides information about partial correlative short-time interaction

properties of non-stationary signals, with f as the frequency and n the number of windows

$$\pi_{ij}(f,n) = \frac{\bar{A}_{ij}(f,n)}{\sqrt{\bar{a}_j^H(f,n)\bar{a}_j(f,n)}} \tag{53}$$

The basis of the NSTPDC represents an m-dimensional AR model with the order p and allows determining linear Granger causality in the frequency domain for bivariate as well as multivariate coupled systems. For the selection of the optimal model order p_{opt} of the AR model and its coefficients I applied the stepwise least squares algorithm (Neumaier & Schneider, 2001) and the Schwarz's Bayesian Criterion (SBC) (Schneider & Neumaier, 2001).

The basic features of the NSTPDC approach I co-developed are to determine the coupling direction and coupling strength. For the determination of the causal coupling direction I introduced a Normalized Factor (eq. 57, 58), and for the determination of the coupling strength I applied a trapezoidal numerical integration function to approximate the areas generated in space by the underlying coupling factor (eq. 54). Moreover, I introduced a normalization procedure (eq. 59) to address the problems of stationarity and scale-invariance of the investigated time series.

3.3.2 Coupling direction – Normalized factor

To estimate the coupling direction between two time series, x and y with the covariate z I introduced a coupling factor (CF). The NSTPDC approach works in principle like that CF (eq. 54) was derived by dividing the mean value $\pi_{xy}(f,n)$ (eq. 55) by the mean value of $\pi_{yx}(f,n)$ (eq. 56).

$$\mathrm{CF} = \frac{\frac{1}{n}\sum \pi_{xy}(f,n)}{\frac{1}{n}\sum \pi_{yx}(f,n)} \tag{54}$$

$$\overline{a} = \frac{1}{n}\sum \pi_{xy}(f,n) \tag{55}$$

$$\overline{b} = \frac{1}{n}\sum \pi_{yx}(f,n) \tag{56}$$

Afterwards, I introduced the Normalized Factor (NF) (eq. 57, 58) that normalized the results of CF to characterises the coupling direction.

$$\max(\overline{a}, \overline{b})$$

$$\mathrm{NF} = \begin{cases} 2, if\ \left(max = \overline{a}\ \&\ \frac{\overline{a}}{\overline{b}} > 5\right) \\ 1, if\ (max = \overline{a}\ \&\ 2 < \frac{\overline{a}}{\overline{b}} \leq 5) \\ 0, if\ (max = \overline{a}\ \&\ 0 \leq \frac{\overline{a}}{\overline{b}} \leq 2) \end{cases} \tag{57}$$

$$\mathrm{NF} = \begin{cases} -2, if\ \left(max = \overline{b}\ \&\ \frac{\overline{b}}{\overline{a}} > 5\right) \\ -1, if\ (max = \overline{b}\ \&\ 2 < \frac{\overline{b}}{\overline{a}} \leq 5) \\ 0, if (max = \overline{b}\ \&\ 0 \leq \frac{\overline{b}}{\overline{a}} \leq 2) \end{cases} \tag{58}$$

Thereby, NF={−2, −1, 0, 1, 2} allows for the determination of the causal coupling direction between the set of time series (x and y, with covariate z) as a function of frequency f (**Figure 15**).

Coupling direction:

- NF={−2 ∣ 2} (where −2 denotes y as the driver):

  Strong unidirectional coupling

- NF={−1.5, < −2} or NF={1.5, < 2}:

  Weak unidirectional coupling

- NF={−1 ∣ 1} (−1 denotes y as the driver):

  Strong bidirectional coupling

- NF={−0.5, < −1} or NF={0.5, < 1}:

  Weak bidirectional coupling, and

- NF=0:

  Equal influence in both directions and/or no coupling in respect to the coupling strengths (If both area indices reveal equal values larger than zero an equal influence in both directions is present if both area indices reveal equal values but are zero no coupling is present).

- NF={> 1, < 1.5} or NF={> −1, < −1.5}:

  Not clearly determinable.

NF allows the differentiation between uni- and bidirectional couplings and if these couplings are of weak or strong origin.

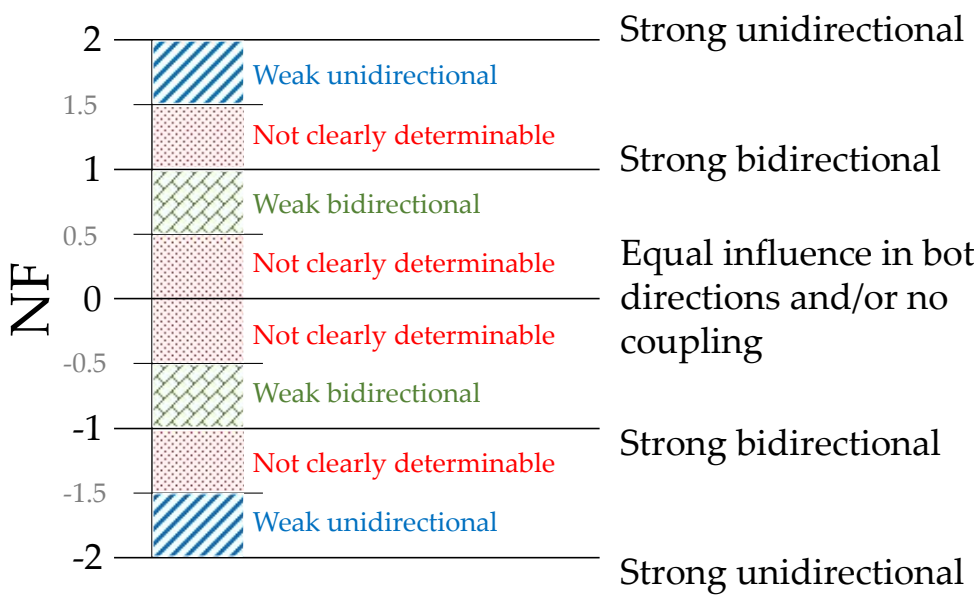

Figure 15. *Normalized Factor (NF) direction derived from the normalized short-time partial directed coherence approach for the determination of the causal coupling.*

3.3.3 Coupling strength – Areas

For determining the coupling strength between two time series x and y with covariate z I calculated the areas ($A_{x\to y(z)}$, $A_{y\to x(z)}$, [a.u.]). Therefore, I applied a trapezoidal numerical integration function to approximate the areas generated in space by CF in each window within the frequency band (f=0-2 Hz) which were afterwards averaged. $A_{x\to y(z)}$ and $A_{y\to x(z)}$ ranges between 0 and 1 [0,1].

Coupling strength:

- $A_{x\to y(z)} = 1$:
  Indicates that all causal influence originating from time series x are directed toward (→) time series y

- $A_{y\to x(z)} = 1$:
  Indicates that all causal influence originating from time series y are directed toward (→) time series x

- $A_{x\to y(z)} = 0$ and $A_{y\to x(z)} = 0$:
  Indicates that no causal influence between time series x and y exists

In order to take advantage of the aspect of stationarity and scale-invariance for NSTPDC analyses, I applied a normalization procedure (zero mean and unit variance) of the time series (Schulz et al, 2015a). Therefore, each sample i of the time series $x = \{x_i, i = 1, \dots N\}, y = \{y_i, i = 1, \dots N\}$ and $z = \{z, i = 1, \dots N\}$ with N as the

maximal number of samples i (temporal index) were first normalized by subtracting the mean of $\bar{x}$ and, then divided by the standard deviation (std) of x or y and z respectively. Thus, I obtained the normalized time series x_{norm}, y_{norm} and z_{norm} (eq. 59) with zero mean and unit variance:

$$x_{\mathrm{norm}}(i) = \frac{x(i)-\bar{x}}{\mathrm{std}(x)},\ y_{\mathrm{norm}}(i) = \frac{y(i)-\bar{y}}{\mathrm{std}(y)} \text{ and } z_{\mathrm{norm}}(i) = \frac{z(i)-\bar{z}}{\mathrm{std}(z)}. \quad (59)$$

For the determination of the NSTPDC indices I applied a window (Hamming) of lengths l, where each window n was shifted by 25% of l per each iteration step.

3.3.4 Simulations

3.3.4.1 Simple coupled oscillators

In a first very simple simulation, I applied the Wolfram Demonstrations Project, "Coupled Oscillators" (Domke, 2011) to simulate two simple cases of coupled time series of 1000 samples length (**Figure 16**).

For the first simulation, I considered two simulated signals (**Figure 16**, ***a***) from an idealized system with two oscillators coupled together by a third one (first time series=driver; second time series=responder). The NF value was 2 (**Figure 16**, ***b***) in all windows over time, clearly indicating strong unidirectional coupling with x as the driver and y as the responder, as already simulated.

For the second simulation (**Figure 16**, ***c***), I applied the same time series, but the coupling direction was changed after 800 samples. Thereby, the second time series became the driving time series and the first time series became the responder. The NF value was 2 (**Figure 16**, ***d***) up to n=14 windows and changed to –2 (n=16 ≙ 800 samples) indicating a strong unidirectional coupling with x as the driver and y as the responder for 800 samples, and changed afterwards to strong unidirectional coupling with y as the driver and x for 200 samples as the responder, as already simulated.

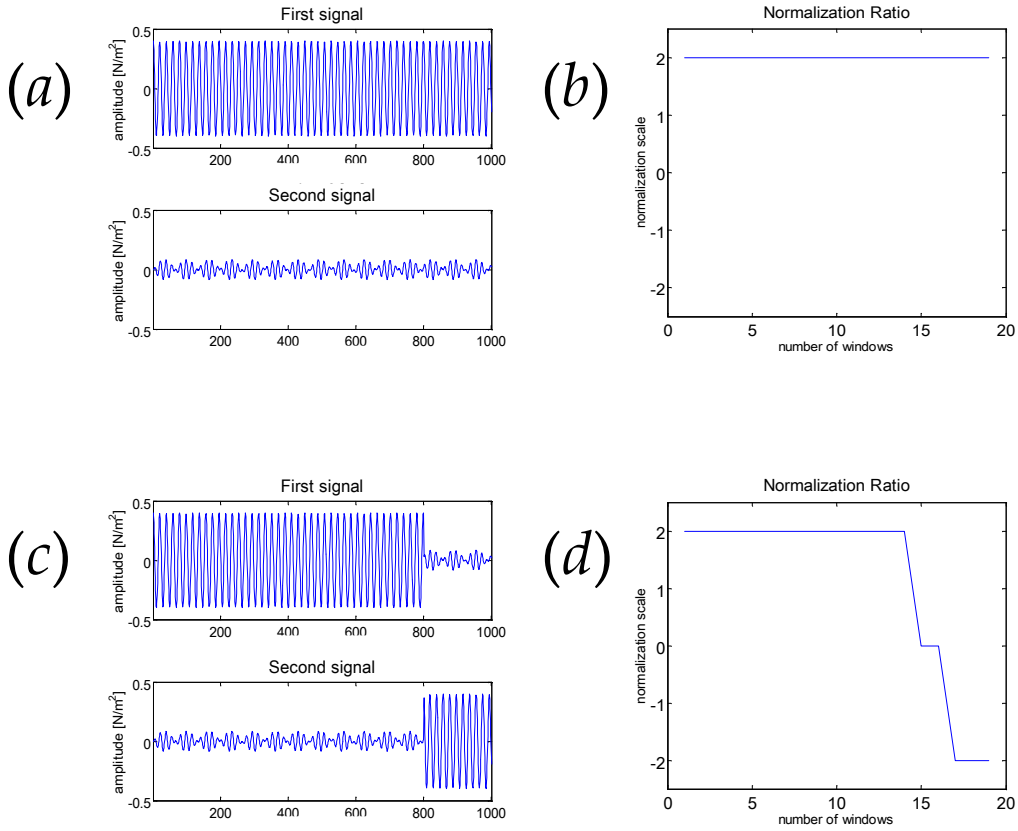

Figure 16. *Simulation of coupled oscillators. (a) showed the simulated input signals where the first time series is the driver and the second time series is the responder; (b) Normalized factor for the coupling direction resulting from (a); (c) showed the simulated input signals where the first time series is the driver that changed to the responder after 800 samples and the second time series is the responder that changed to the driver after 800 samples; (d) Normalized factor for the coupling direction resulting from (c).*

3.3.4.2 Multivariate coupled linear and non-linear systems

For the coupled linear and the non-linear system three different multivariate coupled AR models were applied (see 3.1.4.1) with different mutual influences (unidirectional, bidirectional) between the time series (**Figure 5**). From these simulated systems the NF was derived and determined (**Table 7**).

In Table 7 the results of the 3 coupled linear systems (LS1, LS2, LS3) and the 3 coupled non-linear systems (NLS1, NLS2, NLS3) are shown. Here, the simulated driver-response relationship, the type of coupling (linear or non-linear), the applied AR model (linear or non-linear) and the detected NF and driver-response relationship, and the characteristics of the coupling direction (weak, strong, unidirectional, bidirectional).

Table 7. *Results of coupled multivariate linear and non-linear AR models to validate the Normalized Factor (NF). (blue: driver variable, red: incorrect classification)*

System	Simulated driver-response relationship	Coupling	AR model	NF	Detected driver-response relationship	Characteristic of the coupling direction
LS1	1→2	linear	linear	2.0	1=driver	Strong unidirectional
	1→3			2.0	1=driver	Strong unidirectional
LS2	1→2	linear	linear	2.0	1=driver	Strong unidirectional
	1→3			2.0	1=driver	Strong unidirectional
	2→3			1.8	2=driver	Weak unidirectional
LS3	1→2	linear	linear	2.0	1=driver	Strong unidirectional
	1→3			2.0	1=driver	Strong unidirectional
	2⇄3			-0.5	3=driver	Weak bidirectional
NLS1	1→2	non-linear	non-linear	1.0	1=driver	Strong bidirectional
	1→3	linear		2.0	1=driver	Strong unidirectional
NLS2	1→2	non-linear	non-linear	1.4	1=driver	not determinable
	1→3			2.0	1=driver	Strong unidirectional
	2→3			2.0	2=driver	Strong unidirectional
NLS3	1→2	non-linear	non-linear	1.5	1=driver	Weak unidirectional
	1→3			2.0	1=driver	Strong unidirectional
	2⇄3			1.5	2=driver	Weak unidirectional

Coupled multivariate linear AR model:

Linear system 1, LS1 (Figure 5, *a*):

$x_1 \rightarrow x_2$: NF=2; correct classification of a strong unidirectional coupling direction with x_1 as the driver.

$x_1 \rightarrow x_3$: NF=2; correct classification of a strong unidirectional coupling direction with x_1 as the driver.

Linear system 2, LS2 (Figure 5, *b*):

$x_1 \rightarrow x_2$: NF=2; correct classification of a strong unidirectional coupling direction with x_1 as the driver.

$x_1 \rightarrow x_3$: NF=2; correct classification of a strong unidirectional coupling direction with x_1 as the driver.

$x_2 \rightarrow x_3$: NF=1.8; correct classification of a weak unidirectional coupling direction with x_2 as the driver.

Linear system 3, LS3 (Figure 5, *c*):

$x_1 \rightarrow x_2$: NF=2; correct classification of a strong unidirectional coupling direction with x_1 as the driver.

$x_1 \rightarrow x_3$: NF=2; correct classification of a strong unidirectional coupling direction with x_1 as the driver.

$x_2 \rightleftarrows x_3$: NF=–0.5; correct classification of a weak bidirectional coupling direction with x_3 as the driver (**Figure 17**).

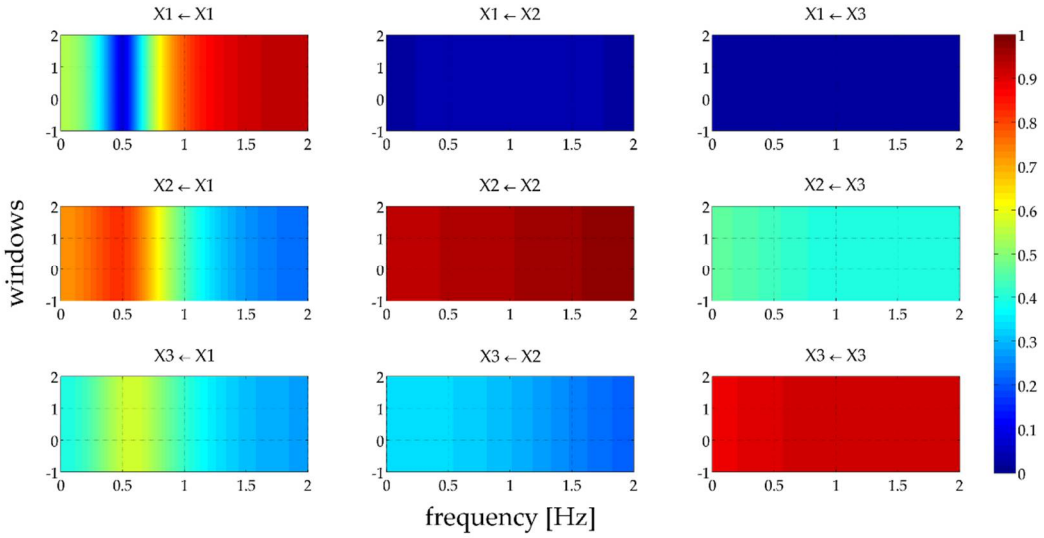

Figure 17. *Averaged NSTPDC plots for the simulated linear system 3. Arrows indicating the causal coupling direction from one time series to another, e.g., $x_2 \leftarrow x_1$, indicating the causal link from x_1 to x_2. Coupling strength ranges from blue (no coupling) to red (maximum coupling).*

Figure 17 shows the results of the averaged NSTPDC plots for the linear system 3. Each plot contain the causal coupling direction (←) from one time series to another, and the related coupling strength (ranging from 0 to 1).

Coupled multivariate non-linear AR model:

Non-linear system 1, NLS1 (Figure 5, *a*):

! $x_1 \rightarrow x_2$: NF=1; correct classification of the driver-response relationship with x_1 as the driver but incorrect classification of the coupling direction characteristic as strong bidirectional (simulated: strong unidirectional)

$x_1 \rightarrow x_3$: NF=2; correct classification of a strong unidirectional coupling direction with x_1 as the driver.

Non-linear system 2, NLS2 (Figure 5, *b*):

! $x_1 \rightarrow x_2$: NF=1.4; correct classification of the driver-response relationship with x_1 as the driver but not clearly determinable classification of the coupling direction characteristic (simulated: unidirectional).

$x_1 \rightarrow x_3$: NF=2; correct classification of a strong unidirectional coupling direction with x_1 as the driver.

$x_2 \rightarrow x_3$: NF=2; correct classification of a strong unidirectional coupling direction with x_2 as the driver.

Non-linear system 3, NLS3 (Figure 5, *c*):

$x_1 \rightarrow x_2$: NF=1.5; correct classification of the driver-response relationship with x_1 as the driver with a weak unidirectional coupling direction characteristic.

$x_1 \rightarrow x_3$: NF=2; correct classification of a strong unidirectional coupling direction with x_1 as the driver.

! $x_2 \rightleftarrows x_3$: NF=1.5; correct classification of the driver-response relationship with x_2 as the driver but incorrect classification of the coupling direction characteristic as weak unidirectional (simulated: bidirectional)

3.3.5 Summary of Normalized Short Time Partial Directed Coherence

I proposed the NSTPDC approach as an improvement of the standard PDC approach to overcome its restrictions, and to allow a better classification of the coupling strength and direction in multivariate linear and non-linear systems.

The NSTPDC approach is based on an m-dimensional AR model with the order p and allows determining linear Granger causality in the frequency domain for bivariate as well as multivariate coupled systems. The optimal model order p_{opt} of the AR model and its coefficients were determined by the stepwise least squares' algorithm and the Schwarz's Bayesian Criterion.

The NSTPDC approach is able to investigate couplings of short non-stationary and scale-invariant time series (which are the most biosignals) using a normalization procedure (zero mean and unit variance).

The introduced Normalized Factor (NF) allows a clear and differentiable characterization of the coupling direction (strong uni- or bidirectional coupling; weak uni- or bidirectional coupling; equal coupling influence in both directions and/or no coupling; not clearly determinable coupling direction).

The coupling strength was determined by a trapezoidal numerical integration function approximating area generated in space in each window within a frequency band. The coupling strength ranges between 0 and 1 [0,1].

The NSTPDC approach can distinguish between both direct and indirect causal information transfer.

The NSTPDC approach is very sensitive in detecting the correct driver-responder relationships in multivariate linear coupled systems, but is only partly able to detect the correct driver-responder relationships in non-linear coupled systems. This means that for purely nonlinear systems, a bias could arise if only the NSTPDC approach is applied, and thus misclassification could occur. Due to this limitation, in detailed investigations to determine the driver-responder relationships, other methods should be used in addition to the NSTPDC approach (e.g. MuTe), which are able to determine the driver-response relationships in non-linear systems.

3.4 Summary and discussion of the novel coupling analyses methods

3.4.1 High Resolution Joint Symbolic Dynamics

The new introduced HRJSD approach which is based on a redundancy reduction strategy to group single word types into 8 pattern families allows a new detailed quantification of bivariate short-term autonomic coupling patterns. This redundancy reduction strategy and the bivariate pattern family density matrix as novel features allows for a more robust statistical analysis of autonomic regulatory processes than already existing symbolization approaches (JSD, SCT). Thereby, my bivariate redundancy reduction strategy based on the idea of the classification of frequent deterministic patterns overcomes classical univariate symbolization strategies and creates a bridge between univariate and bivariate symbolic analyses so far. As new outstanding features in contrast to the standard JSD and SCT. The HRJSD approach emphasizes a clear characterization of how the couplings are composed by regulatory aspects of the ANS; is able to quantify the coupling direction (directionality index: D_{HRJSD}) in linear and partly in non-linear coupled systems which was not possible with existing symbolization approaches neither for bivariate nor for multivariate systems; and assesses the driver-response relationships in bivariate (n=2) and multivariate (n=3) systems. However, due to this limitation to determine the coupling direction only partly in non-linear coupled systems, other methods should be used in addition to D_{HRJSD} (e.g. MuTe), which can also correctly determine the dominant driver-response relationships in pure non-linear systems.

Due to, that the JSD and the SCT approach apply only 2 symbols and a threshold l=0 for the symbol coding decreased and equilibrium changes between two successive intervals (e.g. BBI) were coded with the same symbol and therefore miss important aspects of regulatory aspects of the system under investigation. The HRJSD approach overcomes this limitation by using 3 symbols and different threshold levels l≠0 based on individual dynamic variability and physiological settings. Thereby, it is possible to differentiate between noise, artefacts or ectopic events) and fluctuations that arise from (patho)physiological regulatory processes. Here, I was able clearly to demonstrate that the threshold level based on the non-invasive estimation of the spontaneous baroreflex sensitivity is superior to standard non-invasive baroreflex sensitivity analysis and the JSD approach in uncovering detailed changes of short-term cardiovascular regulation (family patterns), and that the threshold with 25% of the standard deviation of individual cardiorespiratory time series (dynamical threshold level) reveals specific cardiorespiratory coupling patterns, which cannot be detected with other symbolization approaches.

3.4.2 Multivariate High Resolution Joint Symbolic Dynamics

As a further enhancement to already existing symbolization approaches (JSD, SCT, HRJSD) I introduced the multivariate high-resolution joint symbolic dynamics approach (mHRJSD) that overcome the limitation of the previously introduced HRJSD approach. The HRJSD approach and other symbolization approaches are only able to analyse bivariate couplings, whereas the HRJSD approach is also able to determine the driver-responder relationship; facing this, the mHRJSD approach is able to quantify multivariate couplings and to determine the dominant driver-responder relationship in multivariate coupled systems. These are outstanding new features for coupling analyses based on symbolizations. To enable the multivariate analyses based on a coarse graining of the dynamics of the time series under investigation the mHRJSD approach includes a third time series enables multivariate time series coupling analyses. In addition, a statistical significance level (Bonferroni-Holm adjusted) for the probabilities of occurrences of the coupling pattern has been introduced to exclude and prevent unwanted couplings. As outstanding and unique features of the mHRJSD approach are the implemented multivariate directionality indices D_{mHRJSD} ($D_{\mathrm{mHRJSD}}(x,y|z)$, $D_{\mathrm{mHRJSD}}(x,z|y)$, and $D_{\mathrm{mHRJSD}}(y,z|x)$). These indices enabling the determination of a primary- and secondary driver, the dominant responder and direct causal information transfer within a multivariate coupled systems.

The introduced multivariate redundancy reduction strategy in combination with the multivariate directionality indices provide more detailed information about short-term physiological regulatory processes of complex linear multivariate networks than the exiting symbolization approaches and partly other bivariate coupling approaches can do.

3.4.3 Normalized Short Time Partial Directed Coherence

The introduced NSTPDC approach represents a clear improvement of the standard PDC and the time-variant PDC (tvPDC) by overcoming their restrictions and limitations. The NSTPDC approach allows a better classification of the coupling strength and coupling direction of short-term multivariate, non-stationary, scale-invariant, linear and non-linear (only partly possible) coupled time series through the introduced Normalized Factor and the normalization procedure (zero mean and unit variance). Since the NSTPDC approach is only partly able to detect the correct driver-responder relationships in non-linear coupled systems a bias could arise if only the NSTPDC approach is applied, and thus misclassification could occur. Due to this limitation, in detailed investigations other methods should be used in addition to the

NSTPDC approach (e.g. MuTe), which are able to determine the driver-response relationships in non-linear systems.

As outstanding new features of the NSTPDC approach for coupling analyses in contrast to other coupling approaches (LGC, F-test, Wald-test, MDA, PDC versions, DFT) that are asses linear Granger causality in the time- and frequency domain; it provides a clear normalized and defined measure for the coupling strength ranging between 0 and 1, and a clear and differentiable characterization of the coupling direction (strong or weak, unidirectional or bidirectional, not clearly determinable). Moreover, the NSTPDC approach can distinguish between both direct and indirect causal information transfer that is only restricted to other linear Granger causality based approaches.

Chapter 4

4. Analyses of the central-autonomic-network in schizophrenia

The following content was previously published in:

Schulz, S., Haueisen, J., Bär, K. J. & Voss, A. (2019) Altered Causal Coupling Pathways within the Central-Autonomic-Network in Patients Suffering from Schizophrenia. Entropy, 21(8), 733.

Schulz, S., Haueisen, J., Bär, K. J. & Voss, A. (2018) Multivariate assessment of the central-cardiorespiratory network structure in neuropathological disease. Physiol Meas, 39(7), 074004.

Schulz, S., Bolz, M., Bär, K. J., and Voss, A. (2018) Quantification of the Central Cardiovascular Network Applying the Normalized Short-time Partial Directed Coherence Approach in Healthy Subjects. Methods Inf Med 57, 129-134.

Schulz, S., Bolz, M., Bär, K. J. & Voss, A. (2016) Central- and autonomic nervous system coupling in schizophrenia. Philos Trans A Math Phys Eng Sci, 374(2067), 20150178.

4.1 Materials and Methods

4.1.1 Overview

The interdisciplinary field of Network Physiology is getting more and more into the focus of interest in medicine (Bartsch et al, 2015). It aims to characterise healthy and diseased states by analysing structural, dynamical and regulatory alterations in the interaction of physiological systems and sub-systems, and bridging the genetic and sub-cellular level with intercellular interactions and communications among integrated organ systems and sub-systems (Ivanov et al, 2016).

In this study I aimed to characterise short-term instantaneous central-autonomic-network coupling pathways (top-to-bottom and bottom-to-top) by analysing the interaction of heart rate, systolic blood pressure, respiration and central activity in schizophrenic patients. Therefore, I applied the new developed as already established causal and non-causal, linear and non-linear multivariate coupling approaches (HRJSD, mHRJSD, NSTPDC, MuTE) that are able to determine coupling strengths and directions within the CNS-ANS network. I believe that these findings are of importance for a full comprehension of (patho)physiological regulation processes and might allow improvement in treatment strategies in schizophrenic patients, and finally, possibly contribute to cardiac risk stratification strategies able to identify those patients at higher risk for cardiovascular disease.

4.1.2 Subjects

For this investigation, 17 patients with paranoid schizophrenia (SZO; 2 females, 37.5±10.4 years) and 17 healthy subjects as controls (CON; 4 females, 37.7±13.1 years) were enrolled. The diagnosis of schizophrenia was reached through an assessment of patient-specific signs and symptoms, as described in the Diagnostic and Statistical Manual of Mental Disorders, 4th edition (DSM-IV) (Bell, 1994). The positive and negative syndrome scale was applied to quantify psychotic symptoms. Depot antipsychotic medication (77% being atypical neuroleptics [Seroquel, Risperdal, Olanzapin, Leponex, Seroquel, Zypadhera, Clozapin, Xeplion, Solian], and 23% being a mixture of antidepressant and atypical neuroleptics [Remergil, Zyprexa, Haloperidol, Seroquel, Flunxol, Leponex]) were used to treat SZO. Thorough interviews and clinical investigations were performed for CON to exclude any potential psychiatric (DSM-IV) or other diseases, as well as to double-check for any interfering medication. The structured clinical interview and a personality inventory (Freiburger Persönlichkeitsinventar a factor-analytically and item-metrically based method) were also applied to CON to detect personality traits and any disorders which might influence autonomic function (LeBlanc et al, 2004). The written informed consent to a protocol approved by the local ethics committee of the Jena University

Hospital was provided by all subjects. This study complies with the Declaration of Helsinki.

4.1.3 Data recordings and pre-processing

For all schizophrenic patients and healthy subjects, a 3-channel ECG (500 Hz), a synchronized non-invasive continuous blood pressure (200 Hz, photoplethysmography (volume-clamp), Portapres Model-2, TNO Biomedical Instrumentation, Netherlands), a calibrated respiratory inductive plethysmography signal (LifeShirt®, Vivometrics, Inc., Ventura, CA, USA), and a 64-channel EEG were recorded synchronously for 15 minutes. An extended 10-20-system using an electrode cap of 64 active Ag/AgCl electrodes was used to acquire the EEG (Brain Products, Germany, AFZ: ground, FCZ: reference, 500 Hz). The impedance levels (<25 KΩ) were checked for each electrode before starting recordings. Investigations were performed between 14.00 and 18.00 in a quiet room that was kept comfortably warm (22–24°C) and began after subjects had rested in a supine position for 10 min. Subjects were asked to close their eyes, relax and breathe normally to avoid hyperventilation.

The following time series with respect to autonomous regulation were automatically extracted from the raw data records (using in-house software; programming environment DELPHI v. 3 and MatlabR2011b):

- Time series of HR (lead I) consisting of successive beat-to-beat intervals (BBI, (msec)),
- Time series consisting of the maximum successive systolic blood pressure amplitude values over time in relation to the previous R-peak (the given RR-interval) (SYS, (mmHg)), and
- Time series of respiratory frequency (RESP, (sec)) as time intervals between consecutive breathing cycles.

With respect to each extracted BBI(i) from the ECG raw data the related time intervals EEG(i) (msec) from EEG raw data were extracted. Within each EEG(i), with i (i=1:R–1) as the successive number of R-peaks (R), the mean power $P_{EEG}(i)$ (μV^2) of EEG(i) was derived representing time series of EEG activity (Schulz et al, 2016) (**Figure 18**) (eq. 60).

$$P_{EEG}(i) = \frac{1}{T} \sum_{j=t(i)\times fs}^{t(i+1)\times fs} |EEG(j)|^2 \quad (60)$$

with T representing the number of samples within BBI(i) or EEG(i), respectively; $t(i)$ represents the current point in time of BBI(i) and fs represents the sampling frequency.

For the central-cardiovascular-network from the EEG raw data recordings, new time series consisting of the EEG spectral band components as delta (0.5–3.5 Hz), theta (3.5–7.5 Hz), alpha (7.5–12.5 Hz), alpha1 (7.5–9.5 Hz), alpha2 (9.5–12.5 Hz), beta (12.5–25 Hz), beta1 (12.5–17.5 Hz), beta2 (17.5–25 Hz) and gamma (25–60 Hz) activity were derived (Butterworth filter, order=3) for each electrode. For example, for the EEG channel Fp1 (EEG_{Fp1}) the 9 time series as $EEG_{Fp1\delta}$, $EEG_{Fp1\theta}$, $EEG_{Fp1\alpha}$, $EEG_{Fp1\alpha1}$, $EEG_{Fp1\alpha2}$, $EEG_{Fp1\beta}$, $EEG_{Fp1\beta1}$, $EEG_{Fp1\beta2}$ and $EEG_{Fp1\gamma}$ were obtained. All EEG recordings (pre-processing) were band-pass filtered (0.05-60 Hz, Butterworth filter, order=3) to eliminate slow drifts coming from slow body movements or sweating, and to exclude noise resulting from higher frequency contents. For the quantitative EEG analysis. EEG time series were visually inspected and automatically classified as artefact-free applying the Brain Products Software Analyzer 2.0 to get artefact-free time series (Delorme & Makeig, 2004; Maiorana et al, 2016; Tong & Thakor, 2009).

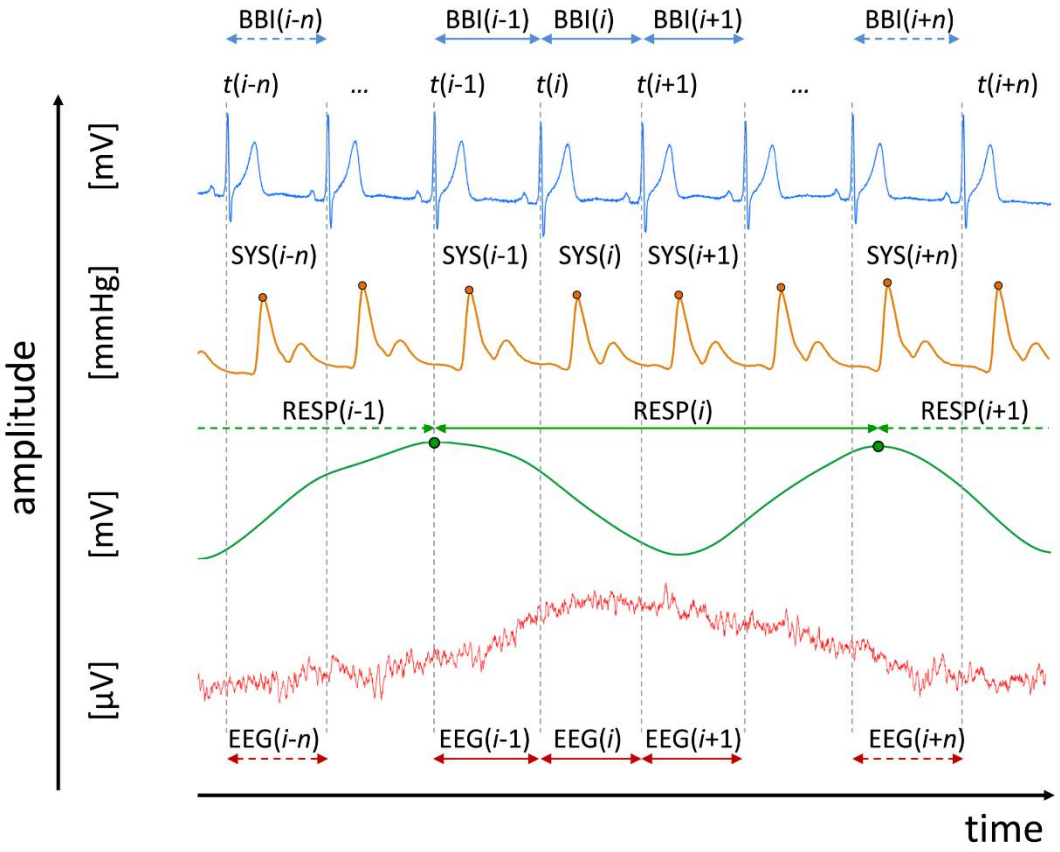

Figure 18. *Visualization example of analysed raw data records and their extracted time series. Raw data are, from top to bottom: ECG, non-invasive continuous systolic blood pressure (SYS), synchronized calibrated respiratory inductive plethysmography signal (RESP), and electroencephalogram (EEG). RR(i) represents the beat-to-beat intervals, SYS(i) represents the maximum systolic blood pressure amplitude values over time in relation to the previous R-peak, RESP(i) represents the respiratory frequency as time intervals between consecutive breathing cycles, and EEG(i) specified the time intervals of the EEG raw data (electrode: Fp2) in relation to BBI(i). Within each EEG(i) the mean power $P_{EEG}(i)$ was calculated.*

All extracted time series were adaptive filtered (adaptive variance estimation algorithm (Wessel et al, 2000) to exclude and interpolate ventricular premature events and/or artefacts to obtain normal-to-normal beat time series (NN). For coupling analyses all time series (BBI, SYS, RESP, and P_{EEG}) were synchronized and resampled with a linear interpolation algorithm (2 Hz).

For central-cardiovascular network analyses, three areas with the corresponding EEG channels were analysed, as:

- The frontal area (Fp1, Fp2, AF3, AF4, AF7, AF8, Fz, F1-F8, FC1-FC6, FT7-FT10),
- The left frontal area (Fp1, AF3, AF7, F1, F3, F5, F7), and
- The right frontal area (Fp2, AF4, AF8, F2, F4, F6, F8). (**Figure 19**)

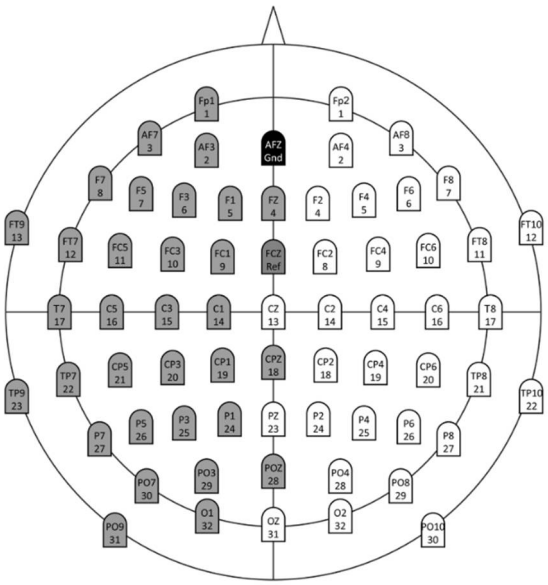

Figure 19. *The applied extended 10-20 EEG system (actiCAP, Brain Products) for central-autonomic-network analyses. (grey marked channels belong to the left hemisphere and white marked channels belong to the right hemisphere, AFZ=ground (black), FCZ=reference (dark grey))*

For central-cardiorespiratory network analyses, five areas with the corresponding EEG channels were analysed, as:

- A0: All EEG channels (n=64),
- A1: The frontal area (Fp1, Fp2, AF3, AF4, AF7, AF8, Fz, F1-F8),
- A2: The central area (FC1-FC6, FCZ, C1-C6, CZ, CP1-CP6, CPZ),
- A3: The temporal area (FT7-FT10, T7, T8, TP7-TP10), and
- A4: The parietal-occipital area (P1-P8, PZ, PO3, PO4, PO7-PO10, POZ, O1, O2, OZ). (**Figure 19**)

Performing central-autonomic coupling analyses, the autonomic time series (e.g. BBI and RESP) were combined with all EEG channels, and averaged from each subject. For example, when coupling heart rate (BBI) with the mean power of EEG (P_{EEG}) (e.g. temporal area), 10 different coupling combinations per subjects of BBI-P_{EEG}(FT7), BBI-P_{EEG}(FT8), BBI-P_{EEG}(FT9), BBI-P_{EEG}(FT10), …, BBI-P_{EEG}(TP10) were obtained. These 10 combinations were analysed applying the coupling approaches HRJSD, mHRJSD, NSTPDC and MuTE. Furthermore, for each combination, the methods related indices were derived and averaged for each subject.

4.1.4 Standard indices

Electroencephalogram in the frequency domain

From the EEG raw data the power spectral density (PSD) function (window length=5 sec, overlap=50%) applying an autoregressive model (Welch's method) (Tong & Thakor, 2009) was used to estimate the mean power (P; 0.5–60 Hz) to quantify the electroencephalogram.

Additionally, for the central-cardiovascular-network: delta (P_{δ}: 0.5–3.5 Hz), theta (P_{θ}: 3.5–7.5 Hz), alpha (P_{α}: 7.5–12.5 Hz), alpha1 ($P_{\alpha 1}$: 7.5–9.5 Hz), alpha2 ($P_{\alpha 2}$: 9.5–12.5 Hz), beta (P_{β}: 12.5–25 Hz), beta1 ($P_{\beta 1}$: 12.5–17.5 Hz), beta2 ($P_{\beta 2}$: 17.5–25 Hz) and gamma (P_{γ}: 25–60 Hz) band power.

Heart rate-, blood pressure-, and respiratory variability in the frequency and time domains

Heart rate variability (HRV), blood pressure- (BPV) and respiratory variability (RESPV) were quantified by calculating standard parameters from time (TD) and frequency domains (FD) (Schulz et al, 2012a; Task Force, 1996; Voss et al, 2009) as:

- meanNN: The mean value of the NN intervals of BBI (msec), of systolic (SYS) blood pressure (mmHg) values, and RESP (sec) as respiratory cycle length;
- sdNN: The standard deviation of the NN intervals of BBI (msec), of systolic (SYS) blood pressure (mmHg) values, and RESP (sec);
- BF: The breathing frequency characterizing the number of breaths per minute (1/min);
- t_{in} and t_{ex}: Inspiration time and expiration time intervals for each breath cycle (sec);
- LF/HF: The ratio between the low- and high-frequency power spectrums (LF: 0.04–0.15 Hz, HF: 0.15–0.4 Hz) (a.u.) of BBI. In FD the power spectra of the time

series were estimated using the fast Fourier transform. The Blackman Harris window function was applied to avoid leakage effects.

Baroreflex sensitivity

The Dual Sequence Method (DSM) (Malberg et al, 1999) was applied to estimate the spontaneous baroreflex sensitivity based on the sequence technique. Here, a minimum change of 1 mmHg increase or decrease in SYS and 5 msec in BBI was defined as the inclusion criterion for a spontaneous baroreflex related cardiovascular oscillation. The slopes of the regression lines between SYS and BBI sequences were taken as an index for local BRS (msec/mmHg). Two kinds of BBI responses were derived:

- bslope: The slope of the regression line between all bradycardic baroreflex fluctuations (msec/mmHg), and
- tslope: The slope of the regression line between all tachycardic baroreflex fluctuations (msec/mmHg).

Respiratory Sinus Arrhythmia

Respiratory Sinus Arrhythmia (RSA) represents the coupling between the cardiac and respiratory system characterized by heart rate fluctuations that are in phase with inspiration and expiration (Grossman et al, 2004). RSA is based on the shortening BBI (cardiac acceleration) during inspiration and the lengthening of BBI (cardiac deceleration) during expiration. RSA is frequently employed as an index of cardiac vagal tone or even believed to be a direct measure of vagal tone (Grossman & Taylor, 2007). RSA was quantified in the time domain using the peak-to-valley approach (Grossman et al, 1990) (RSA_{P2V}, (msec)).

4.1.5 Central–autonomic coupling analyses

For the quantification of linear and non-linear central-autonomic couplings different approaches can be used (Schulz et al, 2013a). I analysed the information transfer between BBI, SYS, RESP and P_{EEG} time series with the normalized short-time partial directed coherence (NSTPDC) (Adochiei et al, 2013), the multivariate Transfer Entropy (MuTE) (Montalto et al, 2014), the high resolution joint symbolic dynamics (HRJSD) (Schulz et al, 2013c), and the multivariate version of HRJSD (mHRJSD) (Schulz et al, 2018; Schulz et al, 2017b).

4.1.6 Surrogate data

When applying non-linear analysis approaches, it must be considered that the linear properties of the signals, like e.g. autocorrelation or spectral features, are likely to affect the measure. To demonstrate the statistical validity of the obtained network pathways between CON and SZO, surrogate tests were performed to determine a threshold for statistical significance for the obtained results (Schreiber & Schmitz, 2000; Theiler et al, 1992). The idea behind this technique is to apply the non-linear method in question to independent time series that are the same or as close as possible to the statistical properties of the original time signals, while randomizing the expressions of the non-linear property to be measured. This procedure makes it possible to define a threshold below which any result is considered to be false. In practice, when deriving couplings even from very weakly coupled (or completely decoupled) systems, the methods always capture some nonzero values of the apparent coupling strength. Surrogate testing can then be used to establish the "zero-level" of apparent coupling corresponding to uncoupled signals (Stankovski et al, 2017). Therefore, for each subject (CON, SZO) and each original time series (BBI, SYS, RESP and P_{EEG}) 15 independent surrogates were derived by random permutation of the temporal structure of the original samples to remove any temporal relationship for the newly derived surrogate time series (CONsu, SZOsu). This technique preserves the linear structures of the signals, but changes the non-linear properties.

A statistical significance thresholds t_{su} was defined, beneath which any coupling result derived from the original time series is considered spurious. This threshold was calculated independently for each subject and then set as the mean+2*SD of the resultant distributions. As a result, I tested the couplings from the original time series by comparison with the significance threshold t_{su}. Hence, if couplings were higher (original time series) than t_{su}, and no significant differences between CONsu and SZOsu existed, then the null hypothesis was rejected, and significant couplings within the original time series were present. The non-parametric paired Mann-Whitney *U*-test was used to determine the significance of differences between the CONsu and SZOsu distributions. The test rejected the null hypothesis at significance level $p<0.00041$ (Bonferroni-Holm adjustment).

4.1.7 Statistics

Significant differences between CON and SZO were estimated applying the nonparametric exact two-tailed Mann-Whitney *U*-Test (SPPS 21.0). The significances were considered at $*p<0.05$, $**p<0.01$, $***p<0.00041$ (Bonferroni-Holm adjustment), and # not confirmed by surrogate analysis. Results in tables are presented as mean±SD. An overview of all performed analyses steps are presented in (**Figure 20**).

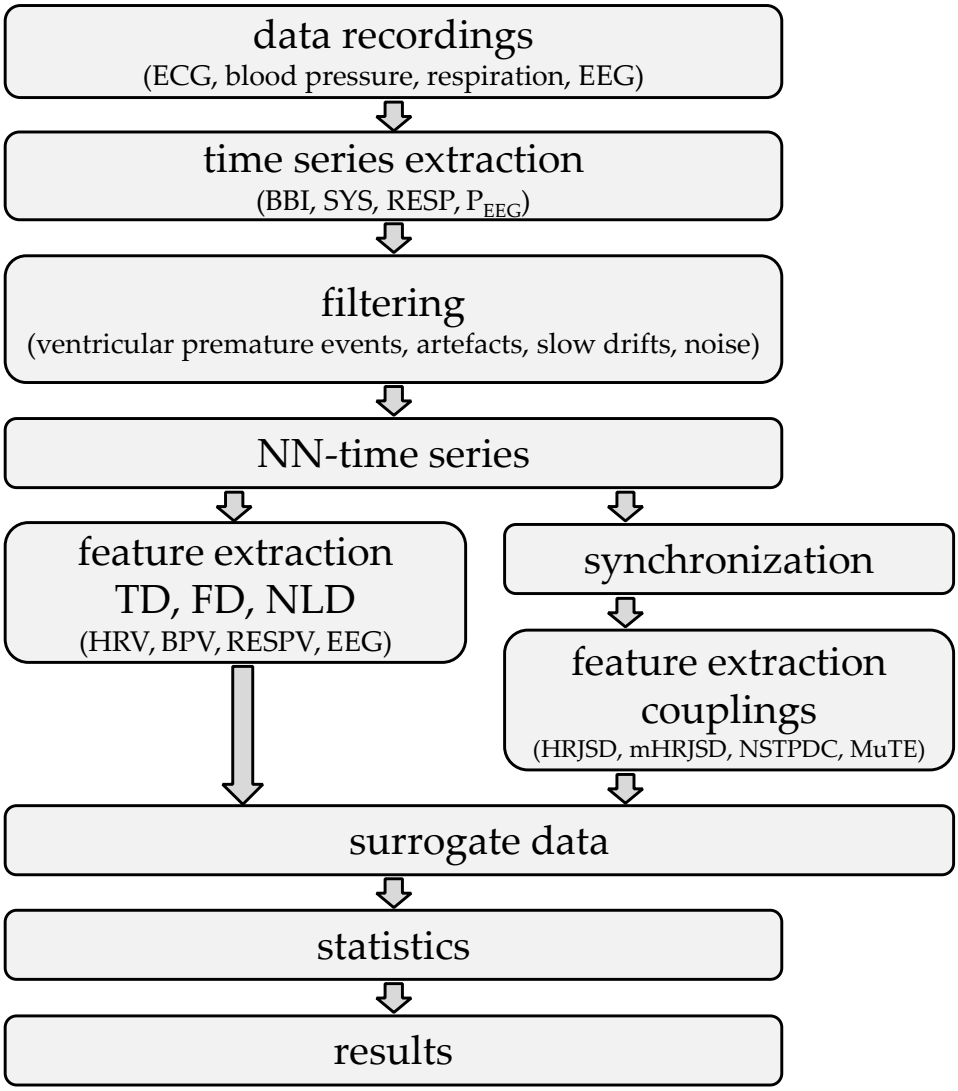

Figure 20. *Flowchart of performed analyses steps. (BBI represents the beat-to-beat intervals, SYS represents the maximum systolic blood pressure amplitude values over time in relation to the previous R-peak, RESP represents the respiratory frequency as time intervals between consecutive breathing cycles, P_{EEG} specified the mean power in the time intervals of the EEG raw data in relation to each BBI, NN: normal-to-normal beat interval, TD: time domain, FD: frequency domain, NLD: non-linear dynamics, HRV: heart rate variability, BPV: blood pressure variability, RESPV: respiratory variability, HRJSD: high resolution joint symbolic dynamics, mHRJSD: multivariate high resolution joint symbolic dynamics, NSTPDC: normalized short-time partial directed coherence, and MuTE: multivariate Transfer Entropy)*

4.2 The electroencephalogram in the frequency domain

4.2.1 Results for the central-cardiovascular areas

Considering EEG-related standard frequency domain spectral component indices, it was found that when comparing SZO with CON in terms of the frontal area, the left frontal area and the right frontal area, highly significant (p<0.00041) differences between both groups were apparent (**Table 8**). Thereby, a significant decrease in the mean power of all spectral bands (delta P_δ to gamma P_γ) and in the whole power P was obviously present for SZO in comparison with CON. In both groups, a lower power has been shown in the left frontal area when compared with the right frontal area.

Table 8. *Results of electroencephalogram (EEG) in the frequency domain which discriminates between paranoid schizophrenia patients (SZO) and healthy subjects (CON). (*p<0.05, **p<0.01, ***p<0.00041, n.s.=not significant)*

	Index	all frontal		left frontal		right frontal	
		CON	SZO	CON	SZO	CON	SZO
		mean ± std	mean ± std	mean ± std	mean ± std	mean ± std	mean ± std
EEG	P_δ	496 ± 761***	417 ± 1341	498 ± 805***	460 ± 1683	494 ± 711***	367 ± 793
	P_θ	64 ± 65***	40 ± 57	63 ± 67***	39 ± 62	65 ± 63***	40 ± 50
	P_α	56 ± 54***	17 ± 14	54 ± 54***	17 ± 14	58 ± 54***	18 ± 14
	$P_{\alpha1}$	34 ± 41***	10 ± 8.8	33 ± 40***	9.3 ± 8.8	35 ± 41***	10 ± 8.8
	$P_{\alpha2}$	20 ± 15***	5.8 ± 5.2	19 ± 16***	5.6 ± 5.6	21 ± 15***	6.0 ± 4.7
	P_β	47 ± 42***	14 ± 10	46 ± 47***	12 ± 9.4	49 ± 34***	15 ± 10
	$P_{\beta1}$	7.0 ± 4.9***	2.2 ± 1.5	6.8 ± 5.2***	2.0 ± 1.5	7.3 ± 4.5***	2.4 ± 1.6
	$P_{\beta2}$	12 ± 10***	3.4 ± 2.4	11 ± 10***	3.2 ± 2.3	12 ± 9.3***	3.7 ± 2.4
	P_γ	21 ± 32***	5.2 ± 5.7	20 ± 38***	4.5 ± 4.8	21 ± 23***	6.1 ± 6.5
	P	712 ± 886***	506 ± 1402	710 ± 933***	546 ± 1753	714 ± 831***	460 ± 843

4.2.2 Results for the central-cardiorespiratory areas

Considering EEG-related frequency domain spectral analyses I found for the comparison of SZO with CON for all areas (A0, A1, A2, A3, A4) highly significantly (p<0.00041) differences between both groups. Thereby, significant decreases in the mean power P of all areas were obviously present for SZO in comparison to CON (P_{A0}: SZO=357.8±732.8***; CON=820.6±860.8). For A2 SZO revealed the lowest power P, and for A3 and A4 CON showed the highest power P. In general, SZO showed comparable values for P for A1 to A4 (**Figure 21**).

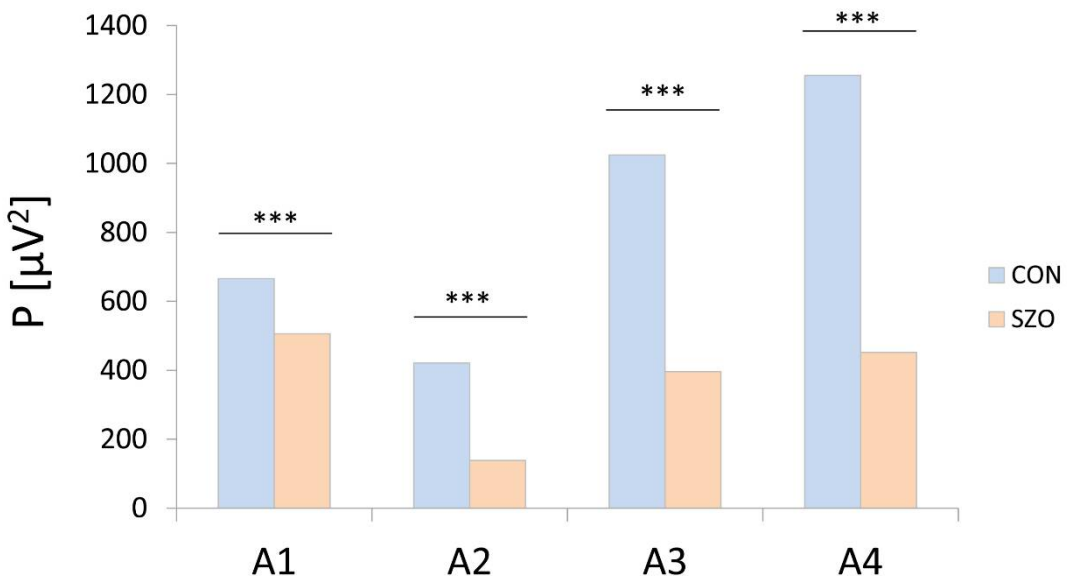

Figure 21. *Bars indicate average mean value of the power P derived from the EEG channels estimated by the power spectral density function (window length: 5 sec, overlap: 50%) for patients suffering from paranoid schizophrenia (SZO) and healthy subjects (CON) for A1 (the frontal area), A2 (the central area), A3 (the temporal area), and A4 (the parietal-occipital area). (*p<0.05; **p<0.01; ***p<0.00041; n.s.=not significant)*

4.2.3 Summary and discussion

4.2.3.1 The central-cardiovascular areas

The results of central activity (via EEG frequency analyses) showed a highly significantly reduced EEG activation (power) in all frequency bands for the frontal area, being much more pronounced in the right frontal hemisphere in SZO when compared to CON. MacCrimmon et al. (Maccrimmon et al, 2012) investigated the effects of the atypical antipsychotic (clozapine) among 64 SZO patients. They found that clozapine augments power globally in the δ and θ bands, but this effect was more pronounced over frontal areas. The authors could demonstrate a significant clozapine-induced α topographic shift frontally and to the right. They suggested further investigations of subcortical structures in the attempt to better understand the diverse aetiologies and optimal treatments of schizophrenia. Small et al. (Small et al, 1987) investigated chronic treatment-resistant patients in relation to placebo, haloperidol, chlorpromazine and clozapine treatment. They found increased frontal δ activity particularly with clozapine and chlorpromazine treatment. Nagase et al. (Nagase et al, 1996) investigated 12 medicated SZO patients, finding that α2 power and slow-wave power were reduced when compared to the neuroleptic-naive state. They concluded that the reduction in α power may occur from the early stage of the disease and progress even further, even though the patients are medicated and clinically improved. Kemali et al. (Kemali et al, 1992) found that after acute treatment,

patients showed a significant decrease of δ and an increase of θ2, β1, and β2. After 28 days of haloperidol treatment, similar changes were observed for δ, together with an increase of α1, and a decrease of fast β. Light et al. (Light et al, 2006) found that schizophrenia patients have frequency-specific deficits in the generation and maintenance of coherent γ-range oscillations, reflecting a fundamental degradation of the basic integrated neural network activity.

In general, γ responses in schizophrenic patients are not necessarily weakened. Depending on the status of the schizophrenic behaviour (negative or positive symptoms) and depending on the difficulty of the applied paradigm, an increase of γ activity may also be observed. Thus, the oscillatory dynamics in schizophrenia also depict the unstable behaviour of electrophysiology in this disease (Basar & Guntekin, 2008). Patients who were treated with clozapine and olanzapine revealed most prominent changes in the anterior cingulate and medial frontal cortex and a decrease in fast frequency activities in the occipital cortex. These results suggest a compensatory mechanism in the neurobiological substrate for schizophrenia (Tislerova et al, 2008). Unfortunately, at the moment, comparative studies between medicated and unmedicated patients are not available in the literature. This makes it difficult to assess the effectiveness of medication and the effect of central activity in schizophrenia patients. It has been shown in many studies on medicated and non-medicated patients that the γ response is lower in SZO patients when compared to healthy subjects (Basar & Guntekin, 2008; Horacek et al, 2006).

Nevertheless, it is strongly justified, based on available literature, to conclude that the δ excess (and to a lesser extent the θ excess) is a strong and bona fide biological marker for schizophrenia, as well as the fact that changes in EEG patterns are not medication-induced (Boutros et al, 2008).

4.2.3.2 The central-cardiorespiratory areas

The results of central activity demonstrated highly significantly reduced power in all clusters (A0-A4) in general, being much more reduced in A2 (central area) and highest in the frontal area (A1) in SZO when compared to CON. On the other side, CON revealed the highest power in A3 and A4 (temporal areas) whereas SZO showed a similar behaviour in all clusters. CON revealed highest EEG spectral power in the A4 area, which is typically related to deep resting or sleeping conditions.

This fact clearly supports these findings and other already published papers that SZO are characterized by an increased sympathetic tone instead of increased vagal tone. Moreover, one should consider that SZO patients were during data recording in acute psychotic state. In general, the central activity in SZO seems to be inhibited independent from local areas of the cortex, and that primary somatosensory cortex and primary visual cortex (A3, A4) are affected in this disease.

In general, the central activity in SZO seems to be inhibited independent from local areas of the cortex, and that primary somatosensory cortex and primary visual cortex (A3, A4) are affected in this disease. These findings are in accordance with the state of the art in literature. For instance, Brenner at al. (Brenner et al, 2009) stated that disruption of both auditory and visual steady state responses in schizophrenia are consistent with neuropathological and magnetic resonance imaging evidence of anatomic abnormalities affecting the auditory and visual cortices. Boning et al found somatosensory stimulation was associated with decreased activity in brain regions participating in an attentional network in SZO (Boning et al, 1989). Individuals with schizophrenia commonly exhibit a variety of symptoms related to the somatosensory system. Impairments related to somatosensory perception are also common, including fine motor touch, temperature, pain (nociception), movement, tension, and vibration (Huang et al, 2010). Impairments in early visual processing have been well documented in schizophrenia using methods, including steady-state and transient event-related potentials (ERP) approaches, along with fMRI, and lead to impairments in processes such as motion detection, object recognition, and reading (Javitt, 2009).

4.3 The cardiovascular and cardiorespiratory network

4.3.1 The cardiovascular network

4.3.1.1 Heart rate- and blood pressure variability

Significant differences between CON and SZO were demonstrated in the time domain of HRV analysis ($meanNN_{BBI}$, $sdNN_{BBI}$). SZO showed an increased heart rate (reduced $meanNN_{BBI}$ ↓) accompanied with reduced variability ($sdNN_{BBI}$ ↓) compared to CON (**Table 9**). The frequency domain index LF/HF was not significantly different between SZO and CON. Blood pressure variability analyses revealed significant difference between both groups in $meanNN_{SYS}$ (reduced in SZO compared to CON) (**Table 9**).

4.3.1.2 Baroreflex sensitivity

BRS measures bslope and tslope revealed significant differences between SZO and CON, namely significant decreases in the BRS measures bslope and tslope were shown for SZO compared to CON (**Table 9**).

Table 9. *Results of standard indices from heart rate variability (HRV), blood pressure variability (BPV), respiratory variability (RESPV), spontaneous baroreflex sensitivity (BRS), respiratory sinus arrhythmia (RSA) which discriminates between paranoid schizophrenia patients (SZO) and healthy subjects (CON). (*p<0.05, **p<0.01, ***p<0.00041, n.s.=not significant)*

	Index	CON			SZO		
		mean	**±**	**std**	**mean**	**±**	**std**
HRV	$meanNN_{BBI}$	904.2	±	153.0	709.4	±	104.7***
	$sdNN_{BBI}$	52.0	±	23.0	32.3	±	23.4*
	LF/HF	5.6	±	6.5	7.3	±	11.4
BPV	$meanNN_{SYS}$	134.9	±	19.8	121.4	±	15.4*
	$sdNN_{SYS}$	9.2	±	3.0	10.0	±	6.8
BRS	bslope	10.2	±	5.8	4.6	±	3.5**
	tslope	11.0	±	5.5	4.8	±	3.2**
RESPV	$meanNN_{RESP}$	4.0	±	1.1	3.7	±	0.8
	$sdNN_{RESP}$	0.7	±	0.6	0.7	±	0.4
	BF	16.2	±	3.0	17.7	±	3.5
	t_{in}	2.3	±	0.6	2.1	±	0.6
	t_{ex}	1.7	±	0.5	1.6	±	0.3
RSA	RSA_{P2V}	62.2	±	42.4	31.1	±	24.4*

4.3.2 The cardiorespiratory network

4.3.2.1 Respiratory variability

Respiratory variability analyses revealed no significant differences between SZO and CON. However, a trend of reduced mean breathing cycle length ($meanNN_{RESP}$=3.7±0.8 sec), increased BF (17.7±3.5 1/min), and reduced inspiration (t_{in}) and expiration (t_{ex}) times in SZO compared to CON were found (**Table 9**).

4.3.2.2 Respiratory sinus arrhythmia

RSA analyses revealed significantly decreased RSA (RSA_{P2V}) for SZO when compared to CON (**Table 9**).

4.3.3 Summary and discussion

4.3.3.1 Heart rate- and blood pressure variability

My findings in relation to HRV are in accordance with other studies that have revealed an altered autonomic tone in treated schizophrenic patients. These results suggest a parasympathetic withdrawal and an ongoing sympathetic predominant activation in cardiac autonomic regulation, highlighted by decreased parasympathetic indices from HRV such as rmssd. Psychiatrists attributed increased heart rate (meanNN ↓) in patients with schizophrenia to antipsychotic treatment. This assumption is only to some extent correct since treatment with clozapine, for instance, is associated with reduced vagal function and increased heart rates (Bär, 2015) and it has been shown that clozapine, quetiapine, amisulpride revealed the strongest anticholinergic side effects of cholinergic or adrenergic receptors on ANS modulation than olanzapine (Schulz et al, 2014a). In addition, Agelink et al. (Agelink et al, 2001) investigated the effects of atypical antipsychotics on autonomic neurocardiac function and showed that amisulpride did not significantly alter HRV because it lacks activity at cholinergic or adrenergic receptors. Excepting amisulpride, the other atypical antipsychotics increased mean HR, an effect largest with clozapine, followed in order by sertindole and olanzapine. Thereby, a significant reduction in parasympathetic dependent HRV indices could only be shown with clozapine. Bär et al (Bär et al, 2008) found a reduction of the complexity of heart rate regulation after olanzapine treatment measured by compression entropy. Thus, the authors suggested a decreased cardiac vagal function which may increase the risk for cardiac mortality. In a study of healthy volunteers' differential effects of single doses of the antipsychotic drugs (olanzapine, thioridazine, risperidone) on HRV were found, and these were independent of their sedative effects. Olanzapine increased, and thioridazine decreased HRV, while risperidone had no effect on HRV (meanNN sdNN, rmssd) (Silke et al, 2002). Due to, that the investigated SZO patients were

treated with atypical neuroleptics a side effect of these drugs cannot be completely excluded on HRV results. However, several studies have reported increased heart rates in the first episode and unmedicated patients too pointing to the significant role of the impaired cardiac modulation in those patients. Interestingly, these drugs seem to be having no effect on blood pressure values and -variability. Although I found some indication for increased sympathetic modulation, results seemed to be restricted to heart rate changes and not to the blood pressure (Bär et al, 2006). Thus, a cardiac dysfunction in SZO does not reflect a simple stress induced arousal but rather chronic and distinct changes of heart rate regulation (Schulz et al, 2015a). Some studies reported an association of the autonomic imbalance with the degree of positive symptoms (i.e. delusions). However, there is no simple relation between cardiac dysfunction and clinical symptoms.

4.3.3.2 Baroreflex sensitivity

Considering baroreflex sensitivity, as a marker for the assessment of autonomic control of the cardiovascular system maintaining blood pressure at a constant level, significantly reduced tachycardic (tslope) and bradycardic (bslope) slopes were found in accordance with other studies investigating unmedicated patients (Bär et al, 2005; Schulz et al, 2013c). These results pointing to a severely impaired fine-tuning of blood pressure and heart rate regulation independent of medication among those patients. Thus, the decrease of efferent vagal activity and the inhibition of baroreflex vagal bradycardia in SZO might be caused by stress due to psychotic experiences or the psychosis itself, a process that allows the organism under physiological conditions to adjust to demanding environmental stress (Bär, 2015).

4.3.3.3 Respiratory variability

In contrast to other studies (Bär et al, 2012; Peupelmann et al, 2009; Schulz et al, 2012a), variability analyses of respiration did not reveal any significant differences between both groups (only trends). However, all these studies were performed with non-medicated SZO patients revealing significantly increased breathing rates and reduced inspiration and expiration times in SZO. The results could be explained by that D2 receptor antagonism in the brain is a general pharmacodynamics property of all antipsychotics. Thus, a dysregulation of dopaminergic circuits with excess dopaminergic activity in the mesolimbic pathway (leading to positive symptoms of psychosis) and reduced dopaminergic signalling in the mesocortical pathway (leading to negative symptoms) seems to be evident in SZO (Lally & MacCabe, 2015). Due to, that antipsychotics are anti-dopaminergic they probably have dopamine's stimulating effect on respiration possibly leading to the reduced respiratory variability. Other studies supporting dopaminergic hypofunction in the cerebral cortex and hyperfunction in subcortical brain regions in SZO, as well as those typical antipsychotics (here: dopamine) inhibit mitochondrial respiration (Ben-Shachar,

2002; Pérez-Neri et al, 2006). The final respiratory output involves a complex interaction between the brainstem and higher centres, including the limbic system and cortical structures. Respiration is primarily regulated for metabolic and homeostatic purposes in the brainstem and also changes in response to changes in emotions, such as sadness, happiness, anxiety or fear (Homma & Masaoka, 2008). Williams et al. (Williams et al., 2004) found a functional disconnection in autonomic and central systems for processing threat-related signals in patients with paranoid schizophrenia. They hypothesized that paranoid cognition may reflect an internally generated cycle of misattribution regarding incoming fear signals due to a breakdown in the regulation of these systems. In addition, it could be shown that personality anxiety is associated with changed respiratory patterns and respiratory frequency (Masaoka & Homma, 1997; 1999). These studies showed that an increase in the respiratory frequency is not related to metabolic factors and is consistent with a mechanism involving the limbic system modulating respiratory drive (Masaoka & Homma, 2001). The found alterations in respiration (trend) likely can be explained that a dysregulation of arousal, as suggested in paranoid schizophrenia in amygdalae prefrontal circuits, might contribute to the correlation of psychopathology and breathing alterations (Bär et al, 2012). Schizophrenic patients who were taking clozapine and olanzapine in comparison to patients who were antipsychotic naive might have a compensatory mechanism in the neurobiological substrate, whereby, alterations in the anterior cingulate, the medial frontal cortex and a decline of fast frequency activities in the occipital cortex were related to clozapine and olanzapine (in this study most patients were treated with these atypical antipsychotic) (Tislerova et al, 2008).

4.3.3.4 Respiratory sinus arrhythmia

The results showed a restricted RSA, which represents the influence of the respiratory system in the regulation of the HR as a measure of cardiac vagal activity. This is in accordance with other studies (Bär et al, 2012; Schulz et al, 2015a) that found impaired cardiorespiratory coupling and reduced RSA in non-medicated SZO. Peupelmann et al. (Peupelmann et al, 2009) did also found decreased cardiorespiratory coupling in SZO as an index for diminished vagal modulation at the brain stem level. Furthermore, they found that regularity of breathing correlated with disease severity and assumed a lack of inhibitory control over brainstem centres in schizophrenia. Based on the findings it can be assumed that decreased vagal activity within the brainstem or its suppression from higher regulatory centres might account for the findings. In a previous study, I was able to show that fractal characteristics (morphological structure) of the RSA signal were increased in SZO indicating that the underlying rhythm of the RSA signal more randomly fluctuates. This indiscriminately wavering of the RSA time series supports the assumption that HR fluctuations are less in phase with inspiration and expiration in SZO providing the

explanation for the lower RSA_{P2V} in SZO in comparison to CON (Schulz et al, 2015a). Moreover, it can be hypothesised that the cardiac dysfunction in SZO does not reflect a simple stress-induced arousal, but rather chronic and distinct changes of heart rate and respiratory regulation (Schulz et al, 2015a).

4.4 The central-cardiovascular-network

For central-cardiovascular coupling analyses I applied the causal and non-causal linear and non-linear coupling approaches (HRJSD, NSTPDC, MuTE) to quantify this network.

4.4.1 Cardiovascular coupling (BBI–SYS)

NSTPDC results demonstrated a significant different coupling direction (NF) in SZO (NF~−0.5) compared to CON, pointing to a decreased bidirectional coupling in the direction from SYS→BBI (SYS is the driver). The coupling strength from SYS→BBI ($A_{SYS\rightarrow BBI(P_{EEG})}$), known as baroreflex loop, was significantly reduced in SZO (↓) in comparison to CON (**Figure 22, *a***) (**Table 10**).

MuTE revealed a highly significant different coupling strength between SZO and CON. Considering the baroreflex loop when SYS influenced BBI ($MuTE_{SYS\rightarrow BBI(PEEG)}$), in contrast to the linear results, the coupling strength was significantly increased in SZO compared to CON, and might point to a stronger non-linear causal information transfer of SYS on BBI. When BBI influenced SYS ($MuTE_{BBI\rightarrow SYS(PEEG)}$), the coupling strength was highly significantly different between SZO (↓) and CON (**Table 11**).

Table 10. *Linear central-cardiovascular (BBI, SYS, and P_{EEG}) coupling analyses results (NSTPDC) to discriminate between patients suffering from paranoid schizophrenia (SZO) and healthy subjects (CON). (BBI=beat-to-beat intervals, SYS=systolic blood pressure amplitude values over time, P_{EEG}=mean power in the BBI-related EEG intervals, *p<0.05, **p<0.01, ***p<0.00041, n.s.=not significant, #=not confirmed by surrogate analysis)*

	Index	CON mean ± std	SZO mean ± std
BBI↔SYS	NF	-0.66 ± 0.52	-0.48 ± 0.81***
	$A_{BBI\rightarrow SYS(PEEG)}$	0.25 ± 0.06	0.27 ± 0.14
	$A_{SYS\rightarrow BBI(PEEG)}$	0.43 ± 0.14	0.39 ± 0.16***
BBI↔P_{EEG}	NF	-0.64 ± 0.86	-0.81 ± 1.03**
	$A_{BBI\rightarrow PEEG(SYS)}$	0.10 ± 0.05	0.09 ± 0.06*
	$A_{PEEG\rightarrow BBI(SYS)}$	0.23 ± 0.16	0.26 ± 0.17*
SYS↔P_{EEG}	NF	0.00 ± 1.07	-0.70 ± 0.94***
	$A_{SYS\rightarrow PEEG(BBI)}$	0.13 ± 0.07	0.10 ± 0.06***
	$A_{PEEG\rightarrow SYS(BBI)}$	0.14 ± 0.10	0.20 ± 0.13***

The results of HRJSD have already been published elsewhere (Schulz et al, 2014a). Here, I demonstrated significantly altered distributed cardiovascular coupling pattern indicating a decreased cardiovascular coupling in patients with acute schizophrenia, especially for medicated patients.

4.4.2 Central-cardiac coupling (BBI–P_{EEG})

Linear couplings analyses (NSTPDC) revealed significant different NF values between both groups. For SZO (NF~−0.8) the coupling direction was characterized as a bidirectional one from P_{EEG}→BBI (P_{EEG} is the driver) (**Figure 22,** ***b***) (**Table 10**).

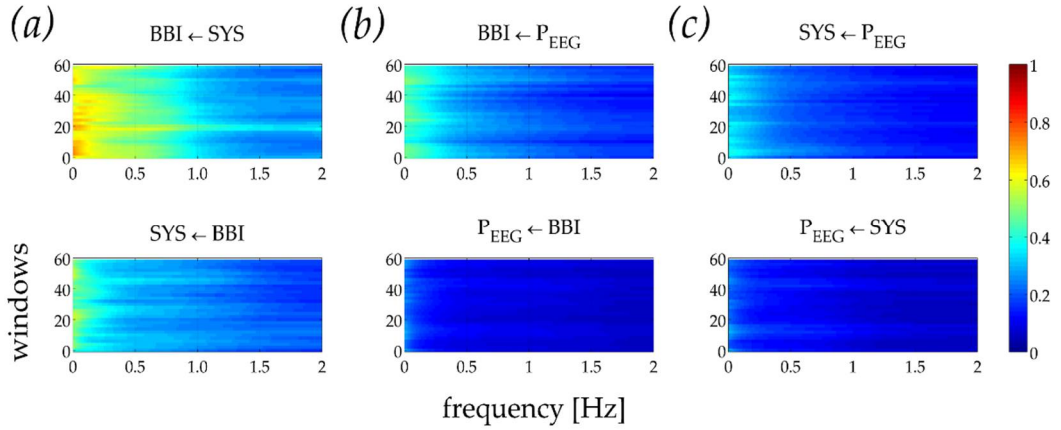

Figure 22. *Averaged NSTPDC plots for central-cardiovascular coupling analyses for (a) cardiovascular couplings, (b) central-cardiac couplings, and (c) central-vascular couplings for schizophrenic patients. Arrows indicating the causal coupling direction from one time series to another, e.g., SYS←P_{EEG}, indicating the causal link from P_{EEG} to SYS. Coupling strength ranges from blue (no coupling) to red (maximum coupling), where BBI represents beat-to-beat intervals, SYS represent successive maximum systolic blood pressure amplitude values over time, and P_{EEG} represents the mean power in BBI-related EEG intervals.*

Please note that the values for central-cardiac couplings in **Table 10** are different from the values in **Table 15**, because in **Table 15** other EEG channels were included for the frontal area (analyses of the central-cardiorespiratory areas). The same is true for **Figure 22** and central-cardiac couplings compared to **Figure 25** (analyses of the central-cardiorespiratory areas).

The non-linear causal information transfer (MuTE) from cardiac system to the central system (BBI→P_{EEG}) as well as from central system to cardiac system (P_{EEG}→BBI) were highly significantly reduced in SZO in comparison to CON, and were nearly equally strong pronounced in SZO (**Table 11**).

Table 11. *Non-linear central-cardiovascular (BBI, SYS, and P_{EEG}) coupling analyses results (MuTE) to discriminate between patients suffering from paranoid schizophrenia (SZO) and healthy subjects (CON). (BBI=beat-to-beat intervals, SYS=systolic blood pressure amplitude values over time, P_{EEG}=mean power in the BBI-related EEG intervals, *p<0.05, **p<0.01, ***p<0.00041, n.s.=not significant, #=not confirmed by surrogate analysis)*

	Index	CON	SZO
		mean ± std	mean ± std
BBI↔SYS	$MuTE_{BBI\rightarrow SYS(PEEG)}$	0.098 ± 0.035	0.064 ± 0.042***
	$MuTE_{SYS\rightarrow BBI(PEEG)}$	0.053 ± 0.034	0.093 ± 0.037***
BBI↔P_{EEG}	$MuTE_{BBI\rightarrow PEEG(SYS)}$	0.012 ± 0.011	0.007 ± 0.009***
	$MuTE_{PEEG\rightarrow BBI(SYS)}$	0.012 ± 0.009	0.007 ± 0.008***
SYS↔P_{EEG}	$MuTE_{SYS\rightarrow PEEG(BBI)}$	0.012 ± 0.011	0.006 ± 0.008***
	$MuTE_{PEEG\rightarrow SYS(BBI)}$	0.008 ± 0.008	0.006 ± 0.008***,#

HRJSD analyses revealed highly significant (p<0.00041) differences between SZO and CON in all 8 central-cardiac coupling pattern families (P_{EEG}/BBI, 8×8=64) for the entire frontal area, the left frontal area and the right frontal area (**Figure 23**) (**Table 12**). The patterns were characterised by decreased absolute values in SZO if the central pattern family P_{EEG}-E0, P_{EEG}-E1, P_{EEG}-E2, P_{EEG}-LU1, P_{EEG}-LD1, P_{EEG}-LA1, P_{EEG}-P and P_{EEG}-V was coupled with BBI-E0, BBI-E1, BBI-E2, BBI-LU1 and BBI-LD1. SZO values significantly increased if the central pattern family was coupled with BBI-LA1, BBI-P and BBI-V. Thereby the central family patterns P_{EEG}-E0 and P_{EEG}-E2 significantly decreased, and P_{EEG}-LA1 significantly increased in SZO, as compared to CON. The cardiac family patterns BBI-E0 and BBI-E2 highly significantly decreased, and BBI-LA1, BBI-P and BBI-V highly significantly increased in SZO, as compared to CON (**Table 13**). The index $HRJSD_{Shannon}$ did not reveal any significant differences between SZO and CON, regardless of the investigated frontal area.

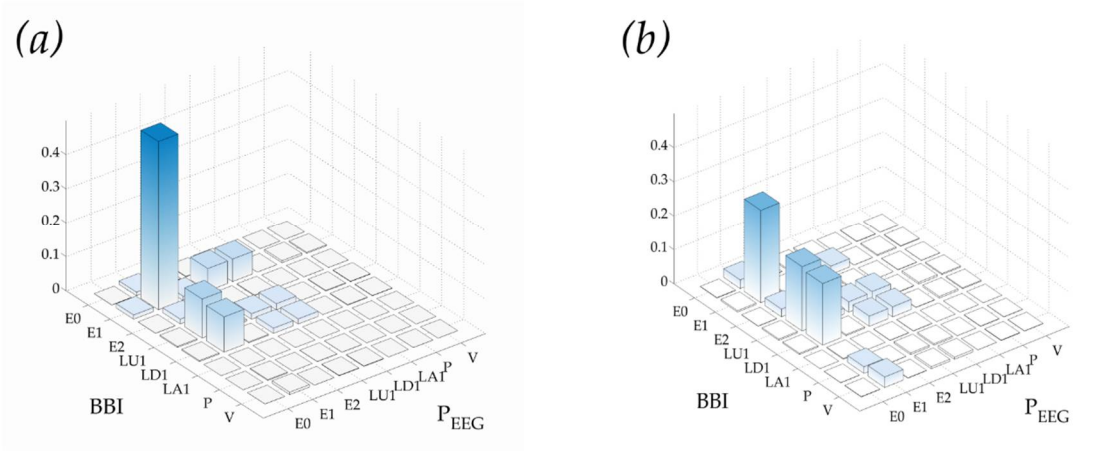

Figure 23. *Three-dimensional plots of the HRJSD pattern family distribution density matrix Wf (8×8) of central-cardiac couplings for the entire frontal area for (a) healthy subjects and (b) schizophrenic patients. (BBI=beat-to-beat intervals, P_{EEG}=mean power in BBI-related EEG intervals)*

Table 12. *Number (N) of significant (p<0.01) central-cardiovascular HRJSD indices p(N) used to discriminate between patients suffering from paranoid schizophrenia (SZO) and healthy subjects (CON) pertaining to the frontal area, the left frontal area and the right frontal area. BBI/P_{EEG} indicates the coupling between beat-to-beat intervals (BBI) and the mean power in BBI-related EEG-intervals (P_{EEG}). SYS/P_{EEG} indicates the coupling between the maximum systolic blood pressure amplitude values over time (SYS) and the mean power in the BBI-related EEG-intervals (P_{EEG}). (e.g., P_{EEG}-E0/BBI describes the coupling of the pattern family E0 from P_{EEG} with all other 8 BBI coupling pattern families)*

	Index	all frontal *p*(*N*)	left frontal *p*(*N*)	right frontal *p*(*N*)
BBI/P_{EEG}	P_{EEG}-E0/BBI	6	5	4
	P_{EEG}-E1/BBI	5	5	5
	P_{EEG}-E2/BBI	5	5	4
	P_{EEG}-LU1/BBI	5	3	3
	P_{EEG}-LD1/BBI	5	4	4
	P_{EEG}-LA1/BBI	8	8	6
	P_{EEG}-P/BBI	5	4	3
	P_{EEG}-V/BBI	4	4	2
SYS/P_{EEG}	P_{EEG}-E0/SYS	5	4	4
	P_{EEG}-E1/SYS	8	8	8
	P_{EEG}-E2/SYS	6	4	5
	P_{EEG}-LU1/SYS	8	6	5
	P_{EEG}-LD1/SYS	8	6	5
	P_{EEG}-LA1/SYS	8	6	5
	P_{EEG}-P/SYS	8	8	8
	P_{EEG}-V/SYS	8	8	4

In addition, all EEG spectral band components were quantified with NSTPDC. NSTPDC results revealed for all spectral bands significantly (p<0.00041) decreased coupling strengths from the EEG spectral power bands towards BBI ($A_{P_{EEGband}\rightarrow BBI}$) for the whole frontal area, the left frontal area and the right frontal area in SZO when compared to CON. Thereby in $P_{EEG\gamma}$ the strongest influence of central γ activity towards BBI was found for both SZO and CON. With regard to the coupling direction of BBI towards $P_{EEGband}$ I found in the coupling strengths for the whole frontal area only in $P_{EEG\beta}$, $P_{EEG\beta1}$, $P_{EEG\delta}$ and $P_{EEG\theta}$ significant increases in $A_{BBI\rightarrow P_{EEGband}}$ for SZO in comparison to CON. Regarding the left frontal area, only in $P_{EEG\beta1}$ and $P_{EEG\theta}$ significant increases in $A_{BBI\rightarrow P_{EEGband}}$ in the couplings strengths were found for SZO, when compared to CON. Regarding the right frontal area in $P_{EEG\alpha1}$, $P_{EEG\beta1}$, $P_{EEG\delta}$ and $P_{EEG\theta}$ significant increases in $A_{BBI\rightarrow P_{EEGband}}$ in coupling strengths could be shown for SZO (**Figure 24**). Considering the NF values for all couplings between BBI and $P_{EEGband}$ SZO revealed generally increased NF values in comparison to CON. For all subjects' entire frontal area, left frontal area and right frontal area, the coupling directions were bidirectional, with BBI acting as the driver (**Table 14**). Only for $P_{EEG\delta}$ and $P_{EEG\gamma}$ was equal influence present in both directions.

Table 13. *Significant HRJSD results showing of the probability of the occurrence of univariate HRJSD pattern families for BBI, SYS and P_{EEG} in % to discriminate between patients suffering from paranoid schizophrenia (SZO) and healthy subjects (CON) for the frontal area, the left frontal area and the right frontal area. (BBI=beat-to-beat intervals, SYS=systolic blood pressure amplitude values over time, P_{EEG}=mean power in the BBI-related EEG intervals, *p<0.05, **p<0.01, ***p<0.00041, n.s.=not significant, #=not confirmed by surrogate analysis)*

	Index	all frontal		left frontal		right frontal	
		CON	SZO	CON	SZO	CON	SZO
		mean ± std	mean ± std	mean ± std	mean ± std	mean ± std	mean ± std
P_{EEG}	P_{EEG}-E0	1.9 ± 1.3***	1.5 ± 0.9	1.9 ± 1.3***	1.5 ± 0.9	1.9 ± 1.3**	1.5 ± 0.9
	P_{EEG}-E2	2.1 ± 1.3**	2.6 ± 2.0	2.0 ± 1.3**	2.6 ± 2.0	2.1 ± 2.0	2.6 ± 2.1
	P_{EEG}-LA1	0.03 ± 0.1***	0.3 ± 0.5	0.03 ± 0.1***	0.3 ± 0.6	0.03 ± 0.1***	0.3 ± 0.8
BBI	BBI-E0	4.6 ± 2.4***	2.1 ± 1.8	4.6 ± 2.4***	2.1 ± 1.8	4.6 ± 2.4***	2.1 ± 1.8
	BBI-E2	6.1 ± 3.5***	3.0 ± 2.3	6.1 ± 3.5***	3.0 ± 2.3	6.1 ± 3.5***	3.0 ± 2.4
	BBI-LA1	0.03 ± 0.1***	1.1 ± 2.1	0.03 ± 0.1***	1.1 ± 2.1	0.03 ± 0.1***	1.2 ± 2.2
	BBI-P	2.4 ± 1.7***	4.5 ± 3.5	2.4 ± 1.7***	4.5 ± 3.4	2.4 ± 1.7***	4.5 ± 3.5
	BBI-V	2.9 ± 2.1***	5.1 ± 4.2	2.9 ± 2.1**	5.0 ± 4.2	2.9 ± 2.1**	5.1 ± 4.3
SYS	SYS-E0	1.7 ± 1.5***	3.6 ± 3.3	1.7 ± 1.5***	3.6 ± 3.4	1.7 ± 1.5***	3.6 ± 3.4
	SYS-E1	61.0 ± 21.9***	33.2 ± 31.3	61.0 ± 21.9***	33.2 ± 31.3	61.0 ± 21.9***	33.2 ± 31.3
	SYS-E2	1.9 ± 1.3***	3.3 ± 2.7	1.9 ± 1.3***	3.3 ± 2.7	1.9 ± 1.3***	3.3 ± 2.8
	SYS-LU1	18.2 ± 9.5***	27.9 ± 11.8	18.2 ± 9.5***	28.0 ± 11.8	18.1 ± 9.5***	27.9 ± 11.8
	SYS-LD1	15.9 ± 9.5***	25.3 ± 11.9	15.9 ± 9.5***	25.3 ± 11.9	15.9 ± 9.5***	25.3 ± 11.9
	SYS-LA1	0.01 ± 0.03***	0.3 ± 1.1	0.01 ± 0.03***	0.3 ± 1.1	0.01 ± 0.03***	0.4 ± 1.1
	SYS-P	0.4 ± 0.7***	3.0 ± 3.1	0.4 ± 0.7***	3.0 ± 3.1	0.4 ± 0.7***	3.0 ± 3.1
	SYS-V	1.2 ± 1.7***	4.6 ± 3.5	1.2 ± 1.7***	4.6 ± 3.5	1.2 ± 1.7***	4.6 ± 3.5

Table 14. *NSTPDC results for the coupling direction (NF: normalized factor) to discriminate between patients suffering from paranoid schizophrenia (SZO) and healthy subjects (CON) for the frontal area, the left frontal area and the right frontal area. (↔ indicates bidirectional coupling, → indicates unidirectional coupling, – indicates equal influence in both directions or no coupling, ↑ increased NF value in SZO compared to CON, ↓ decreased NF value in SZO compared to CON, d denotes the driver variable, BBI=beat-to-beat intervals, SYS=systolic blood pressure amplitude values over time, P_{EEG}=mean power in the BBI-related EEG spectral bands intervals, *p<0.05, **p<0.01, ***p<0.00041, n.s.=not significant, #=not confirmed by surrogate analysis)*

	NF	all frontal			left frontal			right frontal		
		↔	SZO	d	↔	SZO	d	↔	SZO	d
BBI/$P_{EEGband}$	$P_{EEG\delta}$	–	↑**	–	–	↑**	–	–	↑**	–
	$P_{EEG\theta}$	↔	↑**	BBI	↔	↑**	BBI	↔	↑**	BBI
	$P_{EEG\alpha}$	↔	↑**	BBI	↔	↑	BBI	↔	↑**	BBI
	$P_{EEG\alpha1}$	↔	↑**	BBI	↔	↑	BBI	↔	↑**	BBI
	$P_{EEG\alpha2}$	↔	↑*	BBI	↔	↑	BBI	↔	↑	BBI
	$P_{EEG\beta}$	↔	↑**	BBI	↔	↑**	BBI	↔	↑**	BBI
	$P_{EEG\beta1}$	↔	↑**	BBI	↔	↑**	BBI	↔	↑**	BBI
	$P_{EEG\beta2}$	↔	↑**	BBI	↔	↑**	BBI	↔	↑*	BBI
	$P_{EEG\gamma}$	–	↑**	–	–	↑*	–	–	↑*	–
SYS/$P_{EEGband}$	$P_{EEG\delta}$	↔	↑	SYS	↔	↓	SYS	↔	↑	SYS
	$P_{EEG\theta}$	↔	↑	SYS	↔	↑	SYS	↔	↑	SYS
	$P_{EEG\alpha}$	→	↓**	SYS	→	↓**	SYS	→	↓**	SYS
	$P_{EEG\alpha1}$	→	↓**	SYS	→	↓**	SYS	→	↓	SYS
	$P_{EEG\alpha2}$	→	↓**	SYS	→	↓**	SYS	→	↓**	SYS
	$P_{EEG\beta}$	↔	↑	SYS	↔	↑	SYS	↔	↑	SYS
	$P_{EEG\beta1}$	↔	↑*	SYS	↔	↑*	SYS	↔	↑	SYS
	$P_{EEG\beta2}$	↔	↓**	SYS	↔	↓*	SYS	↔	↓*	SYS
	$P_{EEG\gamma}$	–	↑	–	–	↑	–	–	↑	–

4.4.3 Central-vascular coupling (SYS–P_{EEG})

The linear couplings (NSTPDC) between the vascular system (SYS) and the central system (P_{EEG}) a highly significantly different NF value was present for both groups. The coupling directions were characterized as, that CON (NF~0) pointing to an equal information transfer in both directions, and SZO (NF~–0.7) indicating a bidirectional one from P_{EEG}→SYS (driver P_{EEG}). These results were supported by $A_{SYS\rightarrow P_{EEG}(BBI)}$ and $A_{P_{EEG}\rightarrow SYS(BBI)}$ for CON demonstrating similar values for the area indices for both coupling directions. $A_{SYS\rightarrow P_{EEG}(BBI)}$ and $A_{P_{EEG}\rightarrow SYS(BBI)}$ were highly significantly different between SZO and CON. The coupling strength was significantly reduced in SZO when SYS influenced P_{EEG} (SYS→P_{EEG}) compared to CON. If P_{EEG} influences SYS (P_{EEG}→SYS) a significant increase in the coupling strength was present for SZO compared to CON (**Figure 22, *c***) (**Table 10**).

The non-linear central-vascular couplings (MuTE) from the vascular system to the central system (SYS→P_{EEG}) as well as from central system to vascular system (P_{EEG}→SYS) were significantly reduced in SZO compared to CON, and were nearly equally strong pronounced in both groups (**Table 11**).

In contrast to the central-cardiac coupling HRJSD results, a higher number of significantly different central-vascular coupling pattern families (P_{EEG}/SYS, 8×8=64) for the entire frontal area, left frontal area and right frontal area were found (**Table 13**). In SZO patients, the absolute values of central-vascular coupling pattern families significantly decreased if the central pattern family P_{EEG}-E0, P_{EEG}-E1, P_{EEG}-E2, P_{EEG}-LU1, P_{EEG}-LD1, P_{EEG}-LA1, P_{EEG}-P and P_{EEG}-V were coupled with SYS-E1. They significantly increased if the central pattern family P_{EEG}-E0, P_{EEG}-E1, P_{EEG}-E2, P_{EEG}-LU1, P_{EEG}-LD1, P_{EEG}-LA1, P_{EEG}-P and P_{EEG}-V were coupled with SYS-E0, SYS-E2, SYS-LU1, SYS-LD1, SYS-LA1, SYS-P and SYS-V (**Table 12**). In addition, the absolute values of central family patterns P_{EEG}-E0 and P_{EEG}-E2 significantly decreased, and P_{EEG}-LA1 significantly increased in SZO when compared to CON. The values of vascular family patterns SYS-E0, SYS-E2, SYS-LU1, SYS-LD1, SYS-LA1, SYS-P and SYS-V highly significantly (p<0.00041) increased in SZO when compared to CON (**Table 13**). $HRJSD_{Shannon}$ values significantly increased in SZO patients as compared to CON for the entire frontal area (CON: 2.7±0.9, SZO: 3.0±1.2, p<0.00041), the left frontal area (CON: 2.7±0.9, SZO: 3.0±1.2, p<0.00041) and the right frontal area (CON: 2.6±0.9, SZO: 3.0±1.2, p<0.01).

In addition, all EEG spectral band components of the central-vascular network were also quantified with NSTPDC. I found for the direction of EEG spectral power bands towards SYS ($A_{P_{EEGband}\rightarrow SYS}$) an opposite behaviour, as shown by $P_{EEGband}$→BBI (where significant coupling strengths were found here for all bands and all frontal areas) (**Table 14**) (**Figure 24**). Regarding the entire frontal area ($P_{EEG\alpha}$, $P_{EEG\alpha2}$) and the left frontal area ($P_{EEG\alpha}$, $P_{EEG\alpha1}$, $P_{EEG\alpha2}$) significant increases in $A_{P_{EEGband}\rightarrow SYS}$ for SZO in comparison to CON were found. Again in $P_{EEG\gamma}$ the strongest influence of central γ activity towards SYS could be found for both SZO and CON. In the opposite direction, namely from SYS towards $P_{EEGband}$, I found for the frontal area in all spectral bands ($P_{EEGband}$) highly significant decreased coupling strengths in SZO when compared to CON. For the left frontal area besides $P_{EEG\gamma}$ and $P_{EEG\theta}$ and for the right frontal area besides $P_{EEG\delta}$, $P_{EEG\gamma}$ and $P_{EEG\theta}$ for all other bands showed significantly different coupling strengths between SZO and CON. With respect to NF, there was generally a bidirectional coupling for the EEG spectral power bands ($P_{EEG\delta}$, $P_{EEG\theta}$, $P_{EEG\beta}$, $P_{EEG\beta1}$, $P_{EEG\beta2}$) with SYS acting as the driver. Furthermore, there was a unidirectional coupling for $P_{EEG\alpha}$, $P_{EEG\alpha1}$ and $P_{EEG\alpha2}$ and an equal influence in both directions for $P_{EEG\gamma}$ for the entire frontal area, as well as for the left and right frontal areas. In the α bands and $\beta2$ band, NF was decreased in SZO when compared to CON.

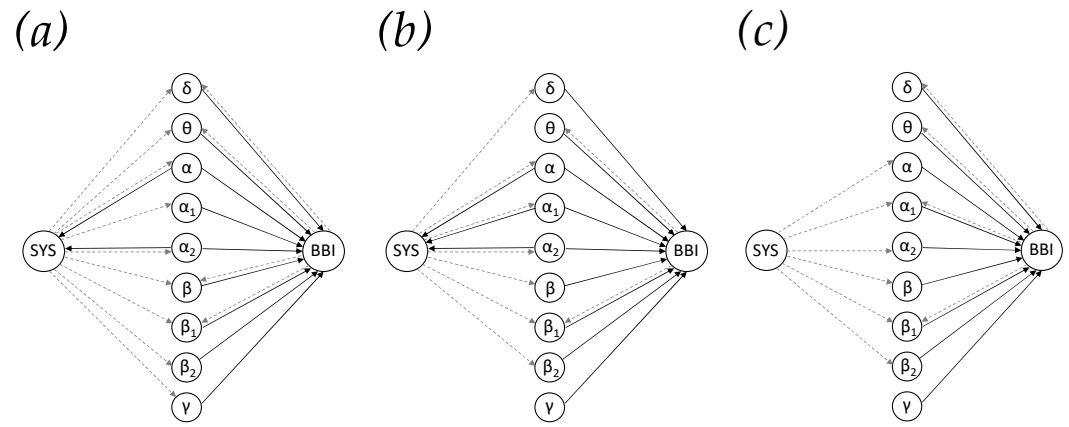

Figure 24. *Visualization of significant differences between patients suffering from paranoid schizophrenia (SZO) and healthy subjects (CON) with respect to the coupling strength (NSTPDC) between autonomic activity (BBI, SYS) and central spectral activity ($P_{EEGband}$) for the (a) whole frontal area, (b) the left frontal area and (c) the right frontal area. Arrows indicate the coupling direction, where black solid lines indicate the direction from central spectral activity towards autonomic target variables. Grey dashed lines indicate the direction from the autonomic variables towards central spectral activity. Note that all arrows were highly significantly ($p<0.00041$) different between SZO and CON; otherwise, the arrows were indicated by *($p<0.01$). (BBI=beat-to-beat intervals, SYS=maximum systolic blood pressure amplitude values over time, $P_{EEGband}$=mean power in BBI-related EEG spectral band intervals)*

4.4.4 Summary and discussion

4.4.4.1 Cardiovascular coupling (BBI–SYS)

Linear cardiovascular coupling results (NSTPDC) showed a decreased bidirectional coupling strength in the direction from SYS→BBI in SZO indicating an inhibited baroreflex control loop, whereas the non-linear part showed contrary results. I was able to show for SZO compared to CON, that the vascular system (SYS) is not affected by antipsychotic treatment leading to the assumption, that the inhibited baroreflex-loop is a result of an impaired cardiac modulation instead of an impairment of the blood pressure regulation circuit. In general, the arterial baroreflex is inhibited under stressful conditions (Nosaka, 1996; Steptoe & Sawada, 1989; Swenne, 2013) (as it has been assumed for SZO). In stressful conditions, when the blood pressure increases, the baroreflex reduces sympathetic outflow and increases parasympathetic tone, which protects the heart, e.g., against arrhythmias. Both blood pressure buffering and cardioprotection are major effects of the arterial baroreflex (Swenne, 2013). Facilitation of stress favours restoration of energy exhausted during a stressful phase in which the subject reacts actively to changing environment. Thereby, brain regions which are related to central baroreflex regulation mechanisms and elicit facilitation of stress are the medial prefrontal cortex, the preoptic/anterior hypothalamus, the ventrolateral part of the periaqueductal grey matter, and the nucleus raphe magnus (Nosaka, 1996).

The coupling results from HRJSD analysis in SZO were mainly characterized by greater amount of low increased, low decreased, alternating and fluctuating patterns (LU1, LD1, LA1, P, V) of SYS and invariable heart rate responses (E1). These results might support previous findings that SZO are characterized by a lack of "finetuning" of baroreflex modulation expressed by the impairment of the baroreflex control feedback loop and reduced efferent vagal activity. This behaviour was independent from medication but was much more formed in medicated patients and seems to be due to the anticholinergic effects of antipsychotics.

4.4.4.2 Central-cardiac coupling (BBI–P_{EEG}) and central-vascular coupling (SYS–P_{EEG})

Linear and non-linear brain-heart information flows (P_{EEG}→BBI) were characterized as top-down from the CNS (brain) towards ANS (heart) in both groups. It leads to the assumption that an impaired brain-heart axis is present in schizophrenia, and more expressed in the linear domain. A functional disconnection between the CNS, impaired interactions of fronto-cingulate and subcortical brain regions, and ANS was suggested for SZO, when these patients process threat-related signals (Williams et al, 2004). Impairments in frontal-subcortical processes are associated with psychopathologies such as schizophrenia (Callicott et al, 2003). Internally generated processes of misjudgements of threat-related signals like anxiety seem to be associated with paranoid cognition due to a breakdown of these processes. This leads to an inhibited central-cardiac coupling influenced by a lack of cortical inhibitory control over sympathetic-excitatory subcortical regions (Williams et al, 2004). Moreover, it was hypothesized that the inhibitory deficit was reflected in impaired cognitive and behavioural inhibition connected with an impaired HRV (Henry et al, 2010; Thayer & Lane, 2009).

Central-cardiovascular interactions revealed that a stronger linear information flow from central activity in the direction of blood pressure regulation (P_{EEG}→SYS) than in the direction of BBI in SZO compared to CON. The central-vascular axis was bidirectionally directed with a stronger central driving mechanism (P_{EEG}→SYS) in SZO, whereas, CON showed equally directed information flows (P_{EEG}↔SYS). In particular, in SZO, the central-cardiac information transfer is more non-linearly defined and significantly bidirectionally decreased. This leads to the assumption that maintaining blood pressure as well as heart rate regulation takes on a greater importance for SZO expressed through increased top down regulation pathways, as for CON. In sum, for SZO it is evident, that the linear central driving is more pronounced in the direction of autonomic activity (BBI, SYS) than in CON, and that the non-linear information transfer within the central-vascular- and as central-cardiac systems are reduced.

This is in accordance with other findings that the coupling between the central and autonomic nervous systems is driven by quite complex regulatory mechanisms

where, in general, the CNS commands and the ANS reflexes (de Zambotti et al, 2018). Recently, it was well demonstrated that beyond a dysfunction of connectivity among different brain areas in schizophrenia, there is also an abnormal asymmetry of functional connectivity and a failure of the left-hemisphere dominance compared with healthy subjects. Moreover, an overall generally attenuated asymmetry of functional connectivity that increases with the duration of the disease and correlates with psychotic symptoms in SZO was found (Ribolsi et al, 2014; Sun et al, 2017). This abnormal asymmetry of connectivity may be related to a dysfunctional inter-hemispheric communication (Ribolsi et al, 2014). This asymmetry is characterized by failure of the left hemisphere dominance (parasympathetic tone) in SZO and is located in several frontal regions and the hippocampus. This asymmetry of functional connectivity in schizophrenia, suggests that this aspect may represent a neurophysiological feature that is unique to this disorder (Ribolsi et al, 2014). In respect to cardiovascular activity extensive research has been conducted on the influence of the frontal, temporal, and parietal regions on heart rate and blood pressure regulation, where, the two hemispheres seem to possess contrasting roles in regulating changes in heart rate and blood pressure. Different studies consistently found a relationship between changes in heart rate and blood pressure and measures of cerebral activity at these locations (temporal and posterior regions), such as electroencephalography (EEG) (Beissner et al, 2013; Foster et al, 2008). Significant correlations between resting heart rate and frontal area lateral asymmetry as well as frontal–parietal asymmetry was found supporting the relative differential associations of the left and right frontal and parietal areas and cardiovascular activity (Foster et al, 2008). Due to this asymmetry, the relative right frontal activation will generate increased inhibition of the right posterior region as well as decreased left frontal area activation, resulting in increased left posterior (parasympathetic) activity. Conversely, relative left frontal area activation will cause increased inhibition of the left posterior region as well as decreased right frontal area activity, resulting in increased right posterior (sympathetic) activity. There is evidence for an inhibitory role of the frontal areas; stimulation of the medial prefrontal regions generates bradycardia and depressor responses and inhibition of conditioned increases in heart rate and blood pressure (Foster et al, 2008). Resting heart rate was associated with lateral asymmetry across the frontal and parietal areas, resting systolic and diastolic blood pressure were related to lateral asymmetry across the temporal and parietal areas (Foster & Harrison, 2006).

What this means for SZO can only be speculated. In general, the CAN represents a dynamic system, with neural structures involved in affective and autonomic regulation, especially cardiovascular activity (Thayer, 2007; Thayer & Lane, 2000). The CAN controls preganglionic sympathetic and parasympathetic, neuroendocrine, respiratory, and sphincter motoneurons and is characterized by reciprocal

interconnections, parallel organization, state-dependent activity, and neurochemical complexity (Benarroch, 1993). Thereby, parasympathetic activation decreases the firing rate of pacemaker cells and heart rate, while sympathetic activity results in an increase of heart rate and firing rate of the pacemaker cells in the heart sinoatrial node (Ardell et al, 2015; Levy, 1997). For SZO, it can be assumed, that through the failure of the left-hemisphere activity in the frontal area, the parasympathetic tone is inhibited and thus the sympathetic tone is overactive resulting in increased heart rate and blood pressure values. As a consequence, within the CAN, the central activity (P_{EEG}) will be increased to counteract these phenomena in the periphery (ANS) to decrease the heart rate and the blood pressure.

The stronger pronounced central information flow in the direction of the cardiac activity (BBI) as well as of vascular regulation (SYS) leads to the assumption that the central-cardiac information flow is probably restricted by the generally impaired cardiac regulation in schizophrenia independently of medication (Bär et al, 2007b; Schulz et al, 2015a). Lesions in the CNS (frontal and temporal areas), as a part of the CAN, can lead to profound changes in heart regulation and even to potentially fatal cardiac arrhythmias or sudden cardiac death (cardiovascular dysfunctions) (Foster & Harrison, 2004). There exists a relationship between increasing magnitude of cerebral activation within the frontal and temporal areas (regions are involved in the regulation of cardiovascular functioning and changes in heart rate and blood pressure. That's why my investigation was focused on EEG electrodes in these regions. Finally, there is a well-known asymmetry between left and right hemisphere with failure of left side dominance that could influence the final coupling results. Thereby, increasing levels of cerebral activation within the left hemisphere would be associated with increasing parasympathetic tone and increasing levels within the right hemisphere with sympathetic tone (Foster & Harrison, 2004). However, it was stated that the two cerebral hemispheres act together to promote changes in cardiovascular functioning (Wittling et al, 1998). Other studies (Foster et al, 2008; Tucker, 1981) showed that the two hemispheres are in a reciprocally balanced condition, with each hemisphere opposing and complementing the other one in respect to parasympathetic and sympathetic modulation of the cardiovascular function.

Peripheral end organs such as the heart (HRV) forward sensory information to the CAN and are directly linked, and thus can be used as a good qualitative characteristic of the central-peripheral neuronal feedback-loop (Thayer, 2007). Dysfunctions within the CNS and their connection to stronger pronounced dysregulation of cardiovascular regulation, characterized by cardiac- and vascular dysregulation expressed through increased abnormal top down modulation (brain to heart), might a reason for the increased risk of sudden cardiac death in SZO (Foster & Harrison, 2004).

HRJSD results demonstrated that central-cardiac coupling in SZO was mainly characterized by a larger amount of decreased short-term strong/weak, increasing/decreasing central pattern families (P_{EEG}-E0, P_{EEG}-E1, P_{EEG}-E2, P_{EEG}-LU1, P_{EEG}-LD1) and an increased alternating and fluctuating of central pattern families (P_{EEG}-LA1, P_{EEG}-P and P_{EEG}-V). This means that central activity is much more variable and more random, with weaker rhythmic oscillatory components. Moreover, fast alterations of increased and subsequently decreased (BBI-P), fast alterations of decreased and subsequently increased (BBI-V) and alternating (BBI-LA1) of heart rate patterns were increased for SZO compared to CON, indicating a more random central-cardiac coupling with weaker rhythmic components of cardiac cycle intervals in relation to central activity in SZO. Central-vascular coupling by HRJSD in SZO was dominated mainly by highly variable SYS patterns in combination with all other 8 central pattern families. This was demonstrated by highly significantly decreased SYS-E1 and highly significantly increased SYS-E0, SYS-E2, SYS-LU1, SYS-LD1, SYS-LA1, SYS-P and SYS-V. It seems to be that the blood pressure regulation is more complex and mainly influences the central-vascular coupling pattern in SZO. Furthermore, it could be shown that central-vascular coupling is strongly affected by reduced blood pressure variability (SYS-E1) and short-term strong/weak, increasing/decreasing, alternating and fluctuating vascular family patterns (SYS-E0, SYS-E2, SYS-LU1, SYS-LD1, SYS-LA1, SYS-P, SYS-V), in combination with central activity. These results suggest an impairment of the baroreflex control feedback loop related to the anti-cholinergic effects of the antipsychotic treatment. One of HRJSD results to be highlighted is the finding that, in schizophrenic patients, the central activity had a much stronger variability and higher degree of randomness with less rhythmic oscillatory components than the central activity in healthy controls.

Considering central-cardiac coupling and central-vascular coupling with respect to central spectral power bands, the strongest influence of cerebral γ activity towards BBI and SYS was found for both SZO (here reduced) and CON, independent of the brain hemisphere. This highlights the role of γ activity in SZO and was also demonstrated in multiple studies (Basar & Guntekin, 2008; 2013). It has been shown that γ and β activity is most augmented in SZO over frontal and temporal brain regions, reflecting a genetic liability for schizophrenia (Venables et al, 2009). It was suggested that impaired neural oscillation (e.g., a reduction in amplitude and altered phase synchronization in all frequency bands with emphasis on the β and γ band activity) in schizophrenia patients can be considered a marker for a functional dysconnectivity between different brain areas and for dysfunctional cortical networks (Uhlhaas & Singer, 2010). Moreover, studies also showed that the parasympathetic and sympathetic nervous systems are lateralized to the left and right central hemispheres, respectively. The central-cardiac and central-vascular coupling directions with respect to central spectral power bands were characterised as

bidirectional with BBI and SYS acting as the driver in each frequency band. This may suggest that the autonomous system provides feedback information towards the different central oscillatory components (with the exception of γ). All these components considered together as the whole central activity provide, in turn, feedforward information to the ANS.

Central-cardiovascular interactions revealed that a stronger linear information flow from central activity in the direction of blood pressure regulation (SYS) than in the direction of BBI in SZO compared to CON. In particular, in SZO, the central-cardiac information transfer is more non-linearly defined and significantly bidirectionally decreased. This suggests for SZO, that the linear central-vascular regulation closed-loop (baroreflex loop) purposefully maintains the blood pressure adaptation and is more aligned than the non-linear part of this regulation closed-loop. Especially, for SZO, within this closed-loop it is obvious that the central regulatory processes (P_{EEG}) are more directed towards the cardiac and vascular system (BBI, SYS) than in the opposite direction (Figure 26).

4.5 The central-cardiorespiratory-network

4.5.1 Cardiorespiratory coupling (BBI–RESP)

NSTPDC revealed a significant differently coupling direction between SZO and CON. SZO (NF~−1.5) showed a bidirectional information transfer (RESP→BBI) (RESP is the driver). The coupling strength for the information transfer from the cardiac system to the respiratory system ($A_{BBI\rightarrow RESP(P_{EEG})}$) was highly significantly decreased for SZO compared to CON. For the RSA loop, when the respiratory system (RESP) transfers information towards the cardiac system (BBI) the coupling strengths were increased for both groups, but not significantly different (**Figure 25**) (**Table 15**).

Table 15. *Linear central-cardiorespiratory (BBI, RESP, and P_{EEG}) coupling analyses results (NSTPDC) to discriminate between patients suffering from paranoid schizophrenia (SZO) and healthy subjects (CON) for the frontal area (A1). (BBI=beat-to-beat intervals, RESP=respiratory frequency, P_{EEG}=mean power in the BBI-related EEG intervals, *p<0.05, **p<0.01, ***p<0.00041, n.s.=not significant, #=not confirmed by surrogate analysis)*

	Index	CON mean ± std	SZO mean ± std
BBI↔RESP	NF	-1.56 ± 0.34	-1.48 ± 0.69
	$A_{BBI\rightarrow RESP(PEEG)}$	0.05 ± 0.02	0.04 ± 0.03***
	$A_{RESP\rightarrow BBI(PEEG)}$	0.25 ± 0.08	0.27 ± 0.17
BBI↔P_{EEG}	NF	-0.48 ± 0.76	-0.13 ± 0.91***
	$A_{BBI\rightarrow PEEG(RESP)}$	0.10 ± 0.05	0.12 ± 0.06***
	$A_{PEEG\rightarrow BBI(RESP)}$	0.16 ± 0.08	0.15 ± 0.07*
RESP↔P_{EEG}	NF	0.99 ± 0.66	1.26 ± 0.62***
	$A_{RESP\rightarrow PEEG(BBI)}$	0.19 ± 0.07	0.24 ± 0.11***
	$A_{PEEG\rightarrow RESP(BBI)}$	0.06 ± 0.03	0.05 ± 0.03***,#

Non-linear cardiorespiratory coupling analyses (MuTE) revealed that the coupling strengths from BBI to RESP and from RESP to BBI (RSA loop) were significantly decreased in SZO in comparison to CON (**Table 16**).

4.5.2 Central-cardiac coupling (BBI–P_{EEG})

For central-cardiac coupling analysis (BBI–P_{EEG}) all indices showed significant differences between both groups. For the coupling direction, SZO (NF~−0.1) showed an equal influence in both directions and/or no coupling (P_{EEG}↔BBI). The coupling strength ($A_{BBI\rightarrow P_{EEG}(RESP)}$) for the information transfer from cardiac system to the central system (BBI→P_{EEG}) showed highly significant differences between SZO and CON. Here, SZO presented a stronger coupling from BBI→P_{EEG} compared to CON.

In the case of, when the information transfer is from central system directed towards the cardiac system (P_{EEG}→BBI) the coupling strength ($A_{P_{EEG}\rightarrow BBI(RESP)}$) was significantly decreased in SZO, and vice versa. (**Figure 25**) (**Table 15**).

Please note that the values for central-cardiac couplings in **Table 15** are different from the values in **Table 10**, because in **Table 10** other EEG channels for the frontal area were included (analyses of the central-cardiovascular areas). The same is true for **Figure 25** and central-cardiac couplings compared to **Figure 22** (analyses of the central-cardiovascular areas).

The causal non-linear central-cardiac couplings (MuTE) were only significantly different between SZO and CON in the case when BBI influenced P_{EEG} ($MuTE_{BBI\rightarrow PEEG(RESP)}$). The non-linear influences from BBI to P_{EEG} as well as from P_{EEG} to BBI were nearly comparable in both directions, and slightly more pronounced in CON than SZO (**Table 16**).

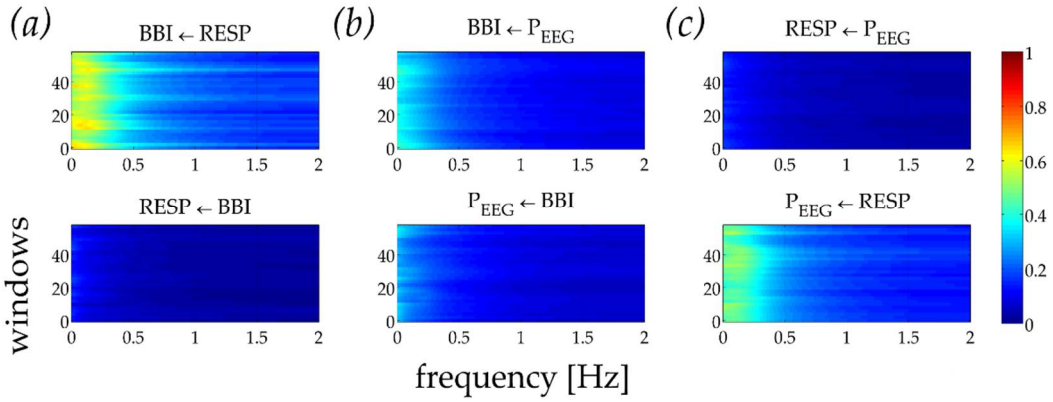

Figure 25. Averaged NSTPDC plots for central-cardiorespiratory coupling analyses for (a) cardiorespiratory couplings, (b) central-cardiac couplings, and (c) central-respiratory couplings for schizophrenic patients for the frontal area (A1). Arrows indicating the causal coupling direction from one time series to another, e.g., RESP←P_{EEG}, indicating the causal link from P_{EEG} to RESP. Coupling strength ranges from blue (no coupling) to red (maximum coupling), where BBI represents beat-to-beat intervals, RESP represents respiratory frequency, and P_{EEG} represents the mean power in BBI-related EEG intervals.

Considering the investigated clusters (A0-A4), SZO demonstrated the highest coupling strengths for A1 and the lowest for A2, in the case of BBI→P_{EEG}. In the opposite direction P_{EEG}→BBI, SZO demonstrated the lowest coupling strengths for A1 and the highest for A3 (**Table 17**). For SZO the most significant differences between the clusters could be found for A1 vs. A2, and A2 vs. A4, whereby for CON it was A1 vs. A2 for the coupling BBI↔P_{EEG}(RESP) (**Table 18**, **Table 19**).

Table 16. *Non-linear central-cardiovascular (BBI, RESP, and P_{EEG}) coupling analyses results (MuTE) to discriminate between patients suffering from paranoid schizophrenia (SZO) and healthy subjects (CON) for the frontal area (A1). (BBI=beat-to-beat intervals, RESP=respiratory frequency, P_{EEG}=the mean power in the BBI-related EEG intervals, *p<0.05, **p<0.01, ***p<0.00041, n.s.=not significant, #=not confirmed by surrogate analysis)*

	Index	CON mean ± std	SZO mean ± std
BBI↔RESP	$MuTE_{BBI\rightarrow RESP(PEEG)}$	0.020 ± 0.013	0.015 ± 0.012***
	$MuTE_{RESP\rightarrow BBI(PEEG)}$	0.033 ± 0.009	0.026 ± 0.012***
BBI↔P_{EEG}	$MuTE_{BBI\rightarrow PEEG(RESP)}$	0.014 ± 0.011	0.012 ± 0.011*
	$MuTE_{PEEG\rightarrow BBI(RESP)}$	0.016 ± 0.010	0.014 ± 0.010
RESP↔P_{EEG}	$MuTE_{RESP\rightarrow PEEG(BBI)}$	0.017 ± 0.010	0.014 ± 0.009***
	$MuTE_{PEEG\rightarrow RESP(BBI)}$	0.015 ± 0.008	0.012 ± 0.009***

4.5.3 Central-respiratory coupling (RESP–P_{EEG})

The coupling direction (central-respiratory) revealed highly significant differences between SZO and CON. SZO (NF~1.3) and CON (NF~1.0) presented both a strong bidirectional one (RESP→P_{EEG}) (RESP is the driver) and were confirmed by highly significantly different coupling strengths ($A_{RESP\rightarrow P_{EEG}(BBI)}$, $A_{P_{EEG}\rightarrow RESP(BBI)}$) between both groups. The coupling strength for the information transfer from the respiratory system to the central system (RESP→P_{EEG}) was significantly increased in SZO compared to CON. For the information transfer from the central system to the respiratory system (P_{EEG}→RESP) the coupling strengths indicated a significant reduction in SZO vs. CON (not confirmed by surrogate analysis). The coupling strength from the ANS (RESP) towards CNS (P_{EEG}) was more pronounced than vice versa, whereby, for CON it was expressed in an opposite way (**Figure 25**) (**Table 15**). For the cluster analyses, SZO demonstrated the highest coupling strengths for A1 and A4, and the lowest again for A2, in the case of RESP→P_{EEG}. In the opposite direction P_{EEG}→RESP, SZO demonstrated the lowest coupling strengths again for A1 and the highest again for A3 (**Table 17**). For SZO the most significant differences between the clusters could be found again for A1 vs. A2, and A2 vs. A4, whereby for CON it was again between A1 and A2 for the coupling RESP↔P_{EEG}(BBI) (**Table 18**, **Table 19**).

Non-linear casual central-respiratory coupling analyses (MuTE) revealed a similar behaviour as shown for central-cardiac coupling analyses. High significant differences were found for both cases, when RESP influences P_{EEG} ($MuTE_{RESP\rightarrow PEEG(BBI)}$)

as well as when P_{EEG} influences RESP ($MuTE_{PEEG \rightarrow RESP(BBI)}$). The non-linear information transfers from respiratory activity towards central activity ($RESP \rightarrow P_{EEG}$) and from P_{EEG} to RESP ($P_{EEG} \rightarrow RESP$) were nearly comparable in both directions and more pronounced in CON than SZO (**Table 16**).

Table 17. *Linear central-cardiorespiratory (BBI, RESP, and P_{EEG}) coupling analyses results (NSTPDC) to discriminate between patients suffering from paranoid schizophrenia (SZO) and healthy subjects (CON) for A0 (all EEG channels), A2 (the central area), A3 (the temporal area), and A4 (the parietal-occipital area). (BBI=beat-to-beat intervals, RESP=respiratory frequency, P_{EEG}=mean power in the BBI-related EEG intervals, *p<0.05, **p<0.01, ***p<0.00041, n.s.=not significant, #=not confirmed by surrogate analysis)*

	Index	A0		A2		A3		A4	
		CON	SZO	CON	SZO	CON	SZO	CON	SZO
		mean ± std	mean ± std	mean ± std	mean ± std	mean ± std	mean ± std	mean ± std	mean ± std
BBI↔P_{EEG}	NF	-0.67 ± 0.75	-0.25 ± 0.91***	-0.82 ± 0.70	-0.43 ± 0.89***	-0.64 ± 0.8	-0.28 ± 0.94***	-0.68 ± 0.73	-0.14 ± 0.87***
	$A_{BBI\rightarrow PEEG(RESP)}$	0.10 ± 0.05	0.12 ± 0.05***	0.09 ± 0.04	0.10 ± 0.05***	0.10 ± 0.1	0.12 ± 0.06***	0.09 ± 0.04	0.12 ± 0.05***
	$A_{PEEG\rightarrow BBI(RESP)}$	0.19 ± 0.10	0.16 ± 0.10***	0.20 ± 0.10	0.16 ± 0.09***	0.21 ± 0.1	0.18 ± 0.15**	0.19 ± 0.09	0.15 ± 0.11***
RESP↔P_{EEG}	NF	0.82 ± 0.74	1.18 ± 0.73***	0.73 ± 0.68	1.15 ± 0.60***	0.74 ± 1	1.04 ± 1.07***	0.84 ± 0.67	1.21 ± 0.70***
	$A_{RESP\rightarrow PEEG(BBI)}$	0.17 ± 0.07	0.23 ± 0.10***	0.16 ± 0.06	0.21 ± 0.09***	0.18 ± 0.1	0.23 ± 0.12***	0.17 ± 0.06	0.24 ± 0.10***
	$A_{PEEG\rightarrow RESP(BBI)}$	0.07 ± 0.06	0.06 ± 0.05***,#	0.07 ± 0.03	0.05 ± 0.03***,#	0.10 ± 0.1	0.08 ± 0.11***	0.07 ± 0.03	0.05 ± 0.04***,#

Table 18. *Central-cardiorespiratory coupling results comparing several EEG-clusters (A1-A4) in patients suffering from paranoid schizophrenia (SZO). A1 (the frontal area), A2 (the central area), A3 (the temporal area), and A4 (the parietal-occipital area). (BBI=beat-to-beat intervals, RESP=respiratory frequency, P_{EEG}=mean power in the BBI-related EEG intervals, *p<0.05, **p<0.01, ***p<0.00041, n.s.=not significant)*

BBI↔P_{EEG}(RESP)		**A1**			**A2**			**A3**		
		NF	$A_{BBI→PEEG}$	$A_{PEEG→BBI}$	NF	$A_{BBI→PEEG}$	$A_{PEEG→BBI}$	NF	$A_{BBI→PEEG}$	$A_{PEEG→BBI}$
	NF	***								
A2	$A_{BBI→PEEG}$		***							
	$A_{PEEG→BBI}$			*						
	NF	n.s.			*					
A3	$A_{BBI→PEEG}$		n.s.			**				
	$A_{PEEG→BBI}$			n.s.			n.s.			
	NF	n.s.			***			n.s.		
A4	$A_{BBI→PEEG}$		n.s.			***			n.s.	
	$A_{PEEG→BBI}$			n.s.			***			*

RESP↔P_{EEG}(BBI)		**A1**			**A2**			**A3**		
		NF	$A_{RESP→PEEG}$	$A_{PEEG→RESP}$	NF	$A_{RESP→PEEG}$	$A_{PEEG→RESP}$	NF	$A_{RESP→PEEG}$	$A_{PEEG→RESP}$
	NF	**								
A2	$A_{RESP→PEEG}$		***							
	$A_{PEEG→RESP}$			**						
	NF	n.s.			n.s.					
A3	$A_{RESP→PEEG}$		n.s.			*				
	$A_{PEEG→RESP}$			n.s.			n.s.			
	NF	n.s.			*			n.s.		
A4	$A_{RESP→PEEG}$		n.s.			***			n.s.	
	$A_{PEEG→RESP}$			n.s.			n.s.			n.s.

Table 19. *Central-cardiorespiratory coupling results comparing several EEG-clusters (A1-A4) in healthy subjects (CON). A1 (the frontal area), A2 (the central area), A3 (the temporal area), and A4 (the parietal-occipital area). (BBI=beat-to-beat intervals, RESP=respiratory frequency, P_{EEG}=mean power in the BBI-related EEG intervals, *p<0.05, **p<0.01, ***p<0.00041, n.s.=not significant)*

BBI↔P_{EEG}(RESP)		**A1**			**A2**			**A3**		
		NF	$A_{BBI→PEEG}$	$A_{PEEG→BBI}$	NF	$A_{BBI→PEEG}$	$A_{PEEG→BBI}$	NF	$A_{BBI→PEEG}$	$A_{PEEG→BBI}$
A2	NF	***								
	$A_{BBI→PEEG}$		***							
	$A_{PEEG→BBI}$			***						
A3	NF	n.s.			**					
	$A_{BBI→PEEG}$		n.s.			*				
	$A_{PEEG→BBI}$			*			*			
A4	NF	*			**			n.s.		
	$A_{BBI→PEEG}$		*			n.s.			n.s.	
	$A_{PEEG→BBI}$			**			**			n.s.

RESP↔P_{EEG}(BBI)		**A1**			**A2**			**A3**		
		NF	$A_{RESP→PEEG}$	$A_{PEEG→RESP}$	NF	$A_{RESP→PEEG}$	$A_{PEEG→RESP}$	NF	$A_{RESP→PEEG}$	$A_{PEEG→RESP}$
A2	NF	***								
	$A_{RESP→PEEG}$		***							
	$A_{PEEG→RESP}$			***						
A3	NF	n.s.			*					
	$A_{RESP→PEEG}$		n.s.			***				
	$A_{PEEG→RESP}$			n.s.			n.s.			
A4	NF	n.s.			**			n.s.		
	$A_{RESP→PEEG}$		***			**			n.s.	
	$A_{PEEG→RESP}$			*			n.s.			n.s.

Table 20. *Probability of the occurrence of mHRJSD coupling pattern, pattern families and entropy values for the central-cardiorespiratory network (BBI, RESP, and P_{EEG}) to discriminate between patients suffering from paranoid schizophrenia (SZO) and healthy subjects (CON) for A0 (all EEG channels), A1 (the frontal area), A2 (the central area), A3 (the temporal area), and A4 (the parietal-occipital area). (BBI=beat-to-beat intervals, RESP=respiratory frequency, P_{EEG}=mean power in the BBI-related EEG intervals, *p<0.05, **p<0.01, ***p<0.00041, n.s.=not significant, #=not confirmed by surrogate analysis)*

	Index	A0						A1						A2					
		CON			SZO			CON			SZO			CON			SZO		
		mean	±	std	mean	±	std	mean	±	std	mean	±	std	mean	±	std	mean	±	std
Coupling pattern	*BBI-LU1/RESP-E1/P_{EEG}-E1*	0.16	±	0.05	0.14	±	0.05***	0.15	±	0.05	0.14	±	0.05	0.16	±	0.05	0.14	±	0.06
	BBI-LD1/RESP-E1/P_{EEG}-E1	0.17	±	0.06	0.15	±	0.06***	0.17	±	0.05	0.15	±	0.06	0.18	±	0.06	0.15	±	0.07
Pattern families	*BBI-E2*	0.06	±	0.04	0.03	±	0.02***	0.06	±	0.04	0.03	±	0.02***	0.06	±	0.04	0.03	±	0.02***
	BBI-LU1	0.25	±	0.06	0.24	±	0.07	0.25	±	0.06	0.24	±	0.07	0.25	±	0.06	0.24	±	0.07
	BBI-LD1	0.28	±	0.06	0.26	±	0.08**	0.28	±	0.06	0.26	±	0.08	0.28	±	0.06	0.26	±	0.08
	BBI-P	0.02	±	0.02	0.05	±	0.04***,#	0.02	±	0.02	0.05	±	0.04***,#	0.02	±	0.02	0.05	±	0.04***,#
	RESP-E1	0.90	±	0.05	0.89	±	0.10*	0.90	±	0.05	0.89	±	0.10	0.90	±	0.05	0.89	±	0.10
	P_{EEG}-E1	0.70	±	0.16	0.64	±	0.17***	0.68	±	0.16	0.65	±	0.16*	0.72	±	0.16	0.65	±	0.15***
	P_{EEG}-LU1	0.12	±	0.06	0.14	±	0.06***,#	0.13	±	0.06	0.14	±	0.06	0.11	±	0.06	0.14	±	0.06***
	P_{EEG}-LD1	0.12	±	0.06	0.14	±	0.06***	0.13	±	0.06	0.14	±	0.06	0.11	±	0.06	0.14	±	0.06***
Entropy	*$mHRJSD_{Shannon}$*	4.0	±	0.7	4.2	±	0.9***	4.1	±	0.7	4.2	±	0.9	3.9	±	0.7	4.2	±	0.8***
	$mHRJSD_{renyi2}$	3.0	±	0.7	3.2	±	0.9***	3.1	±	0.7	3.2	±	0.9	2.9	±	0.7	3.2	±	0.8***

	Index	A3						A4					
		CON			SZO			CON			SZO		
		mean	±	std	mean	±	std	mean	±	std	mean	±	std
Coupling pattern	*BBI-LU1/RESP-E1/P_{EEG}-E1*	0.16	±	0.05	0.14	±	0.06	0.16	±	0.06	0.13	±	0.05***
	BBI-LD1/RESP-E1/P_{EEG}-E1	0.17	±	0.06	0.16	±	0.07	0.17	±	0.06	0.14	±	0.06***
Pattern families	*BBI-E2*	0.06	±	0.04	0.03	±	0.02***	0.06	±	0.04	0.03	±	0.02***
	BBI-LU1	0.25	±	0.06	0.24	±	0.07	0.25	±	0.06	0.24	±	0.07
	BBI-LD1	0.28	±	0.06	0.26	±	0.08	0.28	±	0.06	0.26	±	0.08
	BBI-P	0.02	±	0.02	0.05	±	0.04***,#	0.02	±	0.02	0.05	±	0.04***,#
	RESP-E1	0.90	±	0.05	0.89	±	0.10	0.90	±	0.05	0.89	±	0.10
	P_{EEG}-E1	0.70	±	0.16	0.66	±	0.18*	0.70	±	0.16	0.60	±	0.17***
	P_{EEG}-LU1	0.12	±	0.06	0.13	±	0.07	0.12	±	0.07	0.15	±	0.07***
	P_{EEG}-LD1	0.12	±	0.06	0.13	±	0.07*	0.12	±	0.06	0.16	±	0.07***
Entropy	*$mHRJSD_{Shannon}$*	4.0	±	0.7	4.1	±	0.9	4.0	±	0.6	4.3	±	0.9***
	$mHRJSD_{renyi2}$	3.0	±	0.7	3.1	±	0.9	3.0	±	0.7	3.3	±	0.9***

The mHRJSD approach revealed 2 highly significant central-cardiorespiratory coupling patterns (BBI-LU1/RESP-E1/P_{EEG}-E1, BBI-LD1/RESP-E1/P_{EEG}-E1) between SZO and CON investigating all EEG channels (A0) and the parietal-occipital cluster (A4). Three significant heart rate (E2, LD1, P), one significant respiratory (E1), and three central (E1, LU1, LD1) pattern families showed also differences between SZO and CON (**Table 20**). Central-cardiorespiratory couplings were quantified by the heart rate pattern families LU1 and LD1, the respiratory pattern family E1, and by the central patterns family E1, respectively. Thereby, I found that for the central-cardiorespiratory coupling patterns the heart rate pattern families (BBI-LU1, BBI-LD1), the respiratory pattern family (RESP-E1) and the central patterns family (P_{EEG}-E1) were significantly decreased in SZO in comparison to CON. In addition, SZO were characterized by further significant pattern families which showed increased absolute values as BBI-P, P_{EEG}-LU1, and P_{EEG}-LD1 as well as one significant pattern family with decreased absolute value BBI-E2 in comparison to CON for A0, A2, and A4, and partly for A1 and A3 (**Table 20**). The entropy-based indices $mHRJSD_{Shannon}$ and $mHRJSD_{renyi2}$ were significantly increased in SZO compared to CON for A0, A2, and A4.

4.5.4. Summary and discussion

4.5.4.1 Cardiorespiratory coupling (BBI–RESP)

The direction (NF~−1.5) of the linear information flow within the cardiorespiratory system was bidirectionally pronounced and with the respiration as the driving part in the direction towards cardiac activity (RESP→BBI) in SZO compared to CON (NF~−1.6), who revealed a slightly better RSA-loop. The linear information flow BBI→RESP (significant) within the cardiorespiratory system is suggested as a biomarker complementing RSA as a reciprocal component of cardiorespiratory interaction (Dick et al, 2014). Dick et al. (Dick et al, 2014) believe that this mutual interaction in the function of gas exchange between the respiratory and autonomic system is characterized in a way that the ANS transfers information to the respiratory system in generating breathing patterns is beat-to-beat, whereas the well-known information flow from respiration in the direction to ANS (RSA-loop) is pronounced breath-to-breath. In healthy subjects, it has been shown that the degree of sympathetic activation was associated with a decrease in cardiorespiratory interactions and the RSA-loop during the head-up tilt test (Porta et al, 2012b), confirming the assumption that SZO were associated with higher sympathetic activation. The non-linear cardiorespiratory information transfer was significantly reduced in both directions (BBI→RESP, RESP→BBI) indicating that, in general, non-linear regulatory processes are inhibited. In the study of Peupelmann et al. (Peupelmann et al, 2009), they could show that the severity of schizophrenia is associated with breathing patterns

assuming that an inhibition of vagal control centres at the brainstem are responsible for their findings. The causal information flow RESP→BBI independent of arterial pressure changes characterizes central respiratory driving mechanisms related to alterations in heart rate on the cardiac vagal motor neurons (Faes et al, 2011b). Central respiratory driving mechanisms seem to be inhibited and directly connected to alterations in the cardiac regulatory system in SZO (Schulz et al, 2015a). It was demonstrated that the frontal, central (investigated in this study) and occipital brain regions are involved in central-cardiorespiratory information transfers which are altered to physiological conditions such as wake and sleep (Bartsch et al, 2015).

4.5.4.2 Central-cardiac coupling (BBI–P_{EEG}) and central-respiratory coupling (RESP–P_{EEG})

The closed-loop (feedback-loop) of central-cardiorespiratory regulation seems to be focused on adjusting this increased cardiac activity (heart rate) via the sinus node rather than on regulating respiration. However, whether central chemoreceptors regulate the cardiovagal outflow independently of the respiratory system is an open question (Guyenet, 2014). The respiratory network receives peripheral chemosensory and mechanosensory inputs and modulatory inputs from the other parts of the brain. These inputs are essential for adaptive changes in the respiratory motor output, ensuring appropriate ventilation of the lungs in variable environmental and physiological conditions (Gourine & Spyer, 2009). Lung ventilation, cardiac output, and blood pressure are highly labile physiological states that are continually adjusted by the CNS to match the metabolic requirements of specific behaviours (Guyenet, 2014). It seems to be that in SZO maintaining the oxygen supply takes priority expressed by the stronger feedback from RESP towards P_{EEG}. This feedback-loop from RESP towards central activity is strongly dominated by respiratory activity. This could be originated by reflexes from muscle mechano- and metabotropic receptors cooperate to activate breathing to a degree roughly commensurate with the rise in whole body metabolism and oxygenation. It seems that these cardiorespiratory responses were caused by an initial fast increase in cardiovascular and ventilatory flow parameters that are brought about by neurally mediated muscle mechanoreceptor feedback reflexes and a feedforward 'central motor command'. The combination of these two neural mechanisms will also increase the blood pressure operating point. Thus, the fine control of the matching of cardiac output to ventilation may occur by means of a feedforward ventilatory control of cardiac origin (Turner, 1991).

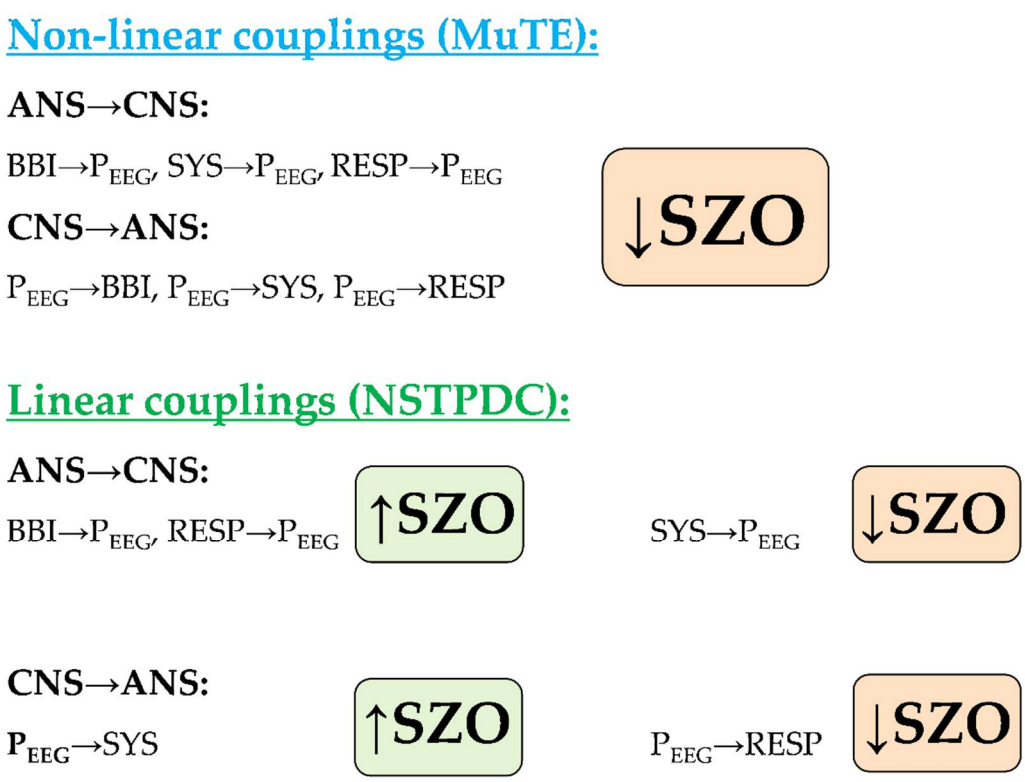

Figure 26. *Summary of significant (p<0.01) linear and non-linear couplings within the central-autonomic-network in schizophrenia (SZO) in comparison to healthy subjects (CON). (BBI=beat-to-beat intervals, SYS=end-systolic blood pressure amplitude values over time, RESP=respiratory frequency, PEEG=mean power in the BBI-related EEG intervals)*

The linear bidirectionally directed central-respiratory information transfer (PEEG↔RESP(BBI)) was dominated towards CNS from respiration. The strongest coupling for PEEG→BBI(RESP) was found for cluster A3 and the weakest coupling for cluster A1. In the opposite direction BBI→PEEG(RESP) the strongest value was found for cluster A1 and the weakest one for cluster A2. For the coupling strength PEEG→RESP(BBI) the highest value was found for cluster A3 again and the lowest value for cluster A1. In the opposite direction RESP→PEEG(BBI) the highest values were found for clusters A1 and A4 and the lowest one for cluster A2. That means that the strongest influence (information transfer) from central activity coming from A3 (temporal area) towards ANS for the cardiorespiratory network. On the other side, it was found that the weakest influence (information transfer) from central activity coming from A1 (frontal area) towards ANS for the cardiorespiratory network. Moreover, the cluster A2 (central area) revealed the weakest information flow from the ANS towards CNS. In addition, it seems to be that, the frontal area (A1) is associated with heart rate activity and the frontal area (A1) and the parietal-occipital area (A4) were associated with respiratory activity. Bartsch et al. (Bartsch et al, 2015) could also show that central-cardiorespiratory couplings change with physiological

states (wake, sleep), and that different brain areas (frontal, central or occipital) play different roles in these couplings. Due to, the respiratory pathway being more pronounced instead of the cardiac one. This leads to the assumption that the closed-loop of central-cardiorespiratory information transfer is less pronounced by central driving on the respiratory system to adapt heart rate but stronger by the ANS. However, it seems that central-cardiorespiratory feedback-loop in the direction from ANS towards CNS is strongly dominated by respiration that functions as a feedback trigger to central regulatory processes for more information transfer towards the ANS for adaptation oxygenation. The brainstem and higher brain centres (limbic system, cortical structures) interacting to maintain the final respiratory output, mainly regulated for metabolic and homeostatic purposes and altered in reaction to emotions (Homma & Masaoka, 2008) such as fear and anxiety present in SZO. Thus, the supposition is that paranoid cognition may reflect an internally generated cycle of misattribution regarding incoming fear signals due to a breakdown in the regulation of these systems resulting in an altered brain–heart interaction, influenced by a lack of cortical inhibitory control over sympatho-excitatory subcortical regions (Williams et al, 2004). Williams et al. (Williams et al, 2004) stated, "that paranoid schizophrenia is characterized by a specific disjunction of arousal and amygdala-prefrontal circuits that leads to impaired processing of significant, particularly threat-related, signals. The pattern of excessive arousal but reduced amygdala activity in paranoid patients points to a dysregulation in the normal cycle of mutual feedback between amygdala function and somatic state (autonomic activity). The concomitant lack of "with-arousal" medial prefrontal engagement suggests that this region cannot undertake its usual role in regulating amygdala-autonomic function, leading to a perseveration and exacerbation of arousal responses." The medial prefrontal area responsible for maintaining amygdala-autonomic working processes seem to be not able to perform its function resulting in a perseveration and exacerbation of arousal responses (threat-related signals (skin conductive response)).

Thus, that the human organism is an integrated network of interconnected and interacting organ systems, each representing a separate regulatory network. The behaviour of one physiological system (network) may affect the dynamics of all other systems in the network of physiologic networks. Due to these interactions, failure of one system can trigger a cascade of failures throughout the entire network (Ivanov & Bartsch, 2014).

MHRJSD results demonstrated that central-cardiorespiratory coupling in SZO was mainly characterized by a lower amount of weak, increasing/decreasing heart rate pattern families (BBI-LU1, BBI-LD1), and a lower amount of invariable respiratory patterns and central patterns (RESP-E1, P_{EEG}-E1). Being a unique feature of the mHRJSD approach (in contrast to other coupling approaches), I was able clearly to identify different altered central-autonomic physiological regulatory patterns

generated by the interplay of the CNS and the ANS in patients with schizophrenia. One of my results to be highlighted is the finding that, in schizophrenic patients, the central activity had a much lower variability (P_{EEG}-E1) and less strong rhythmic oscillatory components (P_{EEG}-LU1, P_{EEG}-LD1) than the central activity in healthy controls. Considering the complexity of central-cardiorespiratory network, I found increased complexity for mHRJSD results. Increased Shannon ($mHRJSD_{Shannon}$) and Renyi ($mHRJSD_{renyi2}$) entropies describe the complexity and randomness of deterministic regulatory coupling patterns (mHRJSD) occurrences in SZO when compared to CON. That means that the higher complexity of central-cardiorespiratory network in SZO is a result of that there are less frequently or missing patterns in trivariate word types or coupling patterns.

The altered central-cardiorespiratory couplings in SZO are characterized by a weaker linear and non-linear central information transfer (P_{EEG}→BBI) in the direction of the cardiac system, and a stronger linear respiratory information flow in the direction of the central system (RESP→P_{EEG}) compared to CON (Figure 26). In addition, central-cardiorespiratory coupling patterns in SZO were mainly characterized by a lower amount of an unchanging central pattern (P_{EEG}-E1), weak increasing/decreasing heart rate patterns (LU1, LD1), and an unchanging respiratory pattern (RESP-E1) as well as a higher complexity of the central-cardiorespiratory network. The scientific impact of this study provides a further step towards a more comprehensive understanding of the interplay of neuronal and autonomic regulatory processes in schizophrenia.

Chapter 5

5. Conclusions

This thesis aimed to characterize short-term instantaneous central-autonomic-network coupling pathways (top-to-bottom and bottom to top) by analysing the coupling of heart rate, systolic blood pressure, respiration and central activity (EEG) in schizophrenic patients and healthy participants. Therefore, new multivariate causal and non-causal linear and non-linear coupling approaches (HRJSD, mHRJSD, NSTPDC) that are able to determine the coupling strength and direction as well as the quantification and classification of deterministic regulatory coupling patterns within and between the cardiovascular- the cardiorespiratory system and the central-autonomic-network were developed (chapter 3). These new coupling approaches allow a new understanding and insight into (patho)physiological regulation processes of the central-autonomic-network in schizophrenia and healthy subjects. Moreover, the findings of the clinical studies (chapter 4) might further allow an improvement in treatment strategies in those patients, and finally, possibly contribute to cardiac risk stratification strategies in order to be able to identify those patients at higher risk for cardiovascular diseases.

In ***chapter 2***, I presented a review of the most frequently applied linear and non-linear coupling approaches (Granger causality, non-linear prediction, entropy, symbolization, and phase synchronization) applied to quantify causal and non-causal direct and indirect couplings that allow for new insights regarding alterations of cardiovascular, cardiorespiratory, and central regulatory networks and may lead to an improved knowledge of the interacting regulatory mechanisms under different physiological and pathophysiological conditions. I outlined their basic theoretical background and requirements as well as important points when applying these approaches to time series analysis, their main features, influencing factors and application examples in the medical field. However, one consideration necessary is that the application of these coupling approaches cannot be restricted to a single favourable since this mainly depends on the problem to be solved. Currently, no generally superior approach that can solve all problems exists. Coupling approaches represent promising tools for detecting information flows in a multivariate sense. They also may be able to provide additional prognostic information in the medical field and might overcome or at least complement other traditional univariate analysis techniques. The interest in coupling analyses of (patho)physiological networks has grown considerably, and therefore, this will potentially lead to an increasing demand for additional applications in the near future, thereby improving the knowledge about interacting regulatory subsystems.

In ***chapter 3.1***, I introduced the HRJSD approach based on a redundancy reduction strategy to group single word types into 8 pattern families, allowing a detailed quantification and classification of bivariate short-term cardiovascular-, cardiorespiratory- and central-autonomic coupling patterns which were due to changes of the different autonomic and central regulatory control mechanisms. This redundancy reduction strategy and the bivariate pattern family density matrix allows for a more robust statistical analysis of regulatory processes. These are very promising and novel features of coupling analyses, emphasizing the novelty of the HRJSD approach. My bivariate redundancy reduction strategy was based on the idea of the classification of frequent deterministic patterns lasting three beats (symbols), as proposed by Porta et al. (Porta et al, 2001). The proposed HRJSD approach was enlarged to create a bridge between univariate and bivariate symbolic analyses. As a quite new feature in contrast to the classical JSD approach or other coupling approaches (Schulz et al, 2013a) the HRJSD approach emphasizes a clear characterization of how the couplings are composed by the different regulatory aspects of the ANS and CNS. Moreover, the HRJSD approach includes different threshold levels and a directionality index D_{HRJSD}. The validation studies showed that the directionality index D_{HRJSD} is able to correctly detect the dominating coupling direction in linear coupled systems, but is only partly able to detect the dominating coupling direction in non-linear coupled systems. Furthermore, the baroreflex-related

threshold (*BRS_TH*) illustrated its potential and significance to characterise short-term non-linear cardiovascular coupling patterns, whereas the thresholds *1/4sd_TH* seem to be the most suitable thresholds to characterise short-term non-linear cardiorespiratory coupling patterns.

In ***chapter 3.2***, I introduced the mHRJSD approach to overcome the limitation of the HRJSD approach that was only able to analyse bivariate couplings and to determine the driver-responder relationship. Therefore, the bivariate HRJSD was an enhanced approach by including a third time series allowing the quantification of multivariate couplings and the determination of the driver-responder relationships in multivariate coupled systems. For the mHRJSD approach a statistical significance level was applied to prevent that spurious couplings were detected whereby the probabilities of occurrences of the coupling patterns has been set to $p(w_f)>0.05$ and has to fulfil the Bonferroni-Holm adjustment ($p<0.000098$, $n=512$ coupling patterns). The multivariate redundancy reduction strategy with the multivariate pattern family density matrix allows for a robust statistical analysis and provides more detailed information about short-term physiological regulatory processes of complex multivariate physiological networks. The mHRJSD approach contains multivariate Directionality indices D_{mHRJSD} ($D_{\mathrm{mHRJSD}}(x,y|z)$, $D_{\mathrm{mHRJSD}}(x,z|y)$, and $D_{\mathrm{mHRJSD}}(y,z|x)$) allowing to determine the primary driver $^{**}D_{\mathrm{mHRJSD}}$, the secondary driver $^{*}D_{\mathrm{mHRJSD}}$ and dominant responder $\bar{D}_{\mathrm{mHRJSD}}$ in multivariate systems (assumption: weakly coupled system). The simulation procedure revealed that the proposed directionality index D_{mHRJSD} derived from the mHRJSD approach is only able to correctly detect the driver-responder relationships in linear coupled systems, but is not able to detect the driver-responder relationships in non-linear coupled systems (limitation). Moreover, the mHRJSD approach is able to evaluate the direct causal information transfer in multivariate systems.

In ***chapter 3.3***, I proposed the NSTPDC approach as an enhanced version of the classical PDC approach to overcome its restrictions, and to allow the classification of couplings (coupling strength and direction) of non-stationary and scale-invariant short time series of multivariate linear and non-linear coupled systems. The NSTPDC approach is based on an m-dimensional AR model and determines linear Granger causality in the frequency domain. The NSTPDC approach has the following properties: the optimal model order of the AR model and its coefficients were determined by the stepwise least squares' algorithm and the Schwarz's Bayesian Criterion; a normalization procedure (zero mean and unit variance) enables to analyse non-stationary and scale-invariant time series; the Normalized Factor (NF) allows a clear and differentiable characterization of the coupling directions; the coupling strength [0,1] in each window within a predefined frequency band. Moreover, the simulations showed that the NSTPDC approach is able to distinguish between both direct and indirect causal information transfer, and is very sensitive in

detecting the correct driver-responder relationships in multivariate linear coupled systems (only partly for non-linear coupled systems).

In ***chapter 4***, I conducted a validation study aimed to characterise central-autonomic-network coupling pathways (top-to-bottom and bottom-to-top) by analysing the interaction of heart rate, systolic blood pressure, respiration and central activity in schizophrenic patients and healthy subjects. Here, I applied the newly developed causal and non-causal, linear and non-linear multivariate coupling approaches (HRJSD, mHRJSD, NSTPDC, MuTE) to determine the coupling strengths and directions within the CNS-ANS network. This study provides new insights within central-autonomic-network pathways in respect to central and cardiovascular-cardiorespiratory regulation processes in schizophrenia. I was able to demonstrate significantly weaker non-linear central-cardiovascular and central-cardiorespiratory coupling pathways, and significantly stronger linear central information flow in the direction of the cardiac- and vascular system, and a significantly stronger linear respiratory information transfer towards the central nervous system in schizophrenia.

For schizophrenia, there is a continuing debate as to what the defined reasons for the dysregulation of the ANS, and thereby, the impaired brain-heart couplings are caused by. It has been suggested that antipsychotic medications which suppress dopamine activity in the mesolimbic pathway of the brain, genetics and neurobiological processes are important contributory factors also because different brain areas (cortical, subcortical, brainstem) are involved in autonomic regulation. The dynamically interacting network of physiological systems and subsystems within the human body are connected in a close way, in that a failure of one system or subsystem can lead to a chain of faults and thus impairing the dynamical interplay within the whole network (Ivanov & Bartsch, 2014). For schizophrenia, it has been shown that autonomic dysfunction is closely associated with deficits of prefrontal cortex activity in executive function and inhibition (Henry et al, 2010; Thayer & Lane, 2009). It has also been suggested (Thayer & Lane, 2009) that the lack of inhibition of amygdala mediating cardiovascular and autonomic responses to stress by the prefrontal cortex is one reason for ANS dysregulation. The medial prefrontal cortex is involved in the regulation of both behavioural and physiological responses, including the regulation of anxiety, heart rate changes associated with social threat, and a variety of other peripheral responses to stressors associated with the brain stem regulatory function. Limitations of the validation studies that should be stated are: 1) the treatment with antipsychotic drugs as a standard therapeutic measure, and 2) no comparative fMRI analyses were performed to prove which parts of the frontal cortex are involved in cerebral activation of the cortical as well as subcortical centres. As an outlook, the combination of fMRI and EEG analysis to achieve new perspectives in cognitive

functions in respect to the central-autonomic-network in schizophrenia seem to be very promising (He & Liu, 2008).

In summary, this thesis provides an enhanced understanding of the interrelationship of central and autonomic regulatory mechanisms in schizophrenia. The detailed findings on how the different pronounced central-autonomic-network pathways are associated with paranoid schizophrenia may allow for a better understanding on how cerebral activation and autonomic responses and/or activation are connected in physiology networks under pathophysiological conditions.

The novel-developed coupling approaches have their own special features that make them unique, even as compared to well-established coupling approaches. They expand the spectrum of novel coupling approaches for biosignal analysis and thus contribute in their own way to obtaining detailed information, and thus contribute to improved diagnostics/therapy.

References

Adochiei, F., Schulz, S., Edu, I., Costin, H. & Voss, A. (2013) A New Normalised Short Time PDC for Dynamic Coupling Analyses. *Biomed Tech (Berl)*, 58 Suppl 1.

Agelink, M. W., Majewski, T., Wurthmann, C., Lukas, K., Ullrich, H., Linka, T. & Klieser, E. (2001) Effects of newer atypical antipsychotics on autonomic neurocardiac function: a comparison between amisulpride, olanzapine, sertindole, and clozapine. *J Clin Psychopharmacol*, 21(1), 8-13.

Aguirre, R. R., Mustafa, M. Z., Dumenigo, A., Schulz, S., Voss, A., Goubran, B., Dumenigo, R. & Sanchez-Gonzalez, M. A. (2018) Influence of Acute Antipsychotic Treatment on Cardiorespiratory Coupling and Heart Rate Variability. *Cureus*, 10(1), e2066.

Ancona, N., Marinazzo, D. & Stramaglia, S. (2004) Radial basis function approach to nonlinear Granger causality of time series. *Phys Rev E Stat Nonlin Soft Matter Phys*, 70(5 Pt 2), 056221.

Ancona, N. & Stramaglia, S. (2006) An invariance property of predictors in kernel-induced hypothesis spaces. *Neural Comput*, 18(4), 749-59.

Ardell, J. L., Rajendran, P. S., Nier, H. A., KenKnight, B. H. & Armour, J. A. (2015) Central-peripheral neural network interactions evoked by vagus nerve stimulation: functional consequences on control of cardiac function. *Am J Physiol Heart Circ Physiol*, 309(10), H1740-52.

Arnhold, J., Grassberger, P., Lehnertz, K. & Elger, C. E. (1999) A robust method for detecting interdependences: application to intracranially recorded EEG. *Physica D: Nonlinear Phenomena*, 134(4), 419-430.

Baccala, L. A. & Sameshima, K. (2001a) Overcoming the limitations of correlation analysis for many simultaneously processed neural structures. *Prog Brain Res*, 130, 33-47.

Baccala, L. A. & Sameshima, K. (2001b) Partial directed coherence: a new concept in neural structure determination. *Biol. Cybern.*, 84,, 463-474.

Bär, K. J. (2015) Cardiac Autonomic Dysfunction in Patients with Schizophrenia and Their Healthy Relatives - A Small Review. *Front Neurol*, 6, 139.

Bär, K. J., Boettger, M. K., Berger, S., Baier, V., Sauer, H., Yeragani, V. K. & Voss, A. (2007a) Decreased baroreflex sensitivity in acute schizophrenia. *J Appl Physiol (1985)*, 102(3), 1051-6.

Bär, K. J., Boettger, M. K., Koschke, M., Schulz, S., Chokka, P., Yeragani, V. K. & Voss, A. (2007b) Non-linear complexity measures of heart rate variability in acute schizophrenia. *Clin Neurophysiol*, 118(9), 2009-15.

Bär, K. J., Boettger, M. K. & Voss, A. (2006) Differences between heart rate and blood pressure variability in schizophrenia. *Biomed Tech (Berl)*, 51(4), 237-9.

Bär, K. J., Koschke, M., Berger, S., Schulz, S., Tancer, M., Voss, A. & Yeragani, V. K. (2008) Influence of olanzapine on QT variability and complexity measures of heart rate in patients with schizophrenia. *J Clin Psychopharmacol*, 28(6), 694-8.

Bär, K. J., Letzsch, A., Jochum, T., Wagner, G., Greiner, W. & Sauer, H. (2005) Loss of efferent vagal activity in acute schizophrenia. *J Psychiatr Res*, 39(5), 519-27.

Bär, K. J., Rachow, T., Schulz, S., Bassarab, K., Haufe, S., Berger, S., Koch, K. & Voss, A. (2012) The phrenic component of acute schizophrenia--a name and its physiological reality. *PLoS One*, 7(3), e33459.

Barnett, L., Barrett, A. B. & Seth, A. K. (2009) Granger causality and transfer entropy are equivalent for Gaussian variables. *Phys Rev Lett*, 103(23), 238701.

Bartsch, R. P., Liu, K. K., Bashan, A. & Ivanov, P. (2015) Network Physiology: How Organ Systems Dynamically Interact. *PLoS One*, 10(11), e0142143.

Basar, E. & Guntekin, B. (2008) A review of brain oscillations in cognitive disorders and the role of neurotransmitters. *Brain Res*, 1235, 172-93.

Basar, E. & Guntekin, B. (2013) Review of delta, theta, alpha, beta, and gamma response oscillations in neuropsychiatric disorders. *Suppl Clin Neurophysiol*, 62, 303-41.

Bashan, A., Bartsch, R. P., Kantelhardt, J. W., Havlin, S. & Ivanov, P. (2012) Network physiology reveals relations between network topology and physiological function. *Nat Commun*, 3, 702.

Bassani, T., Magagnin, V., Guzzetti, S., Baselli, G., Citerio, G. & Porta, A. (2012) Testing the involvement of baroreflex during general anesthesia through Granger causality approach. *Comput Biol Med*, 42(3), 306-12.

Baumert, M., Walther, T., Hopfe, J., Stepan, H., Faber, R. & Voss, A. (2002) Joint symbolic dynamic analysis of beat-to-beat interactions of heart rate and systolic blood pressure in normal pregnancy. *Med Biol Eng Comput*, 40(2), 241-5.

Beissner, F., Meissner, K., Bar, K. J. & Napadow, V. (2013) The autonomic brain: an activation likelihood estimation meta-analysis for central processing of autonomic function. *J Neurosci*, 33(25), 10503-11.

Bell, C. C. (1994) DSM-IV: Diagnostic and statistical manual of mental disorders. *JAMA*, 272(10), 828-829.

Ben-Shachar, D. (2002) Mitochondrial dysfunction in schizophrenia: a possible linkage to dopamine. *J Neurochem*, 83(6), 1241-51.

Benarroch, E. E. (1993) The central autonomic network: functional organization, dysfunction, and perspective. *Mayo Clin Proc*, 68(10), 988-1001.

Bertinieri, G., Di Rienzo, M., Cavallazzi, A., Ferrari, A. U., Pedotti, A. & Mancia, G. (1988) Evaluation of baroreceptor reflex by blood pressure monitoring in unanesthetized cats. *Am J Physiol*, 254(2 Pt 2), H377-83.

Boning, J., Drechsler, F. & Neuhauser, B. (1989) Somatosensory event-related potentials and selective attention impairment in young chronic schizophrenics. *Neuropsychobiology*, 21(3), 146-51.

Boutros, N. N., Arfken, C., Galderisi, S., Warrick, J., Pratt, G. & Iacono, W. (2008) The status of spectral EEG abnormality as a diagnostic test for schizophrenia. *Schizophr Res*, 99(1-3), 225-37.

Brenner, C. A., Krishnan, G. P., Vohs, J. L., Ahn, W. Y., Hetrick, W. P., Morzorati, S. L. & O'Donnell, B. F. (2009) Steady state responses: electrophysiological assessment of sensory function in schizophrenia. *Schizophr Bull*, 35(6), 1065-77.

Broadley, A. J., Frenneaux, M. P., Moskvina, V., Jones, C. J. & Korszun, A. (2005) Baroreflex sensitivity is reduced in depression. *Psychosom Med*, 67(4), 648-51.

Brown, S. (1997) Excess mortality of schizophrenia. A meta-analysis. *Br J Psychiatry*, 171, 502-8.

Brum, P. C., Da Silva, G. J., Moreira, E. D., Ida, F., Negrao, C. E. & Krieger, E. M. (2000) Exercise training increases baroreceptor gain sensitivity in normal and hypertensive rats. *Hypertension*, 36(6), 1018-22.

Callicott, J. H., Mattay, V. S., Verchinski, B. A., Marenco, S., Egan, M. F. & Weinberger, D. R. (2003) Complexity of prefrontal cortical dysfunction in schizophrenia: more than up or down. *Am J Psychiatry*, 160(12), 2209-15.

Caminal, P., Giraldo, B., Zabaleta, H., Vallverdu, M., Benito, S., Ballesteros, D., Lopez-Rodriguez, L., Esteban, A., Baumert, M. & Voss, A. (2005) Joint symbolic dynamic analysis of cardiorespiratory interactions in patients on weaning trials. *Conf Proc IEEE Eng Med Biol Soc*, 2005, 4576-9.

Castro, M. N., Villarreal, M. F., Bolotinsky, N., Papavero, E., Goldschmidt, M. G., Costanzo, E. Y., Drucaroff, L., Wainsztein, A., de Achaval, D., Pahissa, J., Bar, K. J., Nemeroff, C. B. & Guinjoan, S. M. (2015) Brain activation induced by psychological stress in patients with schizophrenia. *Schizophr Res*, 168(1-2), 313-21.

Chang, J. S., Yoo, C. S., Yi, S. H., Hong, K. H., Oh, H. S., Hwang, J. Y., Kim, S. G., Ahn, Y. M. & Kim, Y. S. (2009) Differential pattern of heart rate variability in patients with schizophrenia. *Prog Neuropsychopharmacol Biol Psychiatry*, 33(6), 991-5.

Chen, Y., Rangarajan, G. & Ding, M. (2004) Analyzing multiple nonlinear time series with extended Granger causality. *Physics Letters A* 324,, 26-35.

Cohen, M. A. & Taylor, J. A. (2002) Short-term cardiovascular oscillations in man: measuring and modelling the physiologies. *J Physiol*, 542(Pt 3), 669-83.

Cover, T. M. & Thomas, J. A. (1991) Elements of information theory. *John Wiley and Sons, New York*.

Dampney, R. A. (1994) Functional organization of central pathways regulating the cardiovascular system. *Physiol Rev*, 74(2), 323-64.

de Zambotti, M., Trinder, J., Silvani, A., Colrain, I. M. & Baker, F. C. (2018) Dynamic coupling between the central and autonomic nervous systems during sleep: A review. *Neuroscience & Biobehavioral Reviews*, 90, 84-103.

Delorme, A. & Makeig, S. (2004) EEGLAB: an open source toolbox for analysis of single-trial EEG dynamics including independent component analysis. *Journal of Neuroscience Methods*, 134(1), 9-21.

Dick, T. E., Hsieh, Y. H., Dhingra, R. R., Baekey, D. M., Galan, R. F., Wehrwein, E. & Morris, K. F. (2014) Cardiorespiratory coupling: common rhythms in cardiac, sympathetic, and respiratory activities. *Prog Brain Res*, 209, 191-205.

Domke, H.-J. (2011) *http://demonstrations.wolfram.com/DynamicsOfCoupledPendulums/*, 2011. Available online: [Accessed.

Eckberg, D. L. (2003) The human respiratory gate. *J Physiol*, 548(Pt 2), 339-52.

Eckberg, D. L. (2009) Point:counterpoint: respiratory sinus arrhythmia is due to a central mechanism vs. respiratory sinus arrhythmia is due to the baroreflex mechanism. *J Appl Physiol (1985)*, 106(5), 1740-2; discussion 1744.

Eckmann, J. P., Kamphorst, S. O. & Ruelle, D. (1987) Recurrence plots of dynamical systems. *Europhys Lett*(4), 973-977.

Faes, L., Erla, S. & Nollo, G. (2012a) Measuring connectivity in linear multivariate processes: definitions, interpretation, and practical analysis. *Comput Math Methods Med*, 2012, 140513.

Faes, L., Marinazzo, D., Jurysta, F. & Nollo, G. (2015) Linear and non-linear brain-heart and brain-brain interactions during sleep. *Physiol Meas*, 36(4), 683-98.

Faes, L. & Nollo, G. (2006) Bivariate nonlinear prediction to quantify the strength of complex dynamical interactions in short-term cardiovascular variability. *Med Biol Eng Comput*, 44(5), 383-92.

Faes, L. & Nollo, G. (2010) Extended causal modeling to assess Partial Directed Coherence in multiple time series with significant instantaneous interactions. *Biol Cybern*, 103(5), 387-400.

Faes, L., Nollo, G. & Chon, K. H. (2008a) Assessment of Granger causality by nonlinear model identification: application to short-term cardiovascular variability. *Ann Biomed Eng*, 36(3), 381-95.

Faes, L., Nollo, G. & Porta, A. (2011a) Information-based detection of nonlinear Granger causality in multivariate processes via a nonuniform embedding technique. *Phys Rev E Stat Nonlin Soft Matter Phys*, 83(5 Pt 1), 051112.

Faes, L., Nollo, G. & Porta, A. (2011b) Information domain approach to the investigation of cardio-vascular, cardio-pulmonary, and vasculo-pulmonary causal couplings. *Front Physiol*, 2, 80.

Faes, L., Nollo, G. & Porta, A. (2012b) Non-uniform multivariate embedding to assess the information transfer in cardiovascular and cardiorespiratory variability series. *Comput Biol Med*, 42(3), 290-7.

Faes, L., Porta, A. & Nollo, G. (2008b) Mutual nonlinear prediction as a tool to evaluate coupling strength and directionality in bivariate time series: comparison among different strategies based on k nearest neighbors. *Phys Rev E Stat Nonlin Soft Matter Phys*, 78(2 Pt 2), 026201.

Farmer, J. D. & Sidorowich, J. J. (1987) Predicting chaotic time series. *Phys Rev Lett*, 59(8), 845-848.

Foster, P. S., Drago, V., Ferguson, B. J. & Harrison, D. W. (2008) Cerebral moderation of cardiovascular functioning: a functional cerebral systems perspective. *Clin Neurophysiol*, 119(12), 2846-54.

Foster, P. S. & Harrison, D. W. (2004) The covariation of cortical electrical activity and cardiovascular responding. *Int J Psychophysiol*, 52(3), 239-55.

Foster, P. S. & Harrison, D. W. (2006) Magnitude of cerebral asymmetry at rest: covariation with baseline cardiovascular activity. *Brain Cogn*, 61(3), 286-97.

Fraser, A. M. & Swinney, H. L. (1986) Independent coordinates for strange attractors from mutual information. *Phys Rev A Gen Phys*, 33(2), 1134-1140.

Fritsch, J. M., Eckberg, D. L., Graves, L. D. & Wallin, B. G. (1986) Arterial pressure ramps provoke linear increases of heart period in humans. *Am J Physiol*, 251(6 Pt 2), R1086-90.

Geweke, J. (1982) Measurement of linear dependence and feedback between multiple time series. *Journal of the American Statistical Association*, 77(378), 304-313.

Gilbey, M. P., Jordan, D., Richter, D. W. & Spyer, K. M. (1984) Synaptic mechanisms involved in the inspiratory modulation of vagal cardio-inhibitory neurones in the cat. *J Physiol*, 356, 65-78.

Gourevitch, B., Bouquin-Jeannes, R. L. & Faucon, G. (2006) Linear and nonlinear causality between signals: methods, examples and neurophysiological applications. *Biol Cybern*, 95(4), 349-69.

Gourine, A. V. & Spyer, K. (2009) Autonomic Nervous System: Central Respiratory Control, 883-890.

Granger, C. W. J. (1969) Investigating Causal Relations by Econometric Models and Cross-spectral Methods. *Econometrica*, 37(3), 424-438.

Grossman, P. & Taylor, E. W. (2007) Toward understanding respiratory sinus arrhythmia: relations to cardiac vagal tone, evolution and biobehavioral functions. *Biol Psychol*, 74(2), 263-85.

Grossman, P., van Beek, J. & Wientjes, C. (1990) A comparison of three quantification methods for estimation of respiratory sinus arrhythmia. *Psychophysiology*, 27(6), 702-14.

Grossman, P., Wilhelm, F. H. & Spoerle, M. (2004) Respiratory sinus arrhythmia, cardiac vagal control, and daily activity. *Am J Physiol Heart Circ Physiol*, 287(2), H728-34.

Guyenet, P. G. (2014) Regulation of breathing and autonomic outflows by chemoreceptors. *Compr Physiol*, 4(4), 1511-62.

Hansen, A. L., Johnsen, B. H. & Thayer, J. F. (2003) Vagal influence on working memory and attention. *Int J Psychophysiol*, 48(3), 263-74.

Harvey, P. D., Howanitz, E., Parrella, M., White, L., Davidson, M., Mohs, R. C., Hoblyn, J. & Davis, K. L. (1998) Symptoms, cognitive functioning, and adaptive skills in geriatric patients with lifelong schizophrenia: a comparison across treatment sites. *Am J Psychiatry*, 155(8), 1080-6.

He, B. & Liu, Z. (2008) Multimodal functional neuroimaging: integrating functional MRI and EEG/MEG. *IEEE Rev Biomed Eng*, 1, 23-40.

Heatherton, T. F. & Wagner, D. D. (2011) Cognitive neuroscience of self-regulation failure. *Trends Cogn Sci*, 15(3), 132-9.

Hennekens, C. H., Hennekens, A. R., Hollar, D. & Casey, D. E. (2005) Schizophrenia and increased risks of cardiovascular disease. *Am Heart J*, 150(6), 1115-21.

Henry, B. L., Minassian, A., Paulus, M. P., Geyer, M. A. & Perry, W. (2010) Heart rate variability in bipolar mania and schizophrenia. *J Psychiatr Res*, 44(3), 168-76.

Hesse, W., Moller, E., Arnold, M. & Schack, B. (2003) The use of time-variant EEG Granger causality for inspecting directed interdependencies of neural assemblies. *J Neurosci Methods*, 124(1), 27-44.

Homma, I. & Masaoka, Y. (2008) Breathing rhythms and emotions. *Exp Physiol*, 93(9), 1011-21.

Horacek, J., Bubenikova-Valesova, V., Kopecek, M., Palenicek, T., Dockery, C., Mohr, P. & Hoschl, C. (2006) Mechanism of action of atypical antipsychotic drugs and the neurobiology of schizophrenia. *CNS Drugs*, 20(5), 389-409.

Hoyer, D., Bauer, R., Walter, B. & Zwiener, U. (1998) Estimation of nonlinear couplings on the basis of complexity and predictability--a new method applied to cardiorespiratory coordination. *IEEE Trans Biomed Eng*, 45(5), 545-52.

Hoyer, D., Pompe, B., Chon, K. H., Hardraht, H., Wicher, C. & Zwiener, U. (2005) Mutual information function assesses autonomic information flow of heart rate dynamics at different time scales. *IEEE Trans Biomed Eng*, 52(4), 584-92.

Huang, M. X., Lee, R. R., Gaa, K. M., Song, T., Harrington, D. L., Loh, C., Theilmann, R. J., Edgar, J. C., Miller, G. A., Canive, J. M. & Granholm, E. (2010) Somatosensory system deficits in schizophrenia revealed by MEG during a median-nerve oddball task. *Brain Topogr*, 23(1), 82-104.

Ivanov, P. C. & Bartsch, R. P. (2014) Network Physiology: Mapping Interactions Between Networks of Physiologic Networks, in D'Agostino, G. & Scala, A. (eds), *Networks of Networks: The Last Frontier of Complexity*. Cham: Springer International Publishing, 203-222.

Ivanov, P. C., Liu, K. K. L. & Bartsch, R. P. (2016) Focus on the emerging new fields of Network Physiology and Network Medicine. *New J Phys*, 18.

Javitt, D. C. (2009) Sensory processing in schizophrenia: neither simple nor intact. *Schizophr Bull*, 35(6), 1059-64.

Kaiser, A. & Schreiber, T. (2002) Information transfer in continuous processes. *Physica D*, 166,, 43-62.

Kaminski, M., Ding, M., Truccolo, W. A. & Bressler, S. L. (2001) Evaluating causal relations in neural systems: granger causality, directed transfer function and statistical assessment of significance. *Biol Cybern*, 85(2), 145-57.

Kaminski, M. J. & Blinowska, K. J. (1991) A new method of the description of the information flow in the brain structures. *Biol Cybern*, 65(3), 203-10.

Kemali, D., Galderisi, S., Maj, M., Mucci, A., Di Gregorio, M. & Bucci, P. (1992) Computerized EEG topography findings in schizophrenic patients before and after haloperidol treatment. *Int J Psychophysiol*, 13(3), 283-90.

Kim, J. H., Yi, S. H., Yoo, C. S., Yang, S. A., Yoon, S. C., Lee, K. Y., Ahn, Y. M., Kang, U. G. & Kim, Y. S. (2004) Heart rate dynamics and their relationship to psychotic symptom severity in clozapine-treated schizophrenic subjects. *Prog Neuropsychopharmacol Biol Psychiatry*, 28(2), 371-8.

Kohler, S., Wagner, G. & Bar, K. J. (2019) Activation of brainstem and midbrain nuclei during cognitive control in medicated patients with schizophrenia. *Hum Brain Mapp*, 40(1), 202-213.

Korzeniewska, A., Manczak, M., Kaminski, M., Blinowska, K. J. & Kasicki, S. (2003) Determination of information flow direction among brain structures by a modified directed transfer function (dDTF) method. *J Neurosci Methods*, 125(1-2), 195-207.

Kurths, J., Voss, A., Saparin, P., Witt, A., Kleiner, H. J. & Wessel, N. (1995) Quantitative analysis of heart rate variability. *Chaos*, 5(1), 88-94.

Lally, J. & MacCabe, J. H. (2015) Antipsychotic medication in schizophrenia: a review. *Br Med Bull*, 114(1), 169-79.

Laude, D., Elghozi, J. L., Girard, A., Bellard, E., Bouhaddi, M., Castiglioni, P., Cerutti, C., Cividjian, A., Di Rienzo, M., Fortrat, J. O., Janssen, B., Karemaker, J. M., Leftheriotis, G., Parati, G., Persson, P. B., Porta, A., Quintin, L., Regnard, J., Rudiger, H. & Stauss, H. M. (2004) Comparison of various techniques used to estimate spontaneous baroreflex sensitivity (the EuroBaVar study). *Am J Physiol Regul Integr Comp Physiol*, 286(1), R226-31.

Laursen, T. M., Nordentoft, M. & Mortensen, P. B. (2014) Excess early mortality in schizophrenia. *Annu Rev Clin Psychol*, 10, 425-48.

LeBlanc, J., Ducharme, M. B. & Thompson, M. (2004) Study on the correlation of the autonomic nervous system responses to a stressor of high discomfort with personality traits. *Physiol Behav*, 82(4), 647-52.

Levy, M. N. (1997) Neural control of cardiac function. *Baillieres Clin Neurol*, 6(2), 227-44.

Light, G. A., Hsu, J. L., Hsieh, M. H., Meyer-Gomes, K., Sprock, J., Swerdlow, N. R. & Braff, D. L. (2006) Gamma band oscillations reveal neural network cortical coherence dysfunction in schizophrenia patients. *Biol Psychiatry*, 60(11), 1231-40.

Lombardi, A., Guaragnella, C., Amoroso, N., Monaco, A., Fazio, L., Taurisano, P., Pergola, G., Blasi, G., Bertolino, A., Bellotti, R. & Tangaro, S. (2019) Modelling cognitive loads in schizophrenia by means of new functional dynamic indexes. *Neuroimage*, 195, 150-164.

Maccrimmon, D., Brunet, D., Criollo, M., Galin, H. & Lawson, J. S. (2012) Clozapine augments delta, theta, and right frontal EEG alpha power in schizophrenic patients. *ISRN Psychiatry*, 2012, 596486.

Maiorana, E., Solé-Casals, J. & Campisi, P. (2016) EEG signal preprocessing for biometric recognition. *Machine Vision and Applications*, 27(8), 1351-1360.

Malberg, H., Wessel, N., Schirdewan, A., Osterziel, K. J. & Voss, A. (1999) [Dual sequence method for analysis of spontaneous baroreceptor reflex sensitivity in patients with dilated cardiomyopathy]. *Z Kardiol*, 88(5), 331-7.

Marinazzo, D., Liao, W., Chen, H. & Stramaglia, S. (2011) Nonlinear connectivity by Granger causality. *Neuroimage*, 58(2), 330-8.

Marinazzo, D., Pellicoro, M. & Stramaglia, S. (2006) Nonlinear parametric model for Granger causality of time series. *Phys Rev E Stat Nonlin Soft Matter Phys*, 73(6 Pt 2), 066216.

Marinazzo, D., Pellicoro, M. & Stramaglia, S. (2008) Kernel-Granger causality and the analysis of dynamical networks. *Phys Rev E Stat Nonlin Soft Matter Phys*, 77(5 Pt 2), 056215.

Marwan, N. & Kurths, J. (2002) Nonlinear analysis of bivariate data with cross recurrence plots. *Physics Letters A* 302(2003), 299-307.

Marwan, N., Zou, Y., Wessel, N., Riedl, M. & Kurths, J. (2013) Estimating coupling directions in the cardiorespiratory system using recurrence properties. *Philos Trans A Math Phys Eng Sci*, 371(1997), 20110624.

Masaoka, Y. & Homma, I. (1997) Anxiety and respiratory patterns: their relationship during mental stress and physical load. *Int J Psychophysiol*, 27(2), 153-9.

Masaoka, Y. & Homma, I. (1999) Expiratory time determined by individual anxiety levels in humans. *J Appl Physiol (1985)*, 86(4), 1329-36.

Masaoka, Y. & Homma, I. (2001) The effect of anticipatory anxiety on breathing and metabolism in humans. *Respir Physiol*, 128(2), 171-7.

McAllen, R. M. (1976) Proceedings: Inhibition of the baroreceptor input to the medulla by stimulation of the hypothalamic defence area. *J Physiol*, 257(1), 45P-46P.

McCorry, L. K. (2007) Physiology of the autonomic nervous system. *Am J Pharm Educ*, 71(4), 78.

McGrath, J., Saha, S., Chant, D. & Welham, J. (2008) Schizophrenia: a concise overview of incidence, prevalence, and mortality. *Epidemiol Rev*, 30, 67-76.

Milde, T., Schwab, K., Walther, M., Eiselt, M., Schelenz, C., Voss, A. & Witte, H. (2011) Time-variant partial directed coherence in analysis of the cardiovascular system. A methodological study. *Physiol Meas*, 32(11), 1787-805.

Montalto, A., Faes, L. & Marinazzo, D. (2014) MuTE: a MATLAB toolbox to compare established and novel estimators of the multivariate transfer entropy. *PLoS One*, 9(10), e109462.

Mujica-Parodi, L. R., Yeragani, V. & Malaspina, D. (2005) Nonlinear complexity and spectral analyses of heart rate variability in medicated and unmedicated patients with schizophrenia. *Neuropsychobiology*, 51(1), 10-5.

Nagase, Y., Okubo, Y. & Toru, M. (1996) Electroencephalography in schizophrenic patients: comparison between neuroleptic-naive state and after treatment. *Biol Psychiatry*, 40(6), 452-6.

Negrao, C. E., Irigoyen, M. C., Moreira, E. D., Brum, P. C., Freire, P. M. & Krieger, E. M. (1993) Effect of exercise training on RSNA, baroreflex control, and blood pressure responsiveness. *Am J Physiol*, 265(2 Pt 2), R365-70.

Neumaier, A. & Schneider, T. (2001) Estimation of parameters and eigenmodes of multivariate autoregressive models. *ACM Trans. Math. Softw.*, 27(1), 27-57.

Nollo, G., Faes, L., Porta, A., Pellegrini, B., Ravelli, F., Del Greco, M., Disertori, M. & Antolini, R. (2002) Evidence of unbalanced regulatory mechanism of heart rate and systolic pressure after acute myocardial infarction. *Am J Physiol Heart Circ Physiol*, 283(3), H1200-7.

Nosaka, S. (1996) Modifications of arterial baroreflexes: obligatory roles in cardiovascular regulation in stress and poststress recovery. *Jpn J Physiol*, 46(4), 271-88.

Novak, V., Novak, P., de Champlain, J., Le Blanc, A. R., Martin, R. & Nadeau, R. (1993) Influence of respiration on heart rate and blood pressure fluctuations. *J Appl Physiol (1985)*, 74(2), 617-26.

Palus, M., Komarek, V., Hrncir, Z. & Sterbova, K. (2001) Synchronization as adjustment of information rates: detection from bivariate time series. *Phys Rev E Stat Nonlin Soft Matter Phys*, 63(4 Pt 2), 046211.

Palus, M. & Stefanovska, A. (2003) Direction of coupling from phases of interacting oscillators: an information-theoretic approach. *Phys Rev E Stat Nonlin Soft Matter Phys*, 67(5 Pt 2), 055201.

Pereda, E., Quiroga, R. Q. & Bhattacharya, J. (2005) Nonlinear multivariate analysis of neurophysiological signals. *Prog Neurobiol*, 77(1-2), 1-37.

Pérez-Neri, I., Ramírez-Bermúdez, J., Montes, S. & Ríos, C. (2006) Possible Mechanisms of Neurodegeneration in Schizophrenia. *Neurochemical Research*, 31(10), 1279-1294.

Peupelmann, J., Boettger, M. K., Ruhland, C., Berger, S., Ramachandraiah, C. T., Yeragani, V. K. & Bar, K. J. (2009) Cardio-respiratory coupling indicates suppression of vagal activity in acute schizophrenia. *Schizophr Res*, 112(1-3), 153-7.

Pikovsky, A., Rosenblum, M. & Kurths, J. (2001) *Synchronization: a Universal Concept in Nonlinear Science*. Cambridge: Cambridge University Press.

Porta, A., Baselli, G., Lombardi, F., Montano, N., Malliani, A. & Cerutti, S. (1999) Conditional entropy approach for the evaluation of the coupling strength. *Biol Cybern*, 81(2), 119-29.

Porta, A., Bassani, T., Bari, V., Pinna, G. D., Maestri, R. & Guzzetti, S. (2012a) Accounting for respiration is necessary to reliably infer Granger causality from cardiovascular variability series. *IEEE Trans Biomed Eng*, 59(3), 832-41.

Porta, A., Bassani, T., Bari, V., Tobaldini, E., Takahashi, A. C., Catai, A. M. & Montano, N. (2012b) Model-based assessment of baroreflex and cardiopulmonary couplings during graded head-up tilt. *Comput Biol Med*, 42(3), 298-305.

Porta, A. & Faes, L. (2013) Assessing causality in brain dynamics and cardiovascular control. *Philos Trans A Math Phys Eng Sci*, 371(1997), 20120517.

Porta, A., Furlan, R., Rimoldi, O., Pagani, M., Malliani, A. & van de Borne, P. (2002) Quantifying the strength of the linear causal coupling in closed loop interacting cardiovascular variability signals. *Biol Cybern*, 86(3), 241-51.

Porta, A., Guzzetti, S., Montano, N., Furlan, R., Pagani, M., Malliani, A. & Cerutti, S. (2001) Entropy, entropy rate, and pattern classification as tools to typify complexity in short heart period variability series. *IEEE Trans Biomed Eng*, 48(11), 1282-91.

Porta, A., Guzzetti, S., Montano, N., Pagani, M., Somers, V., Malliani, A., Baselli, G. & Cerutti, S. (2000) Information domain analysis of cardiovascular variability signals: evaluation of regularity, synchronisation and co-ordination. *Med Biol Eng Comput*, 38(2), 180-8.

Quiroga, R. Q., Arnhold, J. & Grassberger, P. (2000) Learning driver-response relationships from synchronization patterns. *Phys Rev E Stat Phys Plasmas Fluids Relat Interdiscip Topics*, 61(5 Pt A), 5142-8.

Rea, P. (2016) Chapter 1 - Overview of the Nervous System, in Rea, P. (ed), *Essential Clinically Applied Anatomy of the Peripheral Nervous System in the Head and Neck*Academic Press, 1-20.

Ribolsi, M., Daskalakis, Z. J., Siracusano, A. & Koch, G. (2014) Abnormal asymmetry of brain connectivity in schizophrenia. *Front Hum Neurosci*, 8, 1010.

Riedl, M., Suhrbier, A., Stepan, H., Kurths, J. & Wessel, N. (2010) Short-term couplings of the cardiovascular system in pregnant women suffering from pre-eclampsia. *Philos Trans A Math Phys Eng Sci*, 368(1918), 2237-50.

Ringen, P. A., Engh, J. A., Birkenaes, A. B., Dieset, I. & Andreassen, O. A. (2014) Increased mortality in schizophrenia due to cardiovascular disease - a non-systematic review of epidemiology, possible causes, and interventions. *Front Psychiatry*, 5, 137.

Rosenblum, M., Pikovsky, A., Schäfer, C., Tass, P. A. & Kurths, J. (2001) *Phase synchronization: from theory to data analysis*. Amsterdam: Elsevier Science.

Rosenblum, M. G., Cimponeriu, L., Bezerianos, A., Patzak, A. & Mrowka, R. (2002) Identification of coupling direction: application to cardiorespiratory interaction. *Phys Rev E Stat Nonlin Soft Matter Phys*, 65(4 Pt 1), 041909.

Rosenblum, M. G. & Pikovsky, A. S. (2001) Detecting direction of coupling in interacting oscillators. *Phys Rev E Stat Nonlin Soft Matter Phys*, 64(4 Pt 2), 045202.

Ruiz-Padial, E., Sollers, J. J., 3rd, Vila, J. & Thayer, J. F. (2003) The rhythm of the heart in the blink of an eye: emotion-modulated startle magnitude covaries with heart rate variability. *Psychophysiology*, 40(2), 306-13.

Saha, S., Chant, D. & McGrath, J. (2007) A systematic review of mortality in schizophrenia: is the differential mortality gap worsening over time? *Arch Gen Psychiatry*, 64(10), 1123-31.

Schäfer, C., Rosenblum, M. G., Kurths, J. & Abel, H. H. (1998) Heartbeat synchronized with ventilation. *Nature*, 392(6673), 239-40.

Schelter, B., Timmer, J. & Eichler, M. (2009) Assessing the strength of directed influences among neural signals using renormalized partial directed coherence. *J Neurosci Methods*, 179(1), 121-30.

Schelter, B., Winterhalder, M., Eichler, M., Peifer, M., Hellwig, B., Guschlbauer, B., Lucking, C. H., Dahlhaus, R. & Timmer, J. (2006) Testing for directed influences among neural signals using partial directed coherence. *J Neurosci Methods*, 152(1-2), 210-9.

Schiff, S. J., So, P., Chang, T., Burke, R. E. & Sauer, T. (1996) Detecting dynamical interdependence and generalized synchrony through mutual prediction in a neural ensemble. *Phys Rev E Stat Phys Plasmas Fluids Relat Interdiscip Topics*, 54(6), 6708-6724.

Schneider, T. & Neumaier, A. (2001) Algorithm 808: ARfit—a matlab package for the estimation of parameters and eigenmodes of multivariate autoregressive models. *ACM Trans. Math. Softw.*, 27(1), 58-65.

Schreiber, T. (2000) Measuring information transfer. *Phys Rev Lett*, 85(2), 461-4.

Schreiber, T. & Schmitz, A. (2000) Surrogate time series. *Physica D* 142, 346-382.

Schulz, S., Adochiei, F. C., Edu, I. R., Schroeder, R., Costin, H., Bar, K. J. & Voss, A. (2013a) Cardiovascular and cardiorespiratory coupling analyses: a review. *Philos Trans A Math Phys Eng Sci*, 371(1997), 20120191.

Schulz, S., Bar, K. J. & Voss, A. (2012a) Respiratory variability and cardiorespiratory coupling analyses in patients suffering from schizophrenia and their healthy first-degree relatives. *Biomed Tech (Berl)*.

Schulz, S., Bär, K. J. & Voss, A. (2012b) Cardiovascular and cardiorespiratory coupling in unmedicated schizophrenic patients in comparison to healthy subjects. *Conf Proc IEEE Eng Med Biol Soc*, 3664-7.

Schulz, S., Bär, K. J. & Voss, A. (2015a) Analyses of Heart Rate, Respiration and Cardiorespiratory Coupling in Patients with Schizophrenia. *Entropy*, 17(2), 483-501.

Schulz, S., Bolz, M., Bär, K. J. & Voss, A. (2016) Central- and autonomic nervous system coupling in schizophrenia. *Philos Trans A Math Phys Eng Sci*, 374(2067), 20150178.

Schulz, S., Castro, M. R., Giraldo, B., Haueisen, J. & Voss, A. (2017a) Multivariate high resolution joint symbolic dynamics (mHRJSD): a new tool to analyze couplings in physiological networks., *Biomedical Engineering / Biomedizinische Technik*.

Schulz, S., Haueisen, J., Bär, K.-J. & Voss, A. (2019) Altered Causal Coupling Pathways within the Central-Autonomic-Network in Patients Suffering from Schizophrenia. *Entropy*, 21(8), 733.

Schulz, S., Haueisen, J., Bär, K. & Voss, A. (2014a) Antipsychotic medication influences cardiovascular coupling in patients suffering from acute schizophrenia, *Computing in Cardiology 2014*. 7-10 Sept. 2014.

Schulz, S., Haueisen, J., Bar, K. J. & Andreas, V. (2015b) High-resolution joint symbolic analysis to enhance classification of the cardiorespiratory system in patients with schizophrenia and their relatives. *Philos Trans A Math Phys Eng Sci*, 373(2034).

Schulz, S., Haueisen, J., Bar, K. J. & Voss, A. (2018) Multivariate assessment of the central-cardiorespiratory network structure in neuropathological disease. *Physiol Meas*, 39(7), 074004.

Schulz, S., Haueisen, J., Bär, K. J. & Voss, A. (2013b) Quantification of cardiorespiratory coupling in acute schizophrenia applying high resolution joint symbolic dynamics. *Computing in Cardiology Conference (CinC), 2013*, 101-104

Schulz, S., Haueisen, J., Bär, K. J. & Voss, A. (2014b) Changed cardiorespiratory phase-coupling pattern in patients suffering from schizophrenia. *Biomed Tech (Berl)*, 59 (s1).

Schulz, S., Haueisen, J., Bär, K. J. & Voss, A. (2020) The Cardiorespiratory Network in Healthy First-Degree Relatives of Schizophrenic Patients. *Front Neurosci*, 14, 617.

Schulz, S., Ricoy Castro, M., Giraldo, B., Haueisen, J., Bär, K. J. & Voss, A. (2017b) Altered Central Cardiovascular Network Pattern in Neuropathological Disease - Application of the Three Dimensional High Resolution Joint Symbolic Dynamics, *Computing in Cardiology 2017; VOL 44* Rennes, France), Sept 24-27, 2017.

Schulz, S., Tupaika, N., Berger, S., Haueisen, J., Bär, K. J. & Voss, A. (2013c) Cardiovascular coupling analysis with high-resolution joint symbolic dynamics in patients suffering from acute schizophrenia. *Physiol Meas*, 34(8), 883-901.

Shannon, C. E. (1948) A mathematical theory of communication. *Bell System Technical Journal. 27*, 379-423 and 623-656.

Shoemaker, J. K., Norton, K. N., Baker, J. & Luchyshyn, T. (2015) Forebrain organization for autonomic cardiovascular control. *Auton Neurosci*, 188, 5-9.

Silke, B., Campbell, C. & King, D. J. (2002) The potential cardiotoxicity of antipsychotic drugs as assessed by heart rate variability. *J Psychopharmacol*, 16(4), 355-60.

Small, J. G., Milstein, V., Small, I. F., Miller, M. J., Kellams, J. J. & Corsaro, C. J. (1987) Computerized EEG profiles of haloperidol, chlorpromazine, clozapine and placebo in treatment resistant schizophrenia. *Clin Electroencephalogr*, 18(3), 124-35.

Staniek, M. & Lehnertz, K. (2008) Symbolic transfer entropy. *Phys Rev Lett*, 100(15), 158101.

Stankovski, T., Ticcinelli, V., McClintock, P. V. E. & Stefanovska, A. (2017) Neural Cross-Frequency Coupling Functions. *Front Syst Neurosci*, 11, 33.

Steptoe, A. & Sawada, Y. (1989) Assessment of baroreceptor reflex function during mental stress and relaxation. *Psychophysiology*, 26(2), 140-7.

Straus, S. M., Bleumink, G. S., Dieleman, J. P., van der Lei, J., t Jong, G. W., Kingma, J. H., Sturkenboom, M. C. & Stricker, B. H. (2004) Antipsychotics and the risk of sudden cardiac death. *Arch Intern Med*, 164(12), 1293-7.

Suhrbier, A., Riedl, M., Malberg, H., Penzel, T., Bretthauer, G., Kurths, J. & Wessel, N. (2010) Cardiovascular regulation during sleep quantified by symbolic coupling traces. *Chaos*, 20(4), 045124.

Sun, J., Li, Z. & Tong, S. (2012) Inferring functional neural connectivity with phase synchronization analysis: a review of methodology. *Comput Math Methods Med*, 2012(2012), 239210.

Sun, Y., Chen, Y., Collinson, S. L., Bezerianos, A. & Sim, K. (2017) Reduced Hemispheric Asymmetry of Brain Anatomical Networks Is Linked to Schizophrenia: A Connectome Study. *Cereb Cortex*, 27(1), 602-615.

Suttkus, S., Schumann, A., de la Cruz, F. & Bar, K. J. (2021) Working memory in schizophrenia: The role of the locus coeruleus and its relation to functional brain networks. *Brain Behav*, 11(5), e02130.

Swenne, C. A. (2013) Baroreflex sensitivity: mechanisms and measurement. *Neth Heart J*, 21(2), 58-60.

Task Force (1996) Heart rate variability: standards of measurement, physiological interpretation and clinical use. Task Force of the European Society of Cardiology and the North American Society of Pacing and Electrophysiology. *Circulation*, 93(5), 1043-65.

Taylor, E. W., Al-Ghamdi, M. S., Ihmied, I. H., Wang, T. & Abe, A. S. (2001) The neuranatomical basis of central control of cardiorespiratory interactions in vertebrates. *Exp Physiol*, 86(6), 771-6.

Thayer, J. F. (2007) What the Heart Says to the Brain (and vice versa) and Why We Should Listen. *Psychological Topics*, 16(2), 241-250.

Thayer, J. F., Ahs, F., Fredrikson, M., Sollers, J. J., 3rd & Wager, T. D. (2012) A meta-analysis of heart rate variability and neuroimaging studies: implications for heart rate variability as a marker of stress and health. *Neurosci Biobehav Rev*, 36(2), 747-56.

Thayer, J. F. & Friedman, B. H. (2004) *A neurovisceral integration model of health disparities in aging*. Translated from English by. Washington, DC: The National Academies Press.

Thayer, J. F. & Lane, R. D. (2000) A model of neurovisceral integration in emotion regulation and dysregulation. *J Affect Disord*, 61(3), 201-16.

Thayer, J. F. & Lane, R. D. (2009) Claude Bernard and the heart-brain connection: further elaboration of a model of neurovisceral integration. *Neurosci Biobehav Rev*, 33(2), 81-8.

Theiler, J., Eubank, S., Longtin, A., Galdrikian, B. & Farmer, J. D. (1992) Testing for nonlinearity in time series: the method of surrogate data. *Phys. D*, 58(1-4), 77-94.

Tislerova, B., Brunovsky, M., Horacek, J., Novak, T., Kopecek, M., Mohr, P. & Krajca, V. (2008) LORETA functional imaging in antipsychotic-naive and olanzapine-, clozapine- and risperidone-treated patients with schizophrenia. *Neuropsychobiology*, 58(1), 1-10.

Tong, S. & Thakor, N. V. (2009) *Quantitative EEG Analysis Methods and Applications*. Boston: Artech House.

Triedman, J. K. & Saul, J. P. (1994) Blood pressure modulation by central venous pressure and respiration. Buffering effects of the heart rate reflexes. *Circulation*, 89(1), 169-79.

Tucker, D. M. (1981) Lateral brain function, emotion, and conceptualization. *Psychol Bull*, 89(1), 19-46.

Turner, D. L. (1991) Cardiovascular and respiratory control mechanisms during exercise: an integrated view. *J Exp Biol*, 160, 309-40.

Uhlhaas, P. J. & Singer, W. (2010) Abnormal neural oscillations and synchrony in schizophrenia. *Nat Rev Neurosci*, 11(2), 100-13.

Vakorin, V. A., Krakovska, O. A. & McIntosh, A. R. (2009) Confounding effects of indirect connections on causality estimation. *J Neurosci Methods*, 184(1), 152-60.

Valkonen-Korhonen, M., Tarvainen, M. P., Ranta-Aho, P., Karjalainen, P. A., Partanen, J., Karhu, J. & Lehtonen, J. (2003) Heart rate variability in acute psychosis. *Psychophysiology*, 40(5), 716-26.

Venables, N. C., Bernat, E. M. & Sponheim, S. R. (2009) Genetic and disorder-specific aspects of resting state EEG abnormalities in schizophrenia. *Schizophr Bull*, 35(4), 826-39.

Verdes, P. F. (2005) Assessing causality from multivariate time series. *Phys Rev E Stat Nonlin Soft Matter Phys*, 72(2 Pt 2), 026222.

Voss, A., Kurths, J., Kleiner, H. J., Witt, A., Wessel, N., Saparin, P., Osterziel, K. J., Schurath, R. & Dietz, R. (1996) The application of methods of non-linear dynamics for the improved and predictive recognition of patients threatened by sudden cardiac death. *Cardiovasc Res*, 31(3), 419-33.

Voss, A., Schulz, S., Schroeder, R., Baumert, M. & Caminal, P. (2009) Methods derived from nonlinear dynamics for analysing heart rate variability. *Philos Trans A Math Phys Eng Sci*, 367(1887), 277-96.

Wagner, G., De la Cruz, F., Schachtzabel, C., Gullmar, D., Schultz, C. C., Schlosser, R. G., Bar, K. J. & Koch, K. (2015) Structural and functional dysconnectivity of the fronto-thalamic system in schizophrenia: a DCM-DTI study. *Cortex*, 66, 35-45.

Wessel, N., Suhrbier, A., Riedl, M., Marwan, N., Malberg, H., Bretthauer, G., Penzel, T. & Kurths, J. (2011) Symbolic coupling traces for causality analysis of cardiovascular control. *Annu Int Conf IEEE Eng Med Biol Soc*, 2011, 5935-8.

Wessel, N., Voss, A., Malberg, H., Ziehmann, C., Voss, H., Schirdewan, A., Meyerfeldt, U. & Kurths, J. (2000) Nonlinear analysis of complex phenomena in cardiological data. *Z. Herzschr. Elektrophys*, 11,, 159–73.

Wiener, N. (1956) The theory of prediction. *Beckenbach, E.F. (Ed.), Modern Mathematics for Engineers.*(vol. series 1, McGraw-Hill, New York).

Williams, L. M., Das, P., Harris, A. W., Liddell, B. B., Brammer, M. J., Olivieri, G., Skerrett, D., Phillips, M. L., David, A. S., Peduto, A. & Gordon, E. (2004) Dysregulation of arousal and amygdala-prefrontal systems in paranoid schizophrenia. *Am J Psychiatry*, 161(3), 480-9.

Winterhalder, M., Schelter, B., Hesse, W., Schwab, K., Leistritz, L., Timmer, J. & Witte, H. (2006) Detection of directed information flow in biosignals. *Biomed Tech (Berl)*, 51(5-6), 281-7.

Wittling, W., Block, A., Schweiger, E. & Genzel, S. (1998) Hemisphere asymmetry in sympathetic control of the human myocardium. *Brain Cogn*, 38(1), 17-35.

Ziegler, G., Dahnke, R., Yeragani, V. K. & Bar, K. J. (2009) The relation of ventromedial prefrontal cortex activity and heart rate fluctuations at rest. *Eur J Neurosci*, 30(11), 2205-10.

List of figures

List of tables

BBI-related EEG intervals, *p<0.05, **p<0.01, ***p<0.00041, n.s.=not significant, #=not confirmed by surrogate analysis)

Publications derived from this thesis

Schulz, S., Haueisen, J., Bär, K. J. & Voss, A. (2020) The Cardiorespiratory Network in Healthy First-Degree Relatives of Schizophrenic Patients. *Front Neurosci*, 14, 617.

Schulz, S., Haueisen, J., Bär, K. J. & Voss, A. (2019) Altered Causal Coupling Pathways within the Central-Autonomic-Network in Patients Suffering from Schizophrenia. *Entropy*, 21(8), 733.

Schulz, S., Haueisen, J., Bär, K. J. & Voss, A. (2018) Multivariate assessment of the central-cardiorespiratory network structure in neuropathological disease. *Physiol Meas*, 39(7), 074004.

Schulz, S., Bolz, M., Bär, K. J., and Voss, A. (2018) Quantification of the Central Cardiovascular Network Applying the Normalized Short-time Partial Directed Coherence Approach in Healthy Subjects. *Methods Inf Med* 57, 129-134.

Schulz, S., Castro, M. R., Giraldo, B., Haueisen, J. & Voss, A. (2017) Multivariate high resolution joint symbolic dynamics (mHRJSD): a new tool to analyze couplings in physiological networks. *Biomedical Engineering / Biomedizinische Technik*.

Schulz, S., Bolz, M., Bär, K. J. & Voss, A. (2016) Central- and autonomic nervous system coupling in schizophrenia. *Philos Trans A Math Phys Eng Sci*, 374(2067), 20150178.

Schulz, S., Haueisen, J., Bär, K. J. & Andreas, V. (2015) High-resolution joint symbolic analysis to enhance classification of the cardiorespiratory system in patients with schizophrenia and their relatives. *Philos Trans A Math Phys Eng Sci*, 373(2034).

Schulz, S., Bär, K. J., & Voss, A., (2015) Analyses of Heart Rate, Respiration and Cardiorespiratory Coupling in Patients with Schizophrenia. *Entropy*, 17(2), 483-501.

Schulz, S., Voss, A., Editors. Cardiovascular and cardiorespiratory coupling analysis—State of the art and future perspectives. Cardiovascular Oscillations (ESGCO), 2014 8th Conference of the European Study Group on; 25-28 May 2014 Trento: IEEE.

Schulz, S., Adochiei, F. C., Edu, I. R., Schroeder, R., Costin, H., Bar, K. J. & Voss, A. (2013a) Cardiovascular and cardiorespiratory coupling analyses: a review. *Philos Trans A Math Phys Eng Sci*, 371(1997), 20120191.

Schulz, S., Tupaika, N., Berger, S., Haueisen, J., Bär, K. J. & Voss, A. (2013) Cardiovascular coupling analysis with high-resolution joint symbolic dynamics in patients suffering from acute schizophrenia. *Physiol Meas*, 34(8), 883-901.

Adochiei, F., **Schulz, S.,** Edu, I., Costin, H. & Voss, A. (2013) A New Normalised Short Time PDC for Dynamic Coupling Analyses. *Biomed Tech (Berl)*, 58 Suppl 1.